The Dissertation Committee for Kelley Elizabeth Hashemi
certifies that this is the approved version of the following dissertation:

Model Reference Adaptive Control for Nonminimum Phase Aerospace Systems

Committee:

Maruthi Akella, Supervisor

Behcet Acikmese

Efstathios Bakolas

Chan-gi Pak

Jayant Sirohi

Model Reference Adaptive Control for Nonminimum Phase Aerospace Systems

by

Kelley Elizabeth Hashemi, B.S.A.E.; M.S.E.

DISSERTATION

Presented to the Faculty of the Graduate School of

The University of Texas at Austin

in Partial Fulfillment

of the Requirements

for the Degree of

DOCTOR OF PHILOSOPHY

THE UNIVERSITY OF TEXAS AT AUSTIN

August 2016

Acknowledgments

I would like to thank my advisor Prof. Maruthi Akella for his extended patience, considerable assistance, and thoughtful encouragement during the course of my degree. I would also like to thank my NASA mentor Dr. Changi Pak and the NASA Harriett Jenkins Fellowship program for providing me with both interesting work and the funding to pursue it. I am grateful for the assistance provided by both the controls and structures branches at NASA Armstrong in helping me learn to span the gap between the two fields. Special thanks to Peter Suh for the copious amount of time spent helping me navigate the control design of such a unique aircraft. Also, thanks to Al Bowers, Randy Thompson, Becky Flick and David Tow for helping me navigate the intricacies of NASA.

I am similarly grateful to my group mates and friends at UT Austin for listening to me complain all along the way. To Kyle Demars, Tyler Summers, Srikant Sukumar, Travis Mercker, Apurva Chunodkar, Divya Thakur, Sonia Hernandez, Hector Escobar, Matt Harris, and Emily Kollin: I was thrilled to see each of you get out the UT door. To Sungpil Yang: you put up with my countless entreaties of "Why won't this work?" and deserve much of the credit for getting me to this point. To Miki Szmuk, Ash Biria, Marcelino Almeida, Kirsten Tuggle, and Marco Gulino: I hope that the time we spent together

got you a little closer to the finish line.

I would also like to thank my both my family and ballet friends for making the time outside of school more enjoyable. Having the option to go see everyone at the farm or taking a class with Eugene at the piano made for some of the most appreciated diversions from work. Finally, I would like to thank Milad, Vega, and Apollo for sticking around through my time in grad school. What else can I say? We'll get that yard soon.

Model Reference Adaptive Control for Nonminimum Phase Aerospace Systems

Publication No. _____

Kelley Elizabeth Hashemi, Ph.D.
The University of Texas at Austin, 2016

Supervisor: Maruthi Akella

Adaptive control techniques are often avoided in aerospace systems due to stringent plant structural requirements and validation difficulties. This dissertation seeks to broaden the range of aerospace engineering applications that can utilize an adaptive controller through the development of an extended model reference adaptive control (MRAC) design. First, a partitioned control framework is presented that permits the combined use of an adaptive control law and a nonadaptive control law. The partitioned framework is used to shift full control authority away from the adaptive portion of the system. Next, two MRAC variations that can accommodate the nonminimum phase zeros often seen in aerospace applications are discussed for use as the adaptive system. The parallel feedforward compensator approach proposes inclusion of a user–defied fictitious model in parallel with the plant that is designed to make the plant appear nonminimum phase. The surrogate tracking error approach modifies the typical MRAC structure to handle nonminimum phase

plants by requiring knowledge of its nonminimum phase zeros. A tracking error convergence proof is provided for this continuous-time MRAC variant. The partitioned design using the surrogate tracking error approach is applied to the control tasks of an experimental, flexible wing aircraft. A simulation is used to demonstrate much improved flight path angle command tracking when compared to use of the aircraft's existing nonadaptive control law, even in the presence of large–scale modeling error. A second simulation is used to show the design applied to flexible motion control of the same aircraft model and exhibits similarly improved performance.

Table of Contents

List of Tables

List of Figures

Chapter 1

Introduction

The use of adaptive control on flight vehicles is a hotly debated topic in the aerospace community. Adaptive controllers involve the use of parameters whose values change, or adapt, in response to measured performance. The changing nature of adaptive control laws means that they have the potential to offer benefits such as unified control design across changing flight conditions or the ability to compensate for aircraft uncertainty or degradation. However, the parameter update also means that adaptive control designs can offer few guarantees with respect to transient behavior and stability margins [1]. These qualities are problematic for flight vehicles that must maintain strict safety assurances [2, 3]. This dissertation attempts to mitigate the potential shortcomings of an adaptive flight controller by combining it with a nonadaptive one.

A new control design is proposed that permits concurrent use of an adaptive and nonadaptive control law. Two types of model reference adaptive controllers investigated for use as the adaptive system including a recent surrogate tracking error formulation whose error convergence proof is provided. Both formulations can accommodate plants with nonminimum phase zeros.

Simulations of the designs are performed using models of an experimental, flexible wing aircraft and are used to demonstrate improved flight control and flexible motion control.

1.1 Overview of the Dissertation's Major Contributions

The dissertation specifically considers the popular model reference adaptive control (MRAC) technique as a solution to flexible aircraft control. A two-part, or partitioned, control structure is proposed such that MRAC can be implemented in conjunction with a nonadaptive control law so as to alleviate some implementation concerns. The partitioned structure utilizes separate control surfaces for the adaptive and nonadaptive portions (i.e. control distribution) and can accommodate most multi–input single–output or multi–input multi–output (MIMO) plants. The partitioned structure also allows control authority to be shifted between the two control laws in response to risk tolerance. The nonadaptive, or nominal, control law should provide acceptable performance for the system when implemented on its own. The adaptive, or delta, control law is based on output feedback MRAC. It is intended to improve upon the performance and robustness of the nominal control law when the two are operated simultaneously. The delta law is not intended to be operated on its own.

The structure of the proposed control design allows the some of the risk associated with implementing an adaptive law to be mitigated by having a portion of the control task managed by a verified and validated nonadaptive

law. Careful selection of design parameters can be used to shift more or less of the reference tracking task to the nominal control system depending on user confidence in the delta control system. Further, since the delta control system is not required for adequate performance, it can be designed such that the expected delta control signal is expected to remain within safe operation limits.

Since the partitioned design is built around an MRAC structure, the typical MRAC implementation requirements become requirements for the proposed design as well. One long–standing MRAC requirement particularly troublesome for many aerospace applications is the need for a minimum phase plant. When considering a linear system, a minimum phase plant is one that has a stable inverse–implying that all zeros are in the open left half of the complex plane. A nonminimum phase plant is therefore one whose zeros are in the closed right half–plane. Such zeros are problematic because they can cause issues such as wrong–way tracking behavior and often eliminate the possibly of using the plant's inverse anywhere in control design. These right half–plane zeros, also denoted as nonminimum phase zeros or unstable zeros, unfortunately arise in aerospace systems frequently. Modification of the standard MRAC scheme will be necessary to implement the partitioned design on a nonminimum phase system.

The dissertation discusses use of two MRAC variants that can handle nonminimum phase systems for the delta control law to accommodate a wider range of applications. The first variant is an existing design that ac-

commodates nonminimum phase systems by introducing a feedforward block in parallel with the plant. This parallel feedforward compensator (PFC) is designed such that the plant and PFC together, known as the augmented plant, are a minimum phase system. The MRAC design is then implemented on the augmented plant. It is desirable to design the PFC such that it has a small output magnitude thus making the output of the augmented plant and the actual plant similar.

To determine the utility of this variant, the partitioned design using the PFC approach for the delta law is applied to flexible motion control of an experimental flexible wing aircraft. Stable but nonminimum phase linear models of the aircraft are generated that satisfy the necessary implementation requirements. An existing, design–reviewed, nonadaptive control law is used for the nominal portion of the proposed control system. The partitioned control design is then implemented in simulation using the models to assess the design's utility. While the PFC approach performs adequately, designing such a PFC block proves to be difficult and several restrictive requirements arise. Further, the feasibility of designing the PFC block when the plant is poorly known is questionable.

A second MRAC variant is proposed as a less restrictive way to handle nonminimum phase systems. This variant is a modification of the previously presented MIMO, continuous–time, output feedback MRAC design based on a quantity known as the surrogate tracking error. The surrogate tracking error is essentially used in place of the tracking error to formulate an adaptive

control law and parameter update law that accomplishes the MRAC task even in the presence of nonminimum phase zeros. However, the user is only able to apply the control design to plants with nonminimum phase zeros if those nonminimum phase zeros are known. The first complete stability proof for the surrogate tracking error MRAC variant is provided using a combination of Lyapunov and signal growth analysis.

The partitioned design using the surrogate tracking error approach is next tested in a flight path angle command tracking simulation for the same experimental aircraft. Here, linear models of the aircraft are generated at flight conditions beyond the body freedom flutter boundary which are both unstable and nonminimum phase. The aircraft's existing nonadaptive control law is used for the nominal law. The performance of the partitioned design using the surrogate tracking error approach is shown to be a significant improvement over a similar implementation using only the nominal control law. The simulation is repeated using estimates of plant information required for implementation, including the nonminimum phase zeros, and performance of the partitioned design is shown to still be preferable to the nominal only implementation. The proposed command tracking control system is the first implementable adaptive design for this aircraft.

The partitioned design using the surrogate tracking error approach is then further tested in a flexible motion control simulation. A simple aeroservoelasic model of the aircraft's wing is created to explore several design choices associated with the partitioned framework before attempting control of the

experimental aircraft. The design choices are then carried over to implementation of the partitioned design on models of the full aircraft where again the aircraft's existing nonadaptive control law is used for the nominal system. The response to a gust-like disturbance at flight conditions past the body freedom flutter boundary is investigated. The partitioned design again demonstrates improved vibration suppression over the nominal-only implementation in both the perfect–knowledge and estimated–knowledge cases. The proposed flexible motion control system is the first adaptive design for this aircraft implementable across the full flight envelope.

1.2 Literature Review

Next a survey of other studies related to the cross–section of adaptive control, nonminimum phase systems, and flight control design is presented.

1.2.1 Adaptive Control for Nonminimum Phase Systems

MRAC is a well established control technique that relies on online parameter update laws to drive a plant's output to match that of a user–selected reference model. The direct formulation has been extensively addressed in previous literature, beginning with works such as [4] and [5], and the solution to the single–input single–output (SISO) MRAC problem is well established [6]. The results can now be found in many textbooks [7–9]. Solutions to the MIMO MRAC problem also exist. The various solution procedures differ however in their treatment of the high frequency gain matrix K_p and the resulting

requirements placed on the plant. Early approaches involved definiteness requirements on K_p which lead to restrictive assumptions on prior knowledge of the unknown system [10]. More recent results propose the use of various matrix factorizations to relax the constraints imposed on K_p [11, 12]. Most versions of the MRAC problem assume that the plant to be controlled satisfies a number of structural requirements including an equal number of inputs and outputs and being minimum phase. Additionally, they require that certain knowledge of the otherwise unknown plant be available—such as relative degree and high frequency gain information [8] (see Chapters 6.4 and 9.7.3).

Although textbook versions of MRAC are restricted to minimum phase systems, other adaptive control techniques have developed to accommodate nonminimum phase plants. Zero annihilation periodic control laws have been proposed to address the minimum phase problem in discrete systems [13] but produce intermittent control. Large uncertainties in the plant can be assumed to compensate for a nonminimum phase structure when attempting MRAC, but perfect tracking is no longer within reach [14]. Certain indirect adaptive control techniques such as adaptive pole placement [15] can also handle nonminimum phase systems. Although, they require some level of parameter knowledge to avoid singularities. An adaptive version of the linear quadratic Gaussian loop transfer recovery (LQG/LTR) procedure is applicable to nonminimum phase plants when it is possible to incorporate fictitious control signals to "square up" the system [16–18].

Extension of MRAC to nonminimum phase systems has been slow to

develop. One possibility is to use the PFC approach and add a feedforward block in parallel with the plant. The block must make the system appear minimum phase to the adaptation mechanism [19]. The output magnitude of the PFC block must be small so as to not significantly disturb the tracking performance of the actual plant. However design of such a structure can be difficult when the plant is poorly known. Retrospective Cost Adaptive Control can also be used in the MRAC framework for discrete-time systems [20]. Here a cost function that relates past error to a computed version of the past error is used to select the parameter update law. Initial attempts to create a similar control law for continuous-time systems using a surrogate tracking error quantity and knowledge of the nonminimum phase zeros have been proposed as well [21, 22]. Although the control design is successfully demonstrated in simulation of simple examples, the assumed plant structure is restrictive. Additionally, the tracking error convergence proof is left open.

1.2.2 Aircraft Control Design

As the topic of aircraft control design is vast, the survey is restricted to topics that are most directly relevant to the dissertation. Foremost, consider the subject of adaptive control law design in the context of flight vehicles. Adaptive control laws are not often implemented on aircraft due in large part to difficulty in providing transient performance assurances and a lack of verification methods [1–3]. Additionally, several common adaptive control techniques, including MRAC, assume linear plant dynamics while aircraft dynamics are

inherently nonlinear. Regardless, significant effort has been made to construct adaptive designs that can serve as viable options for aircraft control. For example, a variant of Retrospective Cost Adaptive Control has been applied to uncertain, nonminimum phase aircraft models [23]. The PFC approach has been recently used in the context of aerospace systems to facilitate autopilot design [24]. A hybrid adaptive controller has been proposed for control of damaged aircraft [25]. Recently, an $\mathcal{L}_1$ adaptive controller was implemented on a Learjet and used for manned flight [26]. Several LQG/LTR designs, both adaptive and nonadaptive, have been applied to aircraft [27]. Additionally, closed–loop reference model adaptive control has been used on its own and in conjunction with LQG/LTR designs to offer improved transient performance of aircraft adaptive control systems [28–30]. Adaptive dynamic inversion has also been used in an MRAC-like framework to control an aircraft model [31]. A survey of other adaptive control designs and implementations for aircraft is provided in [32]. Additionally, alternate verifications frameworks for adaptive control of flight vehicle have been proposed [33].

Next, consider the topic of aircraft flexible motion control design. Control of an aircraft's flexible behavior has received significant attention since the first active flutter suppression demonstration in [34]. Many types of control have now been investigated using models or hardware apparatuses of widely varying complexity. NASA's Benchmark Active Control Technology program in particular spurred many flexible motion control designs including ones based on classical techniques [35], linear parameter varying models [36], and robust

multivariable methods [37].

Adaptive control has also been applied to the task of flexible motion control and flutter suppression in particular. Several designs have been demonstrated on the dynamic model of an aircraft wing's aeroelasitc pitch and plunge motion [38]. The non-trivial dynamics, based on an unsteady aerodynamic theory developed by Theodorsen [39] and approximated by Wagner and Jones [40], have been widely used to investigate control techniques for aeroelastic phenomena. Others have looked at adaptively controlling this model with techniques such as non-certainty equivalence [41] and $\mathcal{L}_1$ [42] adaptive control. A variety of adaptive control techniques were applied to an aircraft model in [43] whose rigid body dynamics were known and flexible body dynamics were treated as unmodeled. A summary of additional adaptive flutter suppression implementations can be found in [44].

Models of an experimental, flexible wing aircraft are used to demonstrate control design performance throughout the dissertation . While further details concerning the aircraft will not be provided, a survey of other control designs for flexible wing aircraft is included. A wide array of control techniques has now been applied to various control tasks for flexible aircraft. In [45], a gain–scheduled controller based on linear parameter–varying models was proposed as a way to provide control design over the flight envelope of a flexible aircraft. An inner and outer loop control system structure was prescribed for a flexible aircraft in [46]. A robust approach to flexible motion control based on modal filtering was also considered in [47]. The recent closed–loop reference

model approach to improved transient adaptive control was even applied to a very flexible aircraft model in [48].

1.3 Dissertation Outline

The dissertation is organized as follows. Chapter 1 provides an introduction to the problem of adaptive control for nonminimum phase aerospace systems and summarizes the steps taken to establish a feasible solution. A review of other related or relevant studies available in the literature is also provided. Chapter 2 contains a collection of established mathematical results and control techniques that provide a foundation for the discussions in later chapters. A discussion of why standard MRAC designs fail for nonminimum phase systems is also provided, with further details on how two of the established error convergence proof procedures break down given in the appendices. An overview of the aeroservoelastic state space modeling approach used in the dissertation included as well. The partitioned control design is presented in Chapter 3. The general structure of the nominal controller and delta controller required by the design is stated. Chapter 4 presents the PFC version of the partitioned design. Simulation results of the design applied to the flexible motion control task of an experimental flexible wing aircraft are shown. Chapter 5 presents the surrogate tracking error version of MRAC which can accommodate nonminimum phase plants. A tracking error convergence proof requiring knowledge of the plant's nonminimum phase zero information is provided. The surrogate tracking error version of the partitioned design is applied

to the flexible aircraft in Chapter 6. Here the design is used to demonstrate improved flight path angle command tracking. Similarly, Chapter 7 applies the surrogate tracking error partitioned design to flexible motion control of the aircraft. Simulation results are used to shown improved rejection of a gust–like disturbance. Finally, some concluding remarks, a summary of the dissertation's contributions, and future research directions are provided in Chapter 8.

Chapter 2

Background

A summary of notation and established results relevant to dissertation is provided in this chapter. After defining some of the notable mathematical operations that will be used, several important properties related to signals and systems and methods to bound them are presented. A framework for relating growth rates of signals is presented next. A brief review of the main of Lyapunov stability analysis results is then provided. Finally, an overview of the theory behind aeroservoelastic modeling is presented. Proofs are omitted unless needed for later discussion. Note that throughout the subsequent chapters of the dissertation arguments of functions are often omitted for notational simplicity whenever no confusion arises.

2.1 Mathematical Preliminaries

For a positive integer n, the n-dimensional identity matrix is denoted by I_n. The i^{th} column of I_n is indicated by the vector e^i.

A matrix $P \in \mathbb{R}^{n\times n}$ has n eigenvalues where the smallest is called $\lambda_{\min}(P)$ and the largest is $\lambda_{\max}(P)$. If P is positive definite, equivalently

written as $P > 0$, then all of its eigenvalues are positive and the inequality

$$\lambda_{\min}(P)\|x\|_2^2 \leq x^T P x \leq \lambda_{\max}(P)\|x\|_2^2 \tag{2.1}$$

holds for any $x \in \mathbb{R}^n$ where $\|\cdot\|_2$ is used to indicate the Euclidean norm.

For matrices $A = (a_{ij}) \in \mathbb{R}^{m\times n}$ and $B \in \mathbb{R}^{p\times q}$, the Kronecker product of A and B is defined as

$$A \otimes B = \begin{bmatrix} a_{11}B & \dots & a_{1n}B \\ \vdots & \ddots & \vdots \\ a_{m1}B & \dots & a_{mn}B \end{bmatrix} . \tag{2.2}$$

2.2 Signal and System Properties

Consider a linear, time–invariant system which can be represented in the time domain by the state space equations

$$\begin{aligned} \dot{x}(t) &= Ax(t) + B(t)u(t) \\ y(t) &= Cx(t) + Du(t) \end{aligned} \tag{2.3}$$

with state $x(t) \in \mathbb{R}^n$. The relationship between input $u(t) \in \mathbb{R}^p$ and output $y(t) \in \mathbb{R}^q$ can also be represented in the Laplace domain (with some abuse of notation) as

$$y = G(s)u \tag{2.4}$$

where s is the Laplace variable and $G(s) = C(sI - A)^{-1}B + D$ is an $l \times m$ transfer function matrix. The same relationship may be expressed as

$$y = G(s)\,[u] \tag{2.5}$$

to be clear what signal constitutes the system's input. The system is called single-input single-output (SISO) if $p = q = 1$ and multiple-input multiple-output (MIMO) if $p, q > 1$. The system is considered stable if all poles of $G(s)$ or all eigenvalues of the A matrix are in the open left half of the complex plane.

The following set of results, each summarized from [8], describes important ways in which signals like $u(t)$ and $y(t)$ and transfer functions like $G(s)$ can be classified and bounded.

Definition 2.2.1 (Signal norms)**.** The $\mathcal{L}_p$ norm of a scalar or vector function of time $x(t)$ is given by

$$\|x\|_p \triangleq \left(\int_0^\infty |x(\tau)|^p d\tau \right)^{\frac{1}{p}} \tag{2.6}$$

for $p \in [1, \infty)$. Note that $x \in \mathcal{L}_p$ when $\|x\|_p$ is finite. Further, the $\mathcal{L}_\infty$ norm is given by

$$\|x\|_\infty \triangleq \sup_{t \geq 0} |x(t)| \tag{2.7}$$

and $x \in \mathcal{L}_\infty$ when $\|x\|_\infty$ is finite.

Theorem 2.2.1 (Barbalat's Lemma)**.** *If* $\lim_{t\to\infty} \int_0^t f(\tau)d\tau$ *exists and is finite, and* $f(t)$ *is uniformly continuous, then* $\lim_{t\to\infty} f(t) = 0$*.*

Corollary 2.2.2 (Corollary to Barbalat's Lemma)**.** *If* f*,* $\dot{f} \in \mathcal{L}_\infty$ *and* $f \in \mathcal{L}_p$ *for some* $p \in [1, \infty)$ *then* $f(t) \to 0$ *as* $t \to \infty$*.*

Theorem 2.2.3 ($\mathcal{L}_2$ gain)**.** *The* $\mathcal{L}_2$ *gain of a stable, linear, time-invariant system described by* $y = H(s)u$ *is given by* $\|H(s)\|_\infty \triangleq \sup_{\omega\in\Re} |H(jw)|$ *such*

that

$$\|y\|_2 \leq \|H(s)\|_\infty \|u\|_2 \tag{2.8}$$

when $u \in \mathcal{L}_2$.

Definition 2.2.2 (PR functions)**.** A rational function $G(s)$ of the complex variable $s = \sigma + j\omega$ is called positive real (PR) if:

i $G(s)$ is real for real s.

ii $\text{Re}[G(s)] \geq 0$ for all $\text{Re}[s] > 0$.

Definition 2.2.3 (SPR functions)**.** Assuming that $G(s)$ is not identically zero for all s, then $G(s)$ is strictly positive real (SPR) is $G(s - \epsilon)$ is PR for some $\epsilon > 0$.

Theorem 2.2.4. *Assume that the rational function* $G(s)$ *is real for real* s *and not identically zero for all* s*. Further, let* $G(s) = \frac{Z(s)}{R(s)}$ *with relative degree* n^**. If* $|n^*| \leq 1$ *then* $G(s)$ *is SPR if and only if:*

i $G(s)$ *is analytic in* $Re[G(s)] \geq 0$.

ii $Re[G(j\omega)] > 0 \ \forall \omega \in (-\infty, \infty)$.

iii (When $n^* = 1$*)* $\lim_{|\omega| \to \infty} \omega^2 Re[G(j\omega)] > 0$.

iv (When $n^* = -1$*)* $\lim_{|\omega| \to \infty} \frac{G(j\omega)}{j\omega} > 0$.

Corollary 2.2.5. *Resulting useful properties of SPR functions include*

i $G(s)$ *is PR (SPR) if and only if 1/*$G(s)$ *is PR (SPR)*

ii If $G(s)$ *is SPR then* $|n^*| \leq 1$ *and the zeros and poles of* $G(s)$ *lie in* $Re[s] < 0$

iii If $|n^*| > 1$ *then* $G(s)$ *is not PR.*

Theorem 2.2.6 (MKY Lemma)**.** *If a stable SISO system given by* $G(s) = C(sI - A)^{-1}B$ *is SPR, then for any* $L = L^T > 0$ *there exists a scalar* $\nu > 0$*, a vector* q*, and a matrix* $P = P^T > 0$ *such that*

$$A^T P + PA = -qq^T - \nu L$$
$$PB = C. \tag{2.9}$$

Theorem 2.2.7 (Swapping Lemma)**.** *Let* $\Psi : \mathbb{R}^+ \to \mathbb{R}^{m \times l}$ *and* $\tilde{\Theta} : \mathbb{R}^+ \to \mathbb{R}^m$ *with* $\tilde{\Theta}$ *differentiable. Let* $W(s)$ *be any strictly proper, stable* $l \times l$ *transfer function matrix with a minimal realization (A,B,C). Then*

$$W(s)\left[\Psi^T \tilde{\Theta}\right] = W(s)\left[\Psi^T\right]\tilde{\Theta} - W_C(s)\left[W_B(s)\left[\Psi^T\right]\dot{\tilde{\Theta}}\right] \tag{2.10}$$

where

$$W_C(s) \triangleq C(sI - A)^{-1} \tag{2.11}$$

$$W_B(s) \triangleq (sI - A)^{-1}B. \tag{2.12}$$

Note that this result is the MIMO version of Appendix A.1 in [8]. A related proof can be found in [49].

Proof. Define the output of $W(s)$ from input $\Psi^T\tilde{\Theta}$ to be $y_1 \in \mathbb{R}^l$ such that

$$\begin{aligned} \dot{x} &= Ax + B\left(\Psi^T\tilde{\Theta}\right) \\ y_1 &= Cx. \end{aligned} \tag{2.13}$$

Define the output of $W(s)$ from input Ψ_i^T (i.e. the i^{th} column of Ψ^T) to be $y_{2,i} \in \mathbb{R}^l$ such that

$$\begin{aligned} \dot{w}_i &= Aw_i + B\left(\Psi_i^T\right) \\ y_{2,i} &= Cw_i \end{aligned} \tag{2.14}$$

for $i = 1...m$. Assembling the state vector and output of each instance of this system as

$$y_2 = [y_{2,1} \;\; y_{2,2} \;\; \cdots \;\; y_{2,m}] \tag{2.15}$$

$$w = [w_1 \;\; w_2 \;\; \cdots \;\; w_m] \tag{2.16}$$

permits a composite system to be stated as

$$\begin{aligned} \dot{w} &= Aw + B\left(\Psi^T\right) \\ y_2 &= Cw. \end{aligned} \tag{2.17}$$

Additionally, define

$$\bar{y}_2 \triangleq Cw\tilde{\Theta}. \tag{2.18}$$

Create a new system by selecting $\bar{x} \triangleq x - w\tilde{\Theta}$. Its dynamics are given

by

$$\begin{aligned}\dot{\bar{x}} &= \dot{x} - \dot{w}\tilde{\Theta} - w\dot{\Theta} \\ &= Ax + B\Psi^T\tilde{\Theta} - Aw\tilde{\Theta} - B\Psi^T\tilde{\Theta} - w\dot{\Theta} \\ &= A(x - w\tilde{\Theta}) - w\dot{\Theta} \\ &= A\bar{x} - w\dot{\Theta}. \end{aligned} \tag{2.19}$$

Its output equation is given by

$$\begin{aligned} y_1 - \bar{y_2} &= C\left(x - w\tilde{\Theta}\right) \\ &= C\bar{x}. \end{aligned} \tag{2.20}$$

Finally, using the new system note that

$$\begin{aligned} W(s)\left[\Psi^T\tilde{\Theta}\right] - W(s)\left[\Psi^T\right]\tilde{\Theta} &= y_1 - \bar{y}_2 \\ &= -W_C(s)\left[w\dot{\Theta}\right] \\ &= -W_C(s)\left[W_B(s)\left[\Psi^T\right]\dot{\Theta}\right] \end{aligned} \tag{2.21}$$

as desired. □

2.3 Signal Growth Relationships

A collection of relevant results relating the growth of signals in a system is provided. Each is taken from Chapter 2 or Appendix B of [9] unless otherwise indicated. Extensions to the MIMO case have been made where needed with a reference provided to existing proofs or without comment if straightforward.

Definition 2.3.1. The class $\mathcal{PC}_{[0,\infty)}$ is defined as the set of all real piecewise continuous functions defined on the interval $[0,\infty)$ that have bounded discontinuities.

Definition 2.3.2 ($\mathcal{O}$ and o notation)**.** For $x, y \in \mathcal{PC}_{[0,\infty)}$, the notation $y(t) = \mathcal{O}[x(t)]$ is used to indicate that there exist positive constants M_1, M_2, and $t_0 \in \mathbb{R}^+$ such that

$$|y(t)| \leq M_1|x(t)| + M_2 \tag{2.22}$$

for all $t \geq t_0$. The notation $y(t) = o[x(t)]$ is used to indicate that there exists a function $\beta(t) \in \mathcal{PC}_{[0,\infty)}$ and $t_0 \in \mathbb{R}^+$ such that

$$|y(t)| = \beta(t)x(t) \tag{2.23}$$

for all $t \geq t_0$ and $\lim_{t\to\infty} \beta(t) = 0$.

Definition 2.3.3 (Same rate of growth)**.** For $x, y \in \mathcal{PC}_{[0,\infty)}$, if $y(t) = \mathcal{O}[x(t)]$ and $x(t) = \mathcal{O}[y(t)]$ then x and y are equivalent which is denoted as

$$x(t) \sim y(t). \tag{2.24}$$

They are said to grow at the same rate if

$$\sup_{\tau\leq t} |y(\tau)| \sim \sup_{\tau\leq t} |x(\tau)|. \tag{2.25}$$

Definition 2.3.4 (Class $\mathcal{M}$ functions)**.** The $\mathcal{M}$ class of positive monotonic functions is defined by

$$\mathcal{M} = \{f|\ f(t) \geq 0,\ f(t_1) \geq f(t_2) \text{ if } t_1 > t_2,\ \forall t, t_1, t_2 \in \mathbb{R}^+\}. \tag{2.26}$$

Note that for any function $f(\cdot) \in \mathcal{PC}_{[0,\infty)}$ it is true that $\sup_{\tau \leq t} |f(\tau)| \in \mathcal{M}$ for $\tau, t \in \mathbb{R}^+$.

Definition 2.3.5 (Class ϵ signals)**.** The ϵ class of signals is defined for $x : \mathbb{R}^+ \to \mathbb{R}^n$ by

$$\epsilon = \{x | \, \|\dot{x}(t)\| \leq M_1 \sup_{\tau \leq t} \|x(\tau)\| + M_2, \;\; M_1, M_2 \in \mathbb{R}^+\}. \tag{2.27}$$

Theorem 2.3.1. *For $x(\cdot) \in \mathcal{PC}_{[0,\infty)}$ and $y(\cdot) \in \mathcal{M}$ it holds that*

$$x(t) = \mathcal{O}[y(t)] \Leftrightarrow \sup_{\tau \leq t} |x(\tau)| = \mathcal{O}[y(t)]. \tag{2.28}$$

Theorem 2.3.2. *Consider a vector $x : \mathbb{R}^+ \to \mathbb{R}^n$*

$$x^T = \begin{bmatrix} x_1^T & x_2^T \end{bmatrix} \tag{2.29}$$

with $x_1 : \mathbb{R}^+ \to \mathbb{R}^{n_1}$, $x_2 : \mathbb{R}^+ \to \mathbb{R}^{n_2}$, and $n_1 + n_2 = n$. If x grows unbounded then

$$\sup_{\tau \leq t} \|x_1(\tau)\| = \mathcal{O}\left[\sup_{\tau \leq t} \|x_2(\tau)\|\right] \Leftrightarrow \sup_{\tau \leq t} \|x_2(\tau)\| \sim \sup_{\tau \leq t} \|x(\tau)\|. \tag{2.30}$$

Theorem 2.3.3. *Define a linear system as*

$$\begin{aligned} \dot{x}(t) &= A(t)x(t) + B(t)u(t) \quad x(t_0) = x_0 \\ y(t) &= C(t)x(t) \end{aligned} \tag{2.31}$$

with $u : \mathbb{R}^+ \to \mathbb{R}^p$, $y : \mathbb{R}^+ \to \mathbb{R}^q$, $x : \mathbb{R}^+ \to \mathbb{R}^n$, and $u \in \mathcal{PC}_{[0,\infty)}$. If the entries of $A(t), B(t), C(t)$ are uniformly bounded and $A(t)$ is exponentially stable, then

$$\sup_{\tau \leq t} \|x(\tau)\| = \mathcal{O}\left[\sup_{\tau \leq t} \|u(\tau)\|\right] \tag{2.32}$$

and

$$\|y(t)\| = \mathcal{O}\left[\sup_{\tau \leq t} \|u(\tau)\|\right]. \tag{2.33}$$

Corollary 2.3.4. *Consider the square transfer function matrix*

$$W(s) = \frac{p(s)}{q(s)} I_m \tag{2.34}$$

with both $p(s)$ and $q(s)$ n^{th}-order stable polynomials. If the input/output relationship is defined as $y = W(s)u$ then $\|y\|$ and $\|u\|$ grow at the same rate.

Theorem 2.3.5. *Consider the linear system*

$$\dot{x} = Ax + Bu \tag{2.35}$$

where $x : \mathbb{R}^+ \to \mathbb{R}^n$ and $u : \mathbb{R}^+ \to \mathbb{R}^p$. If (A, B) is controllable and $u \in \epsilon$ then

$$\sup_{\tau \leq t} \|u(\tau)\| = \mathcal{O}\left[\sup_{\tau \leq t} \|x(\tau)\|\right]. \tag{2.36}$$

Note that this property is a multi-input extension of the standard single-input result. It is most easily obtained from straightforward adjustments to the proof of Lemma 3 in [50].

Theorem 2.3.6. *If $\beta \in \mathcal{L}_2$, $u \in \mathcal{PC}_{[0,\infty)}$, and βu is the input to a time–invariant, asymptotically stable, linear system then the output y adheres to*

$$\|y(t)\| = o\left[\sup_{\tau \leq t} \|u(\tau)\|\right]. \tag{2.37}$$

Theorem 2.3.7. *For two unbounded signals x and $y \in \mathcal{M}$, it holds that*

$$x(t) = \mathcal{O}[y(t)] \Rightarrow y(t) \neq o[x(t)]. \tag{2.38}$$

2.4 Lyapunov Stability Analysis

Consider the system described by

$$\dot{x} = f(t, x), \quad x(t_0) = x_0 \tag{2.39}$$

where $x \in \mathbb{R}^n$, $f : \mathcal{J} \times \mathcal{B}(r) \to \mathbb{R}$, $\mathcal{J} = [t_0, \infty)$, and $\mathcal{B}(r) = \{x \in \mathbb{R}^n, |x| < r\}$. Assume that for each $x_0 \in \mathcal{B}(r)$ and $t_0 \in \mathbb{R}^+$ the function f has only one solution. Several definitions of stability relevant to this system are presented and are then used to summarize Lyapunov's direct method of assessing solution stability.

2.4.1 Stability Definitions

The following definitions of stability provide a basis for the stability discussions in this dissertation and are taken from [9] and [51].

Definition 2.4.1 (Equilibrium point)**.** The quantity x_e is called an equilibrium point of Eq. (2.39) if

$$f(t, x_e) = 0 \quad \forall t \geq t_0. \tag{2.40}$$

Definition 2.4.2 (Bounded, Uniformly bounded)**.** A solution of Eq. (2.39) is said to be bounded if there exists a $\beta > 0$ such that $|x(t)| < \beta$ for all $t \geq t_0$ where β may be dependent on the solution.

The solution is said to be uniformly bounded if for any $\alpha > 0$ and $t_0 \in \mathbb{R}^+$ there exists a $\beta = \beta(\alpha)$ independent of t_0 such that if $|x_0| < \alpha$ then $|x(t)| < \beta$ for all $t \geq t_0$.

Definition 2.4.3 (Stable, Uniformly stable)**.** The equilibrium point of Eq. (2.39) is said to be stable in the sense of Lyapunov if for any t_0 and ϵ there exists a $\delta(\epsilon, t_0)$ such that $|x_0 - x_\epsilon| < \delta$ implies $|x(t) - x_e| < \epsilon$ for all $t \geq t_0$.

The equilibrium point is said to be uniformly stable if δ does not depend on t_0.

Definition 2.4.4 (Asymptotically stable, Asymptotically stable in the large)**.** The equilibrium point of Eq. (2.39) is said to be asymptotically stable if it is stable and there exists a $\delta(t_0)$ such that $|x_0 - x_e| < \delta(t_0)$ implies $\lim_{t\to\infty} |x(t) - x_e| = 0$.

The equilibrium point is said to be asymptotically stable in the large if it is stable and every solution tends to x_e as $t \to \infty$.

Definition 2.4.5 (Uniformly asymptotically stable, Uniformly asymptotically stable in the large)**.** The equilibrium point of Eq. (2.39) is said to be uniformly asymptotically stable if:

i It is stable.

ii For every $\epsilon > 0$ and $t_0 \in \mathbb{R}^+$, there exists a $\delta_0 > 0$ that does not depend on t_0 or ϵ and a $T(\epsilon) > 0$ that does not depend on t_0 such that $|x(t) - x_e| < \epsilon$ for all $t \geq t_0 + T(\epsilon)$ whenever $|x_0 - x_e| < \delta_0$.

The equilibrium point is said to the uniformly asymptotically stable in the large if:

i It is uniformly stable.

ii The solutions are uniformly bounded.

iii For any $\alpha > 0$, any $\epsilon > 0$, and $t_0 \in \mathbb{R}^+$ there exists $T(\epsilon, \alpha) > 0$ independent of t_0 such that if $|x_0 - x_e| < \alpha$ then $|x(t) - x_e| < \epsilon$ for all $t \geq t_0 + T(\epsilon, \alpha)$.

Definition 2.4.6 (Exponentially stable, Exponentially stable in the large)**.** The equilibrium point is said to be exponentially stable if there exists $\alpha > 0$ and for every $\epsilon > 0$ there exists a $\delta(\epsilon) > 0$ such that

$$|x(t) - x_e| \leq \epsilon e^{-\alpha(t-t_0)} \quad \forall t \geq t_0 \tag{2.41}$$

whenever $|x_0 - x_e| \leq \delta(\epsilon)$.

The equilibrium point is said to the exponentially stable in the large if there exits $\alpha > 0$ and for any $\beta > 0$ there exists a $k(\beta) > 0$ such that

$$|x(t)| \leq k(\beta)e^{-\alpha(t-t_0)} \quad \forall t \geq t_0 \tag{2.42}$$

whenever $|x_0| < \beta$.

Definition 2.4.7 (Unstable)**.** The equilibrium state is said to be unstable if it is not stable.

Definition 2.4.8 (Solution stability)**.** If the trajectory $x(t)$ is a solution of Eq. (2.39) then it is said to be stable (or US, AS, UAS, ES, unstable) if the equilibrium point $z_e = 0$ of the system

$$\dot{z} = f(t, z + x(t)) - f(t, x(t)) \tag{2.43}$$

is stable (respectively US, AS, UAS, ES, unstable).

2.4.2 Lyapunov Direct Method

The previous definitions of stability can be used to discuss the stability properties of solutions to systems of the form given in Eq. (2.39) rather than analyzing stability of the explicit solutions themselves. The collection of results is known as Lyapunov's direct method. Here several necessary definition are presented along with two theorems summarizing a portion of the direct method results.

Definition 2.4.9 (Class $\mathcal{K}$ function)**.** A continuous function $\phi : [0, r] \to \mathbb{R}^+$ (or with $r = \infty$) is said to belong to class $\mathcal{K}$ if

i $\phi(0) = 0$

ii ϕ is strictly increasing on $[0, r]$ (or $[0, \infty)$).

Definition 2.4.10 (Class $\mathcal{KR}$ function)**.** A continuous function $\phi : [0, \infty) \to \mathbb{R}^+$ is said to belong to class $\mathcal{KR}$ if

i $\phi(0) = 0$

ii ϕ is strictly increasing on $[0, \infty)$

iii $\lim_{r\to\infty} \phi(r) = \infty$.

Definition 2.4.11 (Same order of magnitude)**.** Two function $\phi_1, \phi_2 \in \mathcal{K}$ defined on $[0, r]$ (or $[0, \infty)$) are said to be the same order of magnitude if there exist positive constants k_1, k_2 such that

$$k_1\phi_1(r_1) \leq \phi_2(r_1) \leq k_2\phi_1(r_1) \quad \forall r_1 \in [0, r] \text{ (or } \forall r_1 \in [0, \infty)) \tag{2.44}$$

Definition 2.4.12 (Positive definite)**.** A function $V(t,x) : \mathbb{R}^+ \times \mathcal{B}(r) \to \mathbb{R}$ with $V(t,0) = 0$ for all $t \in \mathbb{R}^+$ is positive definite if there exists a continuous function $\phi \in \mathcal{K}$ such that $V(t,x) \geq \phi(|x|)$ for all $t \in \mathbb{R}^+$, $x \in \mathcal{B}(r)$, and $r > 0$. $V(t,x)$ is negative definite if $-V(t,x)$ is positive definite.

Definition 2.4.13 (Positive semidefinite)**.** A function $V(t,x) : \mathbb{R}^+ \times \mathcal{B}(r) \to \mathbb{R}$ with $V(t,0) = 0$ for all $t \in \mathbb{R}^+$ is positive semidefinite if $V(t,x) \geq 0$ for all $t \in \mathbb{R}^+$, $x \in \mathcal{B}(r)$, and $r > 0$. $V(t,x)$ is negative semidefinite if $V(t,x) \leq 0$ under the same conditions.

Definition 2.4.14 (Decrescent)**.** A function $V(t,x) : \mathbb{R}^+ \times \mathcal{B}(r) \to \mathbb{R}$ with $V(t,0) = 0$ for all $t \in \mathbb{R}^+$ is decrescent if there exists $\phi \in \mathcal{K}$ such that $|V(t,x)| \leq \phi(|x|)$ for all $t \in \mathbb{R}^+$ and all $x \in \mathcal{B}(r)$ for some $r > 0$.

Definition 2.4.15 (Radially unbounded)**.** A function $V(t,x) : \mathbb{R}^+ \times \mathcal{B}(r) \to \mathbb{R}$ with $V(t,0) = 0$ for all $t \in \mathbb{R}^+$ is radially unbounded if there exists $\phi \in \mathcal{KR}$ such that $V(t,x) \geq \phi(|x|)$ for all $t \in \mathbb{R}^+$ and $x \in \mathbb{R}^n$.

The following two theorems constitute the portion of Laypunov's direct method that will be used here. They concern a function $V(x,t)$ and its derivative along the solution of a system of the form of Eq. (2.39) given by

$$\dot{V} = \frac{\partial V}{\partial t} + (\nabla V)^T f(t,x) \tag{2.45}$$

where $\nabla V = [\frac{\partial V}{\partial x_1}, \frac{\partial V}{\partial x_2}, ..., \frac{\partial V}{\partial x_n}]^T$. Should a given $V(x,t)$ be shown to satisfy any of the results of the direct method theorems it is then known as a Lyapunov function.

Theorem 2.4.1 (Lyapunov local results)**.** *For a positive definite function* $V(t,x) : \mathbb{R}^+ \times \mathcal{B}(r) \to \mathbb{R}$ *for* $r > 0$ *with* $V(t,0) = 0$ *for all* $t \in \mathbb{R}^+$ *and continuous first-order partial derivatives with respect to* x *and* t*, the following hold:*

i If $\dot{V} \leq 0$ *then* $x_e = 0$ *is stable.*

ii If V *is decrescent and* $\dot{V} \leq 0$ *then* $x_e = 0$ *is uniformly stable.*

iii If V *is decrescent and* $\dot{V} < 0$ *then* $x_e = 0$ *is uniformly asymptotically stable.*

iv If V *is decrescent and there exist* $\phi_1, \phi_2, \phi_3 \in \mathcal{K}$ *of the same order of magnitude such that*

$$\phi_1(|x|) \leq V(t,x) \leq \phi_2(|x|), \quad \dot{V}(t,x) \leq -\phi_3(|x|) \tag{2.46}$$

for all $x \in \mathcal{B}(r)$ *and* $t \in \mathbb{R}^+$*, then* $x_e = 0$ *is exponentially stable.*

Theorem 2.4.2 (Lyapunov global results)**.** *Assume that the system in Eq.* (2.39) *has a unique solution for all* $x_0 \in \mathbb{R}^n$*. For a positive definite, decrescent, and radially unbounded function* $V(t,x) : \mathbb{R}^+ \times \mathbb{R}^n \to \mathbb{R}^+$ *with* $V(t,0) = 0$ *for all* $t \in \mathbb{R}^+$ *and continuous first-order partial derivatives with respect to* x *and* t*, the following hold:*

i If $\dot{V} < 0$ *the* $x_e = 0$ *is uniformly asymptotically stable in the large.*

ii If there exist $\phi_1, \phi_2, \phi_3 \in \mathcal{KR}$ *of the same order of magnitude such that*

$$\phi_1(|x|) \leq V(t,x) \leq \phi_2(|x|), \quad \dot{V}(t,x) \leq -\phi_3(|x|) \tag{2.47}$$

then $x_e = 0$ *is exponentially stable in the large.*

Note that if the system in Eq. (2.39) is instead autonomous, i.e.

$$\dot{x} = f(x), \tag{2.48}$$

then $V(t,x) = V(x)$ will always be decrescent and uniformity is automatically implied. Therefore, stability and asymptotic stability of $x_e = 0$ imply uniform stability and uniform asymptotic stability in this case.

Should choice of a function that satisfies the necessary requirements of either Theorem 2.4.1 or 2.4.2 be difficult or impossible, it is often permissible to use a deficient function that resembles a Lyapunov function. The deficient function is called a Lyapunov-like function and it can be used along with its derivative to establish stability. For example, it may be convenient to select a positive semidefinite function for $V(x)$ instead of a positive definite one. This function would not satisfy either theorem and would be considered a Lyapunov-like function.

2.5 Classical MRAC

Consider the a SISO plant with partial state feedback described by the strictly proper transfer function

$$\begin{aligned} y &= G(s)u \\ &= k_p \frac{Z_p(s)}{R_p(s)} \end{aligned} \tag{2.49}$$

where $y, u \in \mathbb{R}$, Z_p and R_p are monic polynomials, and k_p is a constant. The plant can be equivalently represented using the state space description (A_p, B_p, C_p) with state $x_p \in \mathbb{R}^{n_p}$ and initial condition $x_p(0) = x_{p0}$. The user-selected reference model is given by the strictly proper transfer function

$$\begin{aligned} y_m &= W_m(s)r \\ &= k_m \frac{Z_m(s)}{R_m(s)} \end{aligned} \tag{2.50}$$

where Z_m and R_m are monic polynomials, and k_m is a constant. The reference input $r \in \mathbb{R}$ must be uniformly bounded and piecewise continuous. The reference model can be equivalently represented using the state space description (A_m, B_m, C_m) with state $x_m \in \mathbb{R}^{n_m}$ and initial condition $x_m(0) = x_{m0}$.

The goal is to design u such that y is brought to match y_m. Under a variety of assumptions, this is feasible when the parameters of the plant are either known or unknown. In the known plant parameter case, the control law can be specified by selecting its terms based on a matching condition that arises between the controlled plant and reference model. In the unknown plant parameter case, an adaptive control law with terms that are updated online

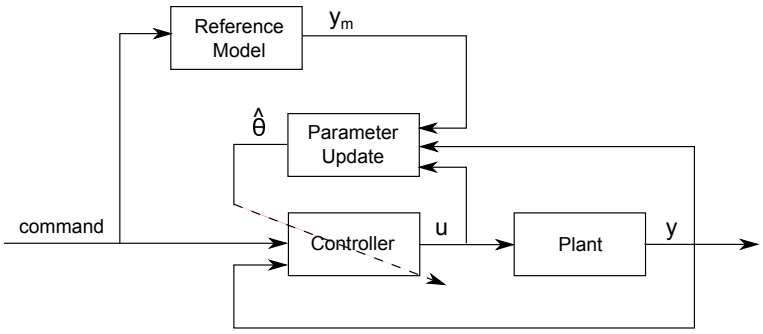

Figure 2.1: Standard MRAC block diagram

can be shown to accomplish the goal in the limit. However, an appropriate update law for the control law terms must also be specified. A block diagram of the standard MRAC design is shown in Fig. 2.1.

In this section the plant and reference model requirements are summarized. Next, the control law that accomplishes the tracking goal in the known plant parameter case is developed. Finally, the adaptive control design for the unknown plant parameter case is described. The methods summarized here follow the notation presented in Chapter 6 of [8], but the same procedures can be found in many adaptive control texts.

2.5.1 MRAC Assumptions

Plant assumptions

i $Z_p(s)$ is a monic, asymptotically stable polynomial of degree m_p

ii Upper bound $n \geq n_p$ is known

iii Plant relative degree $n^* = n_p - m_p$ is known

iv sign(k_p) is known

Reference model assumptions

i $Z_m(s)$ and $R_m(s)$ are monic, asymptotically stable polynomials of degree q_m and $p_m \leq n$, respectively

ii Reference model relative degree $n_m^* = p_m - q_m$ is equal to n^*

2.5.2 Known Parameter Case

Along with the requirements outlined in the previous section, assume that all coefficients appearing in the plant transfer function are known. The control law can then be chosen to force the the closed-loop plant description to match the reference model. An appropriate choice for u is given by

$$u = \theta_1^{*T}\frac{\alpha(s)}{\Lambda(s)}u + \theta_2^{*T}\frac{\alpha(s)}{\Lambda(s)}y + \theta_3^{*T}y + c_0^* r \tag{2.51}$$

where $\theta_1^{*T}, \theta_2^{*T} \in \mathbb{R}^{n-1}$ and $c_0^*, \theta_3^{*T} \in \mathbb{R}$ are parameters that will be specified. Note that $\Lambda(s)$ is an asymptotically stable, monic polynomial of degree $n-1$ of the form

$$\Lambda(s) = \Lambda_0(s)Z_m(s) \tag{2.52}$$

and

$$\alpha(s) = \begin{cases} [s^{n-2}, s^{n-3}, ..., s, 1]^T & \text{for } n \geq 2 \\ 0 & \text{for } n = 1 \end{cases} \tag{2.53}$$

For the control law given in Eq. (2.51), the closed loop plant expression is given by $y = G_{cl}(s)r$ where

$$G_{cl}(s) = \frac{c_0^* k_p Z_p \Lambda^2}{\Lambda[(\Lambda - \theta_1^{*T}\alpha)R_p - k_p Z_p(\theta_2^{*T}\alpha + \theta_3^{*T}\Lambda)]}. \tag{2.54}$$

The choice of the control law parameters can be used to ensure that the "matching condition" $G_{cl}(s) = W_m(s)$, also expressed as

$$\frac{c_0^* k_p Z_p \Lambda^2}{\Lambda[(\Lambda - \theta_1^{*T}\alpha)R_p - k_p Z_p(\theta_2^{*T}\alpha + \theta_3^{*T}\Lambda)]} = k_m \frac{Z_m}{R_m}, \tag{2.55}$$

is satisfied. Note that there must be a number of pole/zero cancellations in G_{cl} to achieve matching. Each of these cancellation will occur in the open left half-plane due to the required stable structure of Z_p and Λ. After some manipulation, the matching condition can be written as

$$\left(\Lambda - \theta_1^{*T}\alpha\right) R_p - k_p Z_p \left(\theta_2^{*T}\alpha + \theta_3^{*}\Lambda\right) = Z_p \Lambda_0 R_m \tag{2.56}$$

or equivalently

$$\theta_1^{*T}\alpha R_p + k_p \left(\theta_2^{*T}\alpha + \theta_3^{*T}\Lambda\right) Z_p = \Lambda R_p - Z_p \Lambda_0 R_m \tag{2.57}$$

after the choice

$$c_0^* = \frac{k_m}{k_p} \tag{2.58}$$

has already been included. Equating coefficients based on the power of s on each side, the matrix equation

$$S\bar{\theta}^* = p \tag{2.59}$$

arises where $\theta^* = [\theta_1^{*T}, \theta_2^{*T}, \theta_3^{*T}]$, S is a matrix containing the coefficients from the left side of Eq. (2.57), and p is a vector containing the coefficients from the right side of Eq. (2.57). It can be shown, though the result is not included here, that a solution θ^* exists [8].

Moving forward, a state space formulation of the problem will facilitate error convergence analysis. The same known parameter control system is now presented in a state space framework to provide a clear approach in more complex versions of the problem. First, the control law in Eq. 2.51 can be stated as

$$u = \theta^{*T}\omega \tag{2.60}$$

where

$$\begin{aligned} \theta^* &= [\theta_1^{*T}, \theta_2^{*T}, \theta_3^{*T}, c_0^*]^T \\ \omega &= [\omega_1^T, \omega_2^T, y, r]^T \end{aligned} \tag{2.61}$$

and

$$\begin{aligned} \dot{\omega}_1 &= F\omega_1 + gu, \quad \omega_1(0) = 0 \\ \dot{\omega}_2 &= F\omega_1 + gy, \quad \omega_2(0) = 0. \end{aligned} \tag{2.62}$$

The matrix F and vector g are prescribed by the state space realization

$$(sI - F)^{-1}g = \frac{\alpha(s)}{\Lambda(s)}. \tag{2.63}$$

A composite state space system of the entire closed loop plant is obtained by augmenting the state of the plant x_p with the filter states ω_1 and ω_2 according to

$$\begin{aligned} \dot{Y}_c &= A_c Y_c + B_c c_0^* r, \quad Y_c(0) = Y_0 \\ y &= C_c^T Y_c \end{aligned} \tag{2.64}$$

where $Y_c = [x_p^T, \omega_1^T, \omega_2^T]^T$ and

$$A_c = \begin{bmatrix} A_p + B_p\theta_3^* C_p^T & B_p\theta_1^{*T} & B_p\theta_2^{*T} \\ g\theta_3^* C_p^T & F + g\theta_1^{*T} & g\theta_2^{*T} \\ gC_p^T & 0 & F \end{bmatrix} \tag{2.65}$$

$$B_c^T = \begin{bmatrix} B_p^T & g^T & 0 \end{bmatrix} \tag{2.66}$$

$$C_c^T = \begin{bmatrix} C_p^T & 0 & 0 \end{bmatrix}. \tag{2.67}$$

Thus, the s-domain representation developed previously is captured in state space by

$$\frac{y(s)}{r(s)} = C_c^T(sI - A_c)^{-1}B_c c_0^*. \tag{2.68}$$

Also, because of the matching condition previously established,

$$\begin{aligned} \frac{y(s)}{r(s)} &= W_m(s) \\ &= \frac{c_0^* k_p Z_p \Lambda^2}{\Lambda[(\Lambda - \theta_1^{*T}\alpha)R_p - k_p Z_p(\theta_2^{*T}\alpha + \theta_3^{*T}\Lambda)]} \end{aligned} \tag{2.69}$$

and therefore

$$\begin{aligned} \det(sI - A_c) &= \Lambda[(\Lambda - \theta_1^{*T}\alpha)R_p - k_p Z_p(\theta_2^{*T}\alpha + \theta_3^{*T}\Lambda)] \\ &= \Lambda Z_p \Lambda_0 R_m \end{aligned} \tag{2.70}$$

where Eq. (2.56) has been used. Since the roots of Z_p are restricted to be stable, A_c is a stable matrix.

A similar, nonminimal state space formulation of the reference model is given by

$$\begin{aligned} \dot{Y}_m &= A_c Y_m + B_c c_0^* r, \quad Y_m(0) = Y_{m0} \\ y_m &= C_c^T Y_m \end{aligned} \tag{2.71}$$

and can be used to define the composite error dynamics. Selecting $e = Y_c - Y_m$ and defining the tracking error $z = y - y_m$ results in the system

$$\begin{aligned} \dot{e} &= A_c e \\ z &= C_c^T e. \end{aligned} \tag{2.72}$$

The tracking error z will therefore converge to zero exponentially due to the stability of A_c.

2.5.3 Unknown Parameter Case

Next consider the same problem formulation and same assumptions, but permit the plant parameters to remain unknown. Additionally, restrict the discussion to plants of relative degree $n^* = 1$ and reference models that are SPR. Similar versions of the design exist for plant of higher relative degree and and MIMO systems but are not included here. The presentation of this and all further adaptive designs will be made directly in the state space framework laid out in the previous section.

An appropriate control law to obtain tracking error convergence in the unknown parameter case is given by

$$u = \theta^T \omega \tag{2.73}$$

where

$$\begin{aligned} \theta^T &= [\theta_1^T, \theta_2^T, \theta_3^T, c_0]^T \\ \omega &= [\omega_1^T, \omega_2^T, y, r]^T \end{aligned} \tag{2.74}$$

and

$$\dot{\omega}_1 = F\omega_1 + gu, \quad \omega_1(0) = 0$$
$$\dot{\omega}_2 = F\omega_1 + gy, \quad \omega_2(0) = 0. \tag{2.75}$$

The vector $\theta(t)$ contains the current estimate of the true but unknown parameters θ^*. It will be necessary to update the estimate during operation based on measured signals, and an update law $\dot{\theta}(t)$ will be prescribed during the course of the design. F and g are prescribed by any stable filter design.

A composite state space representation for the plant is given by

$$\dot{Y}_c = A_0 Y_c + B_c u, \quad Y_c(0) = Y_0$$
$$y = C_c^T Y_c \tag{2.76}$$

where $Y_c = [x_p^T, \omega_1^T, \omega_2^T]^T$ and

$$A_0 = \begin{bmatrix} A_p & 0 & 0 \\ 0 & F & 0 \\ gC_p^T & 0 & F \end{bmatrix} \tag{2.77}$$

$$B_c^T = \begin{bmatrix} B_p & g & 0 \end{bmatrix} \tag{2.78}$$

$$C_c^T = \begin{bmatrix} C_p^T & 0 & 0 \end{bmatrix}. \tag{2.79}$$

Adding and subtracting $B_c\theta^{*T}\omega$ and then absorbing all but the r-dependent portion of the positive term into $A_0 Y_c$ gives

$$\dot{Y}_c = A_c Y_c + B_c c_0^* r + B_c \left(u_p - \theta^{*T}\omega\right), \quad Y_c(0) = Y_0$$
$$y_p = C_c^T Y_c \tag{2.80}$$

where A_c is given by Eq. (2.65). The same nonminimal description for the reference model stated in Eq. (2.71) holds here as well. Again defining $e = Y_c - Y_m$ and the tracking error $z = y - y_m$ produces the error dynamics

$$\begin{aligned} \dot{e} &= A_c e + B_c \left(u_p - \theta^{*T} \omega \right) \quad e(0) = e_0 \\ z &= C_c^T e. \end{aligned} \tag{2.81}$$

Including the control law gives

$$\begin{aligned} \dot{e} &= A_c e + B_c \left(\tilde{\theta}^T \omega \right) \quad e(0) = e_0 \\ z &= C_c^T e. \end{aligned} \tag{2.82}$$

where $\tilde{\theta} = \theta(t) - \theta^*$ is the parameter error. From the reference model composite system it is evident that

$$C_c^T (sI - A_c)^{-1} \bar{B}_c = W_m(s) \tag{2.83}$$

where $\bar{B}_c = B_c c_0^*$. Thus Eq. (2.82) assures that

$$z = W_m(s) \rho^* \tilde{\theta}^T \omega \tag{2.84}$$

where $\rho^* = \frac{1}{c_0^*}$. Note that A_c is unchanged from the known parameter case and is still stable, and $W_m(s)$ is SPR by requirement.

The parameter update law is next specified through Lyapunov analysis. Select the Lyapunov-like function

$$V(\tilde{\theta}, e) = \frac{e^T P_c e}{2} + \frac{\tilde{\theta}^T \Gamma^{-1} \tilde{\theta}}{2} |\rho^*| \tag{2.85}$$

with $\Gamma = \Gamma^T > 0$ and $P_c = P_c^T > 0$ which satisfies

$$P_c A_c + A_c^T P_c = -qq^T - \nu_c L_c$$
$$P_c \bar{B}_c = C_c. \tag{2.86}$$

Here q is a vector, $L_c = L_c^T > 0$, and $v_c > 0$ as indicated by the MKY lemma. Taking the derivative,

$$\dot{V} = -\frac{e^T qq^T e}{2} - \frac{\nu_c}{2} e^T L_c e + e^T P_c \bar{B}_c \rho^* \tilde{\theta}^T \omega + \tilde{\theta}^T \Gamma^{-1} \dot{\theta} |\rho^*|. \tag{2.87}$$

Selecting the update law

$$\dot{\theta} = -\Gamma z \omega \text{sign}(\rho^*) \tag{2.88}$$

gives

$$\dot{V} = -\frac{e^T qq^T e}{2} - \frac{\nu_c}{2} e^T L_c e \leq 0 \tag{2.89}$$

since $z = C_c^T e = e^T P_c \bar{B}_c$. Signal chasing analysis and Barbalat's Lemma assures that $\lim_{t \to \infty} z(t) = 0$.

2.6 Nonminimum Phase Systems

In the context of continuous-time linear plants, which are the structure of concern in this dissertation, a nonminimum phase system can be defined as one which has one or more zeros in the closed right half of the complex plane (i.e. $Re[z] \geq 0$). Such zeros are called nonminimum phase zeros or unstable zeros. Equivalently, a nonminimum phase system is one whose inverse in unstable. A nonminimum phase system will also have a larger phase contribution than a minimum phase system with the same magnitude response and

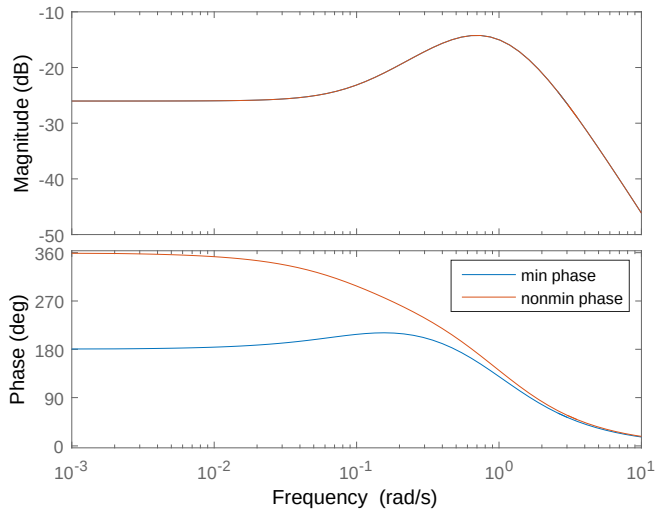

Figure 2.2: Example of larger phase contribution of nonminimum phase system vs. its minimum phase counterpart

can potentially cause the transient response to move in the opposite direction of the ultimate characterization.

Consider a the following two systems as a motivating example of nonminimum phase characteristics:

$$G_1(s) = \frac{-0.5(s+0.1)}{(s+1)^3} \tag{2.90}$$

and

$$G_2(s) = \frac{-0.5(s-0.1)}{(s+1)^3}. \tag{2.91}$$

Here clearly only $G_2(s)$ is nonminimum phase though both $G_1(s)$ and $G_2(s)$ have the same magnitude. The Bode plot of both system, shown in Fig. 2.2, confirms the claims. The so-called "wrong way" transient behavior of some

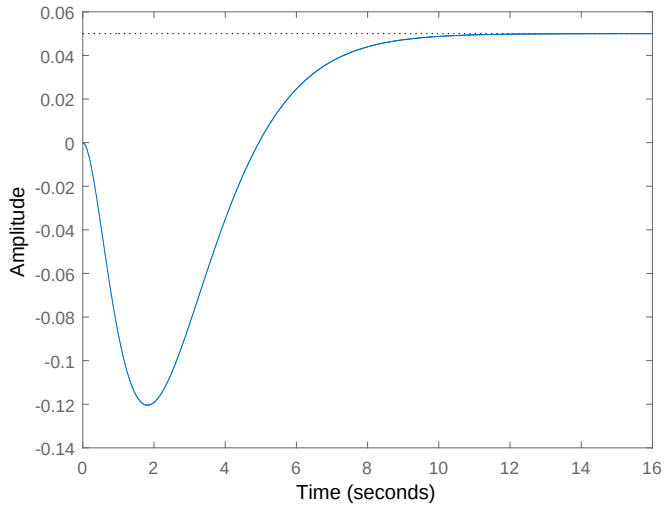

Figure 2.3: Example of nonminimum phase system displaying significant undershoot during unit step response

nonminimum phase systems is also present in the example system. Consider the step response of $G_2(s)$ shown in Fig. 2.3. The system initially displays significant undershoot before heading in the correct direction. Undershoot such as that seen here can be problematic in many practical applications, especially when humans are part of the feedback loop.

From an engineering standpoint nonminimum phase system often arise when sensor and actuators are non-collocated. More generally, they occur when forces act on the system at locations other than those being monitored. Tail-actuated missiles and aircraft pitch dynamics are common examples of this situation. A more in-depth discussion of aircraft nonminimum phase behavior is provided in the following sections.

2.6.1 Aircraft Nonminimum Phase Zero Interpretations

Although nonminimum phase zeros present mathematical difficulties for control design, their presence in an aircraft model has physical implications that impact handling qualities. Generally speaking, an input to output relationship that has nonminimum phase zeros can exhibit an initial response whose direction is different from the direction of the final behavior [52]. Note that this reversal may not alway be present depending on the number and arrangement of nonminimum phase zeros [53]. Several of the commonly analyzed aircraft input to output relationships that contain both nonminimum phase zeros and display the characteristic direction reversal are summarized subsequently.

To simplify the discussion consider the latitude and longitude decoupled, linearized equations for rigid body motion of a standard aircraft with elevator, aileron, and rudder control surfaces. A summary of these equations and a discussion of the assumptions used to obtain them can be found in many textbooks (for example, see Ch. 2 of [52]). Further details are omitted here as the discussion will be qualitative. Transfer functions relating control inputs to relevant outputs can be obtained from the equations facilitating comparison between pole/zero representation and observed physical behaviors.

First consider the simplified longitudinal dynamics and the resulting elevator to pitch rate transfer function. More accurately for control system discussion, consider the elevator to normal acceleration transfer function. Here the normal acceleration is a measurement provided by a vertical axis ac-

celerometer placed somewhere forward of the center of gravity along the line of symmetry. This transfer function will contain nonminimum phase zeros. The presence of the nonminimum phase zeros has obvious physical interpretation when considering the impact of elevator use [52]. For example, a trailing edge up deflection of the elevator generates an intuitive upward normal acceleration. This action also generates a less obvious downward force on the tail. The aircraft's center of gravity and thus the normal acceleration can drop briefly due to the downward force before increasing in a clear display of nonminimum phase behavior. Note that the nonminimum phase zero location in the transfer function and the perceived nonminimum phase effect varies based on where the normal acceleration is monitored. Correspondingly, a pilot may or may not feel the nonminimum phase effect depending on cockpit location.

Next consider the simplified lateral dynamics and the aileron to roll rate transfer function. Here, a nonminimum phase zero appears near the origin. The physical manifestation of this zero is apparent as the aircraft rolls [52]: The aircraft sideslips due to gravity and, if it has positive roll stiffness, it initially rolls in the opposite direction than intended. The rudder to roll rate transfer function also posses a nonminimum phase zero associated with the same rolling behavior, but contains a second nonminimum phase zero associated with rudder deflection. A positive rudder deflection produces both a positive rolling moment and negative yawing moment. The negative yawing moment leads to positive sideslip and, again if the aircraft has positive roll stiffness, results in a negative rolling moment that competes with the rudder's

positive rolling moment.

Several structural modification to the aircraft can alter the presence of the nonminimum phase zeros previously mentioned. For example, canards can be mounted forward of the aircraft's center of mass to mitigate the nonminimum phase behavior associated with elevator use since their deflection produces a pitch up moment that also generates positive lift [54]. A tailless aircraft may also avoid the pitch nonminimum phase behavior for appropriately designed and placed wing control surfaces (see [55] for a specific example). However, note that such structural changes impart other significant changes to aircraft handling which are not discussed here.

2.6.2 Nonminimum Phase Zeros from Non-collocation

While the previous discussion focused on the nonminimum phase zeros associated with the aircraft's rigid body dynamics, it is important to note that additional nonminimum phase behavior arises when considering the aeroelasticity of a flexible aircraft structure. The primary source of nonminimum phase zeros in this context is non-collocation of sensors and actuators. In general, a lightly damped flexible structure with collocated sensors and actuators will result in alternating left half plane poles and zeros in the vicinity of the imaginary axis [56]. However non-collocated sensors and actuators can cause the zeros to migrate from their collocated position, potentially resulting in a nonminimum phase system. Also note that the zero migration can result in pole/zero pairs that flip their ordering. Flipped pole/zero pairs result in a

root locus plot that indicates a significant portion of gain selections leads to an unstable system.

To facilitate a straightforward discussion, consider a beam with force actuator and displacement sensor. Each of the flexible modes considered introduces a left half plane pole/zero pair near the imaginary axis. As the sensor is moved along the beam away from the actuator location the zeros migrate out from their collocated location to a position of increased magnitude [56]. For more complex beam-like systems the migrating zeros can move into the right half plane in response to increasing sensor and actuator separation distance. At a certain separation distance the migrating zeros can reach infinity and return from $\pm\infty$ on the real axis and move in towards the origin [57,58]. Thus non-collocated sensors and actuators have the potential to result in nonminimum phase system descriptions, especially when the sensors and actuators are significantly displaced.

As an example of the zero migration due to non-collocation, consider a pole/zero map of a reduced linear model for the experimental flexible wing aircraft that is the subject of Chapters 4, 6, and 7. An input/output diagram of the aircraft is shown in Fig. 2.4 including the eight wing flaps and two body flaps that are used for control input and a variety of accelerometer locations used for feedback. The map is shown in Fig. 2.5 and contains the pole and zero locations from multiple input/output pairs at flight conditions just beyond the body freedom flutter boundary. Specifically, the poles and zeros from the SISO transfer function relating the nearly collocated sensor ACC RR and

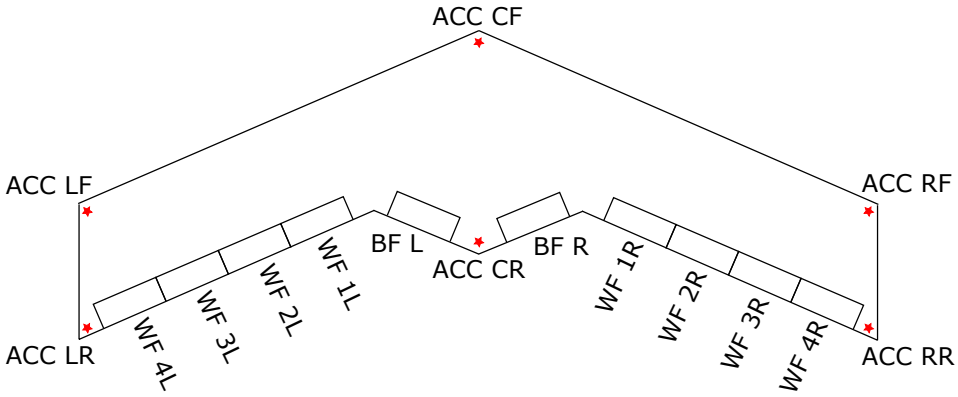

Figure 2.4: Input and output diagram for the experimental flexible wing aircraft

actuator WF 4R are compared to those from increasingly removed actuators WF 3R, WF 2R, and WF 1R. The map clearly shows one pair of zeros near the imaginary axis that migrates out and into the right half plane as sensor and actuator distance increases. Another pair of zeros moves in towards the origin with increasing distance, though the behavior is most clearly seen in the motion of the right half plane zero. From the map it is clear that all of the sensor and actuator arrangements considered in this example result in a nonminimum phase model.

2.6.3 Technical Issues with MRAC

In Section 2.5 it was demonstrated that the in the SISO ideal case the MRAC objective is achieved through satisfaction of the matching condition

$$\frac{c_0^* k_p Z_p(s)\Lambda^2(s)}{\Lambda(s)\left[\left(\Lambda(s)-\theta_1^{*T}\alpha(s)\right)R_p(s)-k_p Z_p(s)\left(\theta_2^{*T}\alpha(s)+\theta_3^{*T}\Lambda(s)\right)\right]}=k_m\frac{Z_m(s)}{R_m(s)}. \tag{2.92}$$

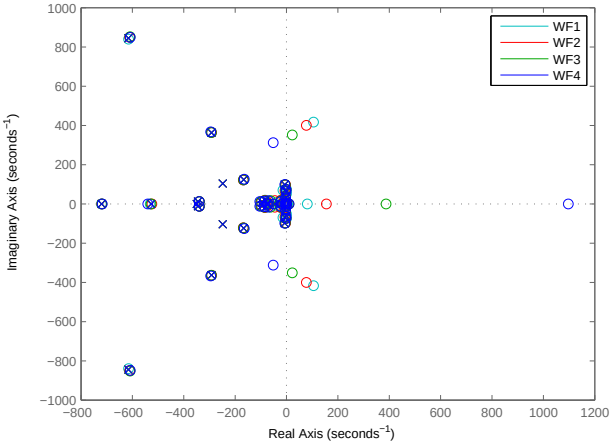

Figure 2.5: Pole/zero maps displaying migrating zeros in response to increasing sensor and actuator non-collocation, utilizes flexible aircraft transfer functions relating each of the four right wing flaps to the right aft wing tip accelerometer

The condition implies that the closed-loop poles of the system are placed at the roots of the polynomial

$$Z_p(s)\Lambda_0(s)R_m(s). \tag{2.93}$$

If the plant to be controlled is nonminimum phase then $Z_p(s)$ will have unstable roots and the closed-loop poles would be placed unstable locations. As this is unacceptable, one apparent solution would be to copy the unstable zeros from the plant and include them as zeros in the reference model. Say that the plant transfer function is given by

$$y = k_p \frac{Z_{p,s}(s)Z_{p,u}(s)}{R_p(s)}u \tag{2.94}$$

where $Z_{p,s}(s)$ contains the stable zeros and $Z_{p,u}(s)$ the unstable zeros. Assume that $Z_{p,u}(s)$ is known (even though the rest of the plant is unknown) and

included in the reference model so that its transfer function is given by

$$y_m = k_m \frac{Z_m(s) Z_{p,u}(s)}{R_m(s)} r. \tag{2.95}$$

After some manipulation the matching condition arising from use of these transfer functions, the previously established design choice $\Lambda(s) = \Lambda_0(s) Z_m(s)$, and $c_0^* = \frac{k_m}{k_p}$ is

$$\left(\Lambda(s) - \theta_1^{*T} \alpha(s)\right) R_p(s) - k_p Z_{p,s}(s) Z_{p,u}(s) \left(\theta_2^{*T} \alpha(s) + \theta_3^{*T} \Lambda(s)\right) = Z_{p,s}(s) \Lambda_0(s) R_m(s) \tag{2.96}$$

The closed-loop poles would then be placed at the roots of the stable polynomial

$$Z_{p,s}(s) \Lambda_0(s) R_m(s). \tag{2.97}$$

Although inclusion of the unstable zeros improves the matching condition, additional problems arise when moving to the case of unknown plant parameters and attempting to prescribe a parameter update law. Previously the update law was determined through the use of a Lyapunov function and the need to cancel undesirable terms in its derivative. The procedure required that the reference model be SPR so that the MKY Lemma could be used. Here, the reference model is no longer SPR because of its unstable zeros, and the parameter update law must be obtained in another way. However, suitable options do exist such as gradient or least square-based update laws (see Chapter 6 of [8]).

The larger problem with inclusion of the unstable zeros is that the now unstable reference model breaks existing error convergence proof procedures. As the presence of these zeros in the reference model forms the basis of the MRAC procedure for nonminimum phase systems discussed in the dissertation, demonstrations of how two established proofs are disrupted are provided in the appendices. Specifically, Appendix A features the dual swapping lemma approach in [8]. Appendix B considers a continuous-time version of the discrete-time proof used in [20]. Both versions are presented in the context of the problem formulation laid out in Chapter 5, and the reader will be better equipped to follow the discussion after surveying the design contained therein.

2.7 Aeroservoelastic Modeling

The ZAERO software package is used throughout the dissertation to produce aeroservoelastic state space models [59]. While many of the general model creation techniques are familiar to controls engineers, the aeroelastic modeling portion of the process should be summarized for clarity.

2.7.1 Aeroelastic Background

The aeroelastic state equations of motion are given by

$$\bar{M}\ddot{x}(t) + \bar{K}x(t) = F(t) \tag{2.98}$$

where $x(t)$ represents structural deformation, $\bar{M}$ and $\bar{K}$ are mass and stiffness matrices obtained using the structural finite element model, and $F(t)$ contains

aerodynamic forces. The force term can be decomposed as

$$F(t) = F_a(x(t)) + F_e(t) \tag{2.99}$$

where $F_a(x(t))$ represents aerodynamic forces caused by structural deformation and $F_e(t)$ represents external forces. Determination of $F_a(x(t))$ is typically based on numerical calculations related to the unsteady aerodynamic forces and will be discussed in further detail later. Ignoring external forces the system can be written as

$$\bar{M}\ddot{x}(t) + \bar{K}x(t) - F_a(x(t)) = 0 \tag{2.100}$$

making it clear that self-excitation is possible. For an aircraft this unstable behavior is known as flutter and the flight conditions that produce such excitation must be identified and avoided.

Practical flutter analysis is carried out by linearizing Eq. (2.100) and turning the stability question into an eigenvalue problem. The linear system permits formulation of a transfer function from $F_a(x(t))$ to $x(t)$ given by

$$F_a(x(s)) = q_\infty \bar{H}\left(\frac{sL}{V}\right) x(s). \tag{2.101}$$

Here q_∞ is the dynamic pressure, $L = \frac{c}{2}$ is the reference length using the reference chord c, and V is the far field flow velocity. The Laplace domain version of (2.100) is thus given by

$$\left[s^2\bar{M} + \bar{K} - q_\infty \bar{H}\left(\frac{sL}{V}\right)\right] x(s) = 0. \tag{2.102}$$

Solving the eigenvalue problem using Eq. (2.102) would be computationally taxing as the structural model typically contains many degrees of freedom.

Instead, the modal approached is used to reduce the order of the system before proceeding. The displacement is expressed as

$$x = \Phi q. \tag{2.103}$$

Φ is a matrix with columns that each describe one of the first few natural modes and q contains the modal coordinates. The modal form of Eq. (2.102) is given by

$$\left[s^2 M + K - q_\infty Q\left(\frac{sL}{V}\right) \right] q = 0 \tag{2.104}$$

where the modal mass matrix, modal stiffness matrix, and generalized aerodynamic forces (GAF) matrix are defined as

$$\begin{aligned} M &= \Phi^T \bar{M} \Phi \\ K &= \Phi^T \bar{K} \Phi \\ Q\left(\frac{sL}{V}\right) &= \Phi^T \bar{H}\left(\frac{sL}{V}\right) \Phi. \end{aligned} \tag{2.105}$$

Eq. (2.104) results in a much smaller eigenvalue problem and is regarded as the classical flutter matrix equation.

The ability to conduct flutter analysis using Eq. (2.104) is tied to the ability to determine the aerodynamic transfer function. This difficult task requires expression of the unsteady aerodynamics in the frequency domain and is ultimately achieved by assuming simple harmonic motion of the elastic structure. The aerodynamic transfer function is then expressed as a matrix equation using information from the approximated unsteady aerodynamic forces. The

matrix used in this expression is called the Aerodynamic Influence Coefficient (AIC) matrix, and its calculation is a primary function of ZAERO.

In the subsonic regime relevant to the experimental aircraft considered in the dissertation, the AIC matrices are ultimately generated by solving integral equations that arise from the unsteady linearized small-disturbance equations. The aircraft is discretized into small panels, termed aerodynamic boxes, each of which requires solution of an elementary integral equation. Each aerodynamic box contains a control point where boundary conditions are applied and, once solutions of the elementary integrals are tabulated, the AIC matrix relating the aerodynamic influence of the aerodynamic boxes to control points can be formed. Ultimately, the relationship between structural deformation and aerodynamic forces utilizes the AIC matrix and can be stated as

$$F_h = q_\infty[\text{AIC}(ik)]h \tag{2.106}$$

where h is the structural deformation defined at the aerodynamic boxes and F_h is the aerodynamic force at the aerodynamic boxes as a result of h.

However, an AIC matrix formed using the panel method is not yet ready for use in place of the GAF matrix of Eq. (2.104). First, the integral equations and resulting AIC matrix are formulated in terms of reduced frequency k. The reduced frequency is given by

$$k = \frac{\omega L}{V} \tag{2.107}$$

where ω is the frequency associated with the simple harmonic motion assumption. Expression as a function of the Laplace variable will require a rational

function approximation (RFA) that will be discussed in the next section. Second, the AIC matrix is formulated based on the panel representation of the aircraft which is likely very different from the structural finite element model. A spline matrix G must be used to relate displacement and forces in terms of the structural grid points (G–set) to those in terms of the aerodynamic control points (K–set). Specifically, deformations are translated from the panel to structural model according to

$$h = Gx \tag{2.108}$$

and forces according to

$$F_a = G^T F_h. \tag{2.109}$$

Combining Eqs. (2.106), (2.108), and (2.109) leads to

$$F_a = q_\infty G^T [\text{AIC}(ik)] G x \tag{2.110}$$

Then, comparing Eqs. (2.101) and (2.110) leads to the realization that

$$Q(ik) = \Phi^T G^T [\text{AIC}(ik)] G \Phi \tag{2.111}$$

where the modal approach of Eq. (2.105) has been used. This final equation expresses the GAFs (in the k domain) in terms of the AIC matrix and will be converted to the Laplace domain for use in the aeroservoelastic equations of motion.

2.7.2 Aeroservoelastic Equations of Motion

It is convenient to couple the aeroelastic dynamics described in the previous section with the control system for controller design. Changing notation

slightly and adding a damping term, consider the coupled equations of motion given by

$$M_{hh}\ddot{\xi} + C_{hh}\dot{\xi} + K_{hh}\xi + M_{hc}\ddot{\delta} = q_\infty Q_{hh}(ik)\xi + q_\infty Q_{hc}(ik)\delta \tag{2.112}$$

where ξ now refers to the modal coordinates and δ refers to the control surface deflections. The subscript h indicates relationship to the structural modes while subscript c indicates the relationship to the control surfaces. Additionally, note that M_{hh}, C_{hh}, and K_{hh} are the modal mass, damping, and stiffness matrices. The matrix M_{hc} is given by

$$M_{hc} = \phi_h^T M_{gg} \phi_c \tag{2.113}$$

where M_{gg} is the G–set mass matrix. The structural modes are contained in ϕ_h and the control surface modes in ϕ_c. The GAFs are split into those due to the structural modes

$$Q_{hh}(ik) = \phi_h^T G^T [\text{AIC}(ik)] G \phi_h \tag{2.114}$$

and those due to the control surfaces

$$Q_{hc}(ik) = \phi_h^T G^T [\text{AIC}(ik)] G \phi_c \tag{2.115}$$

where the AIC matrix relationship from Eq. (2.111) has been used.

Next, an RFA is used to convert the GAFs from the reduced frequency domain to the Laplace domain. The RFA expresses each of the GAFs as a ratio of polynomials according to the general form

$$\tilde{Q}(s) = A_0 + \frac{L}{V}A_1 s + \frac{L^2}{V^2}A_2 s^2 + D\left(sI - \frac{V}{L}R\right)^{-1} Es. \tag{2.116}$$

An analytic continuation argument using $\frac{L}{V}s = g + ik$ permits swapping of $\frac{L}{V}s$ and ik such that

$$\tilde{Q}(ik) = A_0 + A_1(ik) + A_2(ik)^2 + D\left((ik)I - L)R\right)^{-1} E(ik). \tag{2.117}$$

The coefficients in this equation are determined through a least squares fitting process that attempts to match the GAF calculated from the AIC matrix at a given reduced frequency k. Here, Roger's method is used for the RFA which has the specific form

$$\tilde{Q}(ik) = A_0 + A_1(ik) + A_2(ik)^2 + \sum_{j=1}^{N_{\text{lag}}} \frac{ik}{ik + \gamma_j} C_j. \tag{2.118}$$

N_{lag} indicates the number of aerodynamic lag states. The approximation theoretically improves as more aerodynamic lag states are included, although the size of the overall state space model for the system also grows. Eq. (2.118) implies that each of the user–selectable roots γ in the summation are repeated for each of the N_h modes. This leads to the following coefficient expressions for the general form in Eq. (2.117):

$$D = \begin{bmatrix} I_{N_h} & I_{N_h} & \dots & I_{N_h} \end{bmatrix} \tag{2.119}$$

$$\bar{R} = \text{diag}\left(\gamma_j\right), \quad R = -\begin{bmatrix} \bar{R}_1 & 0 & 0 & 0 \\ 0 & \bar{R}_2 & 0 & 0 \\ & & \ddots & \\ 0 & 0 & 0 & \bar{R}_{N_h} \end{bmatrix} \tag{2.120}$$

$$E = \begin{bmatrix} C_1 \\ C_2 \\ \vdots \\ C_{N_{\text{lag}}} \end{bmatrix}. \tag{2.121}$$

After the coefficients have been determined, $\tilde{Q}(s)$ can be recovered from $\tilde{Q}(ik)$. Introducing the partitions

$$\tilde{Q}(s) = \begin{bmatrix} Q_{hh}(s) \\ Q_{hc}(s) \end{bmatrix} \quad A_i = \begin{bmatrix} A_{hh,i} \\ A_{hc,i} \end{bmatrix} \quad E = \begin{bmatrix} E_h \\ E_c \end{bmatrix} \tag{2.122}$$

for $i = 0, 1, 2$ allows the equations of motion from Eq. (2.112) to be expressed as

$$M_{hh}\ddot{\xi} + C_{hh}\dot{\xi} + K_{hh}\xi + M_{hc}\ddot{\delta} = q_\infty Q_{hh}(s)\xi + q_\infty Q_{hc}(s)\delta. \tag{2.123}$$

2.7.3 State Space Model

An LTI state space model can be constructed by combining the aeroservoelastic equations of motion from with a dynamic model of the actuators. Rigid body dynamics can also be incorporated into the state space description but are omitted here for simplicity.

First convert the aeroservoelastic equations of motion given in Eq. (2.123) to a state space representation. Using the partitions defined in Eq. (2.122) and the RFA expression in Eq. (2.116) gives equations of motion of the form

$$\begin{aligned} M_{hh}\ddot{\xi} + C_{hh}\dot{\xi} + K_{hh}\xi + M_{hc}\ddot{\delta} =& q_\infty \left(A_{hh_0}\xi + \frac{L}{V}A_{hh_1}\dot{\xi} + \frac{L^2}{V^2}A_{hh_2}\ddot{\xi} \right) \\ &+ q_\infty \left(A_{hc_0}\delta + \frac{L}{V}A_{hc_1}\dot{\delta} + \frac{L^2}{V^2}A_{hc_2}\ddot{\delta} \right) + q_\infty D x_a. \end{aligned} \tag{2.124}$$

Here, the quantity x_a is defined as

$$x_a = \left(sI - \frac{V}{L}R \right)^{-1} (E_h\xi + E_c\delta)\, s \tag{2.125}$$

for convenience. The state space form of the aeroservoelastic dynamics is given by

$$\dot{x}_{ae} = A_{ae}x_{ae} + B_{ae}u_{ae} \tag{2.126}$$

where

$$x_{ae} = [\xi^T \;\; \dot{\xi}^T \;\; x_a^T]^T \tag{2.127}$$

and

$$u_{ae} = [\delta^T \;\; \dot{\delta}^T \;\; \ddot{\delta}^T]^T. \tag{2.128}$$

The matrices are detailed in the following equations.

$$A_{ae} = \begin{bmatrix} 0 & I & 0 \\ -\bar{M}^{-1}\left(K_{hh} - q_\infty A_{hh_0}\right) & -\bar{M}^{-1}\left(C_{hh} - q_\infty \frac{L}{V} A_{hh_1}\right) & q_\infty \bar{M}^{-1} D \\ 0 & E_h & \frac{V}{L} R \end{bmatrix} \tag{2.129}$$

$$B_{ae} = \begin{bmatrix} 0 & 0 & 0 \\ q_\infty \bar{M}^{-1} A_{hc_0} & q_\infty \frac{L}{V} \bar{M}^{-1} A_{hc_1} & -\bar{M}^{-1}\left(M_{hc} - \frac{q_\infty L^2}{V^2} A_{hc_2}\right) \\ 0 & E_c & 0 \end{bmatrix} \tag{2.130}$$

$$\bar{M} = M_{hh} - \frac{q_\infty L^2}{V^2} A_{hh_2} \tag{2.131}$$

The output equation is of the form

$$y_{ae} = C_{ae}x_{ae} + D_{ae}u_{ae}, \tag{2.132}$$

but the matrix structure varies based on the type of sensor desired. However, accelerometers are primarily selected for use here meaning that for each of the $i = 1...p$ sensors the reading can be extracted from the state space

representation as

$$y_{ae,i} = -\phi_{h,i}\left[\bar{M}^{-1}K_{hh} - q_\infty A_{hh,0} \quad \bar{M}^{-1}\left(C_{hh} - q_\infty \tfrac{L}{V} A_{hh,1}\right) \quad -q_\infty \bar{M}^{-1} D\right] x_{ae}$$
$$- \phi_{c,i}\left[q_\infty \bar{M}^{-1} A_{hc,0} \quad q_\infty \tfrac{L}{V}\bar{M}^{-1} \quad \bar{M}^{-1}\left(M_{hc} - \tfrac{q_\infty L^2}{V^2} A_{hc,2}\right)\right] u_{ae}. \quad (2.133)$$

Note that $\phi_{h,i}$ is the natural mode displacement at the i^{th} sensor location and $\phi_{c,i}$ the corresponding control surface mode displacement. The matrices C_{ae} and D_{ae} are formed by stacking the coefficient matrices in Eq. (2.133) for each of the desired sensors according to the vectors x_{ae} and u_{ae}.

Next consider the actuator dynamics. Each of the $i = 1...m$ control surfaces has 3^{rd} order dynamics given by the transfer function from command u_{act_i} to deflection δ_i as

$$\delta_i = \frac{g_{0_i}}{s^3 + g_{2_i}s^2 + g_{1_i}s + g_{0_i}} u_{\text{act}_i}. \quad (2.134)$$

Collecting all the actuators permits the state space expression

$$\dot{x}_{\text{act}} = A_{\text{act}} x_{\text{act}} + B_{\text{act}} u_{\text{act}} \quad (2.135)$$

where

$$u_{\text{act}} = [u_{\text{act}_1} ... u_{\text{act}_m}]^T \quad (2.136)$$

and

$$x_{\text{act}} = [\delta_1 ... \delta_m \;\; \dot{\delta}_1 ... \dot{\delta}_m \;\; \ddot{\delta}_1 ... \ddot{\delta}_m]^T$$
$$= [\delta^T \;\; \dot{\delta}^T \;\; \ddot{\delta}^T]. \quad (2.137)$$

The matrices are given by

$$A_{\text{act}} = \begin{bmatrix} 0 & I & 0 \\ 0 & 0 & I \\ G_0 & G_1 & G_2 \end{bmatrix} \tag{2.138}$$

$$B_{\text{act}} = \begin{bmatrix} 0 \\ 0 \\ \bar{G}_0 \end{bmatrix} \tag{2.139}$$

where

$$\begin{aligned} G_0 &= \text{diag}(-g_{0_i}) \\ G_1 &= \text{diag}(-g_{1_i}) \\ G_2 &= \text{diag}(-g_{2_i}) \end{aligned} \tag{2.140}$$

and

$$\bar{G}_0 = [g_{0_1} ... g_{0_m}]^T. \tag{2.141}$$

To assemble the full state space system, note from Eqs. (2.128) and (2.137) that $u_{ae} = x_{\text{act}}$. A composite state vector can thus be defined as

$$\begin{aligned} x_p &= [x_{ae}^T \;\; x_{\text{act}}^T]^T \\ &= [\xi \;\; \dot{\xi} \;\; x_a \;\; \delta \;\; \dot{\delta} \;\; \ddot{\delta}]^T. \end{aligned} \tag{2.142}$$

The corresponding system is given by

$$\begin{aligned} \dot{x}_p &= A_p x_p + B_p u_{\text{act}} \\ y &= C_p x_p \end{aligned} \tag{2.143}$$

where the matrices are defined in block form as

$$A_p = \begin{bmatrix} A_{ae} & B_{ae} \\ 0 & A_{\text{act}} \end{bmatrix} \quad B_p = \begin{bmatrix} 0 \\ B_{\text{act}} \end{bmatrix} \quad C_p = \begin{bmatrix} C_{ae} & D_{ae} \end{bmatrix}. \tag{2.144}$$

Chapter 3

Partitioned Model Reference Adaptive Control

The development of the two-part, or partitioned, MRAC scheme is presented in this chapter. The partitioned design assumes a linear, multi-input plant description and combines the use of two control laws: a nonadaptive nominal control law and an adaptive delta control law. The nominal control law should provide acceptable performance when used on its own. The delta control law is intended to be used in addition to the nominal law and seeks to improve upon the performance of the nominal law alone. Simultaneous use of the two control laws is facilitated by partitioning the control surfaces available to each law while permitting the measurements fed back to be used by both laws. A general block diagram of the proposed design is provided in Fig. 3.1.

As an example of the partitioned structure consider a linear plant with four inputs and two outputs described by the transfer function relationship

$$\begin{bmatrix} y_1 \\ y_2 \end{bmatrix} = \begin{bmatrix} G_{11}(s) & G_{12}(s) & G_{13}(s) & G_{14}(s) \\ G_{21}(s) & G_{22}(s) & G_{23}(s) & G_{24}(s) \end{bmatrix} \begin{bmatrix} u_1 \\ u_2 \\ u_3 \\ u_4 \end{bmatrix}. \tag{3.1}$$

Inputs u_1 and u_2 are assigned to the nominal control law and u_3 and u_4 to the delta control law. Both outputs are assigned to both control laws. Output y_1

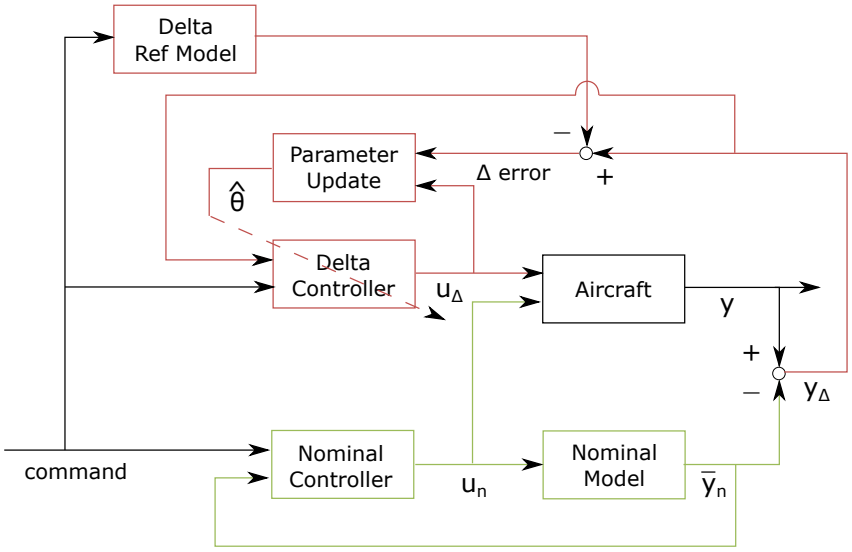

Figure 3.1: Block diagram for partitioned MRAC design, nominal system in green (bottom), delta system in red (top)

thus consists of two independent portions, one resulting from each control law:

$$\begin{aligned} y_1 &= G_{11}(s)u_1 + G_{12}(s)u_2 + G_{13}(s)u_3 + G_{14}(s)u_4 \\ &= G_{1,n}(s)u_n + G_{1,\Delta}(s)u_\Delta \\ &= y_{1,n} + y_{1,\Delta} \end{aligned} \tag{3.2}$$

where $G_{1,n} = [G_{11} \;\; G_{12}]$, $G_{1,\Delta} = [G_{13} \;\; G_{14}]$, $u_n = [u_1 \;\; u_2]^T$, and $u_\Delta = [u_3 \;\; u_4]^T$. A similar result holds for y_2. Note that without further specification concerning the control laws this type of partitioned structure can facilitate any number of outputs and two or more inputs. However the delta law to be used here will require selections that have the same number of inputs and outputs (as is necessary for traditional MRAC designs).

Within this framework the inputs and outputs associated with the nom-

inal portion of the system and the delta portion of the system are user-choice. The assignments greatly impact the performance of the proposed design and must be thoughtfully selected when applied to a physical system. As an example, consider a different input and output division for the same generic 4×2 system in Eq. (3.1). Allow u_1, u_2, and u_3 to be assigned to the nominal control law and only u_4 assigned to the delta law. Due to the anticipated MRAC design for the delta system, assignment of only one delta output is permissible because of the square structure required. Arbitrarily selecting the delta output to be y_1 means that this signal can be partitioned into nominal and delta components as in Eq. (3.2). However for y_2 there is a portion of the signal that is "unmanaged":

$$\begin{aligned} y_2 &= G_{21}(s)u_1 + G_{22}(s)u_2 + G_{23}(s)u_3 + G_{24}(s)u_4 \\ &= G_{2,n}(s)u_n + G_x(s)u_\Delta \\ &= y_{2,n} + y_x. \end{aligned} \tag{3.3}$$

Here $G_x = G_{24}$ and refers to the unmanaged dynamics while y_x is the corresponding unmanaged portion of the output signal. Without the delta law, y_x would not be present and y_2 could be fully controlled by the nominal control law. Use of the delta law however has the potential to disrupt y_2's behavior in this scenario. If a similar type of input and output arrangement is selected for implementation then any output signal contains an unmanaged component must be monitored to ensure that the delta control law does not cause unacceptable behavior.

The input splitting feature permits the general statement that $y = y_n + y_\Delta$. In order to implement MRAC on only the delta portion of the system there must be a way to recover y_Δ from the measured output y. This is accomplished by applying the nominal control to a known model of the nominal portion of the system $\bar{G}_n(s)$. The nominal output y_n is replaced by the quantity $\bar{y}_n$ that is determined by applying the nominal controller to the nominal model, i.e. $\bar{y}_n = \bar{G}_n(s)u_n$. The delta output used for feedback in the adaptive system is thus recovered as $y_\Delta = y - \bar{y}_n$. Figure 3.1 illustrates this feature in the lower feedback loop.

Note that this structure corresponds to a shifted version of MRAC in some ways. Instead of using a full reference model, the reference model is shifted by subtraction of the nominal model to create the delta reference model. The adaptive control law then attempts to match the delta reference signal. Correspondingly, many of the typical MRAC implementation requirements fall on the delta portion of the system.

3.1 Nominal Control Law

The transfer function representation of the open-loop nominal system is given as $y_n = G_n(s)u_n$. An estimated model of nominal system is given by

$$\bar{y}_n = \bar{G}_n(s)u_n. \tag{3.4}$$

Any type of control that permits the closed-loop nominal model to be expressed as

$$\bar{y}_n = \bar{W}_n(s)r \tag{3.5}$$

can be used. Although, the nominal control law should ideally provide acceptable performance when used by itself to control the plant. This structure is intentionally non-specific so that a variety of control methodologies can be used for the nominal law. Further, this structure accommodates the existing experimental aircraft controller which will used in later simulations.

3.2 Delta Control Law

A model-based control formulation for the delta law is appropriate due to the need to operate the delta law in conjunction with a nominal law. The use of a user-selected reference model $y_r = W_r(s)r$ in the design permits the closed-loop nominal model $\bar{W}_n(s)$ to subtracted away leaving a remainder that serves as the delta reference model $W_\Delta(s)$. To demonstrate, note that the goal for a model-based design is to use the control system to bring the output of the plant y to match the output of a reference model y_r. It was noted previously that use of a nominal model permits the expression $y = y_\Delta + \bar{y}_n$. Ideally this expression should become $y_r = y_{\Delta_r} + \bar{y}_n$, where y_{Δ_r} is the output of the delta reference model, through the use of the control system. Substituting the reference model and nominal model expressions then solving for y_{Δ_r} gives

$$y_{\Delta,r} = \left[W_r(s) - \bar{W}_n(s)\right] r. \tag{3.6}$$

Therefore the delta reference model is

$$W_\Delta(s) = W_r(s) - \bar{W}_n(s). \tag{3.7}$$

It is clear that there are input/output size considerations that must be satisfied in order to form the delta reference model. It may be necessary to leave some outputs unmanaged by the delta system as previously discussed. Also, note that in practice it may more useful to instead design the delta reference model directly and recover the corresponding full reference model.

Additionally, note that for any delta output the goal is no longer to track the original command. The partitioned MRAC design means that it is the full reference model $W_r(s)$ whose output y_r should be tracked instead. Further, y_r has both a nominal and delta contribution

$$\begin{aligned} y_r &= y_{\Delta_r} + \bar{y}_n \\ &= \left[W_\Delta(s) + \bar{W}_n(s)\right] r \end{aligned} \tag{3.8}$$

and the delta system is only to track the y_{Δ_r} portion. This is especially important to keep in mind when designing the nominal controller as $\bar{y}_n$ is only part of the total value that will be tracked. Since the full reference model is constructed from $\bar{W}_n(s)$ and $W_\Delta(s)$, two items that the user has some freedom to select, there is an inherent ability to distribute the how much of the y_r tracking task is distributed between the nominal and delta systems. For example, the user can easily alter the design of the delta reference model and modulate the size of y_Δ to be a larger or smaller percentage of the tracked value.

Chapter 4

Parallel Feedforward Compensator

The partitioned design is first used in conjunction with the parallel feedforward compensator approach to MRAC. The PFC method can be used to accommodate nonminimum phase plants in the MRAC scheme by introducing a user–designed system in parallel with the plant to create the appearance of a minimum phase system. This straightforward solution to the problem of MRAC for nonminimum phase systems has been called "simple adaptive control" and has been applied to a diverse range of applications [19]. While undoubtedly useful, the PFC approach does has several potential shortcomings that will be highlighted in the subsequent discussion.

The functionality of the PFC–based partitioned design is explored in this chapter through application to aeroservoelastic control of an experimental, flexible wing aircraft. Nonminimum phase, linear models of the aircraft are produced to simulate performance of the design and can be stable or unstable depending on flight condition. Discussion of appropriate actuator and sensor assignments for the nominal and delta control laws is provided, as well and details regarding aeroservoelastic model generation useful for the purpose of control design.

The design is specified beginning with system level requirements. The general structure of the nominal law and extensive detail of the delta law are the provided. PFC nonminimum phase adaptations are discussed. An overview of the flexible aircraft is provided and state space modeling procedures are outlined. Finally, simulation results of the flexible motion behavior are provided.

4.1 PFC MRAC Design Details

Since the partitioned system is split into the nominal and delta portions and only the delta portion is controlled adaptively, several implementation requirements fall on the delta system. Some comments on assumptions related to the nominal partition are warranted however. Most importantly, a model of the nominal partition is assumed to be known. A control law that permits a transfer function expression of the nominal partition from the reference signal to the output is assumed to have already been designed. Ideally, this nominal control law provides a reasonable level of performance when controlling the entire system on its own. The system-level requirements for the proposed control design are as follows:

R1. The delta partition must be controllable, observable, and strictly proper. Its observability index ν (or at least its upper bound [8]) must be known.

R2. Both the nominal and delta partitions must have m inputs and m outputs.

R3. The delta partition must have relative degree 1.

R4. The signs of the leading principal minors of the high frequency gain matrix K_p of the delta partition must be known.

R5. The delta partition should be minimum phase. If this is not expected to be the case, then an approximate model of the delta partition must be available.

Additionally, there are some restrictions on the delta reference model. Specifically, the product of the delta reference model and a component of high frequency gain matrix decomposition $W_\Delta S$ must satisfy an SPR requirement. Further details will be provided later in the text.

4.1.1 Nominal Control Law

One of the motivating factors behind the model partitioning explored in this paper is the desire to make use of existing nonadaptive control laws that have already been developed for the flexible aircraft. These nominal control laws already meet necessary safety and performance requirements. It is important to note that the design of the the nominal control law is not the focus of this investigation. Any nominal control law that permits the closed-loop nominal model to be expressed in the form $y_n = W_n(s)r$ is permissible. Thus, to simplify subsequent discussion, a straightforward pole placement controller with constant reference tracking is selected as the nominal control law [60]. Of course more sophisticated control techniques could be used here instead, but

it is not necessary for successful implementation of the proposed design. If the frequency representation of the open-loop nominal model is given as

$$\bar{y}_n = \bar{G}_n(s)u_n \tag{4.1}$$

then the model can be equivalently expressed in state space form as

$$\begin{aligned} \dot{\bar{x}}_n &= \bar{A}_n\bar{x}_n + \bar{B}_n u_n \\ \bar{y}_n &= \bar{C}_n\bar{x}_n. \end{aligned} \tag{4.2}$$

The appropriate pole placement control signal is

$$u_n = -K_n\bar{x}_n + \bar{N}r \tag{4.3}$$

where

$$\bar{N} = \left(\bar{C}_n[-\bar{A}_n + \bar{B}_n K_n]^{-1}\bar{B}_n\right)^{-1}. \tag{4.4}$$

The closed-loop system becomes

$$\begin{aligned} \dot{\bar{x}}_n &= (\bar{A}_n - \bar{B}_n K_n)\bar{x}_n + \bar{B}_n\bar{N}r \\ \bar{y}_n &= \bar{C}_n\bar{x}_n \end{aligned} \tag{4.5}$$

and so a transfer function matrix from r to $\bar{y}_n$ can be obtained such that $\bar{y}_n = \bar{W}_n(s)r$ as is necessary.

4.1.2 Delta Control Law Derivation

Next proceed to development of an adaptive control law for the unknown delta system. As stated previously, the delta control law is based on

the direct MRAC scheme for a MIMO system. It is intended to work with the nominal law to ensure that the system's output tracks the output of a reference model. The m x m delta system will be denoted as either $G_\Delta(s)$ or $(A_\Delta, B_\Delta, C_\Delta, D_\Delta)$, and its high frequency gain matrix can be defined as $K_p = C_\Delta B_\Delta$. Several other works addressed in the literature review contain derivations that could be used to carry out design here, but the procedure outlined in [12] has been selected for adaptation to the partitioned structure.

First, define the output signals $y_\Delta = y - \bar{y}_n$ and $y_{\Delta,r} = y_r - \bar{y}_n$ as illustrated in Figure 3.1. Using these definitions note that the full system tracking error $z = y - y_r$ is equivalent to the so-called delta system tracking error

$$\begin{aligned} e_\Delta &= y_\Delta - y_{\Delta,r} \\ &= (y - \bar{y}_n) - (y_r - \bar{y}_n) \\ &= y - y_r. \end{aligned} \tag{4.6}$$

Thus, the goal is to use the delta control law u_Δ to bring the full system tracking error to zero

$$\lim_{t\to\infty} z = \lim_{t\to\infty} (y - y_r) = 0. \tag{4.7}$$

Next, as discussed in Chapter 3, note that the delta reference model can be recovered as $W_\Delta = W_r - \bar{W}_n$. If the true values of the unknown parameters

in the delta control law were known the closed loop delta system would become

$$\begin{aligned} y_\Delta &= G_\Delta u_\Delta \\ &= W_\Delta r. \end{aligned} \tag{4.8}$$

The control law u_Δ^* that would make Eq. (4.8) true is known to be [7]

$$u_\Delta^* = \theta_1^{*T}\omega_1 + \theta_2^{*T}\omega_2 + \theta_3^* y_\Delta + \theta_4^* r = \theta^{*T}\omega \tag{4.9}$$

where

$$\omega_1 = \frac{A(s)}{\Lambda(s)} u_\Delta \tag{4.10}$$

and

$$\omega_2 = \frac{A(s)}{\Lambda(s)} y_\Delta. \tag{4.11}$$

Here define

$$A(s) = [I\ Is ... Is^{\nu-2}]^T \text{ with } I \in \mathbb{R}^{m\text{x}m} \tag{4.12}$$

where ν is the delta system's observability index. Also define

$$L(s) = \lambda_0 + \lambda_1 s + ... + s^{\nu-2} \tag{4.13}$$

where the λ's are user choice, but the resulting $L(s)$ must be Hurwitz. Note that ω_1, $\omega_2 \in \mathbb{R}^{m(\nu-1)}$. Also note that θ_1^*, $\theta_2^* \in \mathbb{R}^{m(\nu-1)\text{x}m}$, $\theta_3^* \in \mathbb{R}^{m\text{x}m}$, and $\theta_4^* = K_p^{-1}$. The θ's refer to unknown parameters and the superscript $*$ denotes their (unknown) true value.

A more useful form of the full system error can now be obtained through manipulation of Eq. (4.9). First set $u_\Delta = u_\Delta^*$ in the expressions for ω_1, ω_2, and

r in Eqs. (4.10),(4.11), and (4.8). Substitute these into Eq. (4.9) to obtain

$$u_\Delta^* = \theta_1^{*T}\frac{A(s)}{\Lambda(s)}u_\Delta^* + \theta_2^{*T}\frac{A(s)}{\Lambda(s)}G_\Delta u_\Delta^* + \theta_3^* G_\Delta u_\Delta^* + \theta_4^* W_\Delta^{-1} G_\Delta u_\Delta^*. \tag{4.14}$$

From here obtain the matching equation

$$I = \theta_1^{*T}\frac{A(s)}{\Lambda(s)} + \theta_2^{*T}\frac{A(s)}{\Lambda(s)}G_\Delta + \theta_3^* G_\Delta + \theta_4^* W_\Delta^{-1} G_\Delta. \tag{4.15}$$

Right multiplying by u_Δ and adding and subtracting equivalent forms of $K_p^{-1}r$ gives

$$u_\Delta = \theta^{*T}\omega - K_p^{-1}r + K_p^{-1}W_\Delta^{-1}G_\Delta u_\Delta \tag{4.16}$$

where K_p is the high frequency gain matrix of the delta system. Next, left multiply by $W_\Delta K_p$, make use of the y_Δ, $y_{\Delta,r}$, and e_Δ expressions to obtain

$$W_\Delta K_p u_\Delta = W_\Delta K_p \theta^{*T}\omega + e_\Delta. \tag{4.17}$$

Finally, remembering that $z = e_\Delta$ and rearranging, arrive at the desired alternative error expression

$$z = W_\Delta K_p(u_\Delta - \theta^{*T}\omega). \tag{4.18}$$

In the SISO case, the certainty equivalence-type control law choice for u_Δ would be straightforward. The update law for θ would be selected from term cancellation in the Lyapunov function, and knowledge of at least the sign of the scalar K_p would be required to complete the implementation. In the MIMO case proceeds similarly but again some type of knowledge of the matrix K_p is required. The design used here requires only that the signs of the leading principal minors of K_p are known [12].

To determine the appropriate control law proceed by restating Eq. (4.18) with a decomposition of K_p. Specifically, the high frequency gain matrix is factored as $K_p = SDU$ where S is a symmetric positive definite matrix, D is diagonal, and U is unity upper triangular [61]. Such a factorization is assured to exist as long as K_p is real, square, and has nonzero leading principal minors– again facilitated by the relative degree one requirement [12]. Substituting the factorization into Eq. (4.18) gives

$$z = W_\Delta SD(Uu_\Delta - U\theta_1^{*T}\omega_1 - U\theta_2^{*T}\omega_2 - U\theta_3^* y_\Delta - U\theta_4^* r). \tag{4.19}$$

Next include the relationship $Uu_\Delta = u_\Delta - (I-U)u_\Delta$ to be explicit that no infeasible dependencies exist among the control terms (i.e. a given control term, u_{Δ_i}, can only depend on higher index control terms, $u_{\Delta_{i+1}}...u_{\Delta_m}$). Also define the place holders $K_1 = U\theta_1^{*T}$, $K_2 = U\theta_2^{*T}$, $K_3 = U\theta_3^*$, and $K_4 = U\theta_4^*$ so that the error equation can be stated as

$$z = W_\Delta SD[u_\Delta - K_1\omega_1 - K_2\omega_2 - K_3 y_\Delta - K_4 r - (I-U)u_\Delta]. \tag{4.20}$$

Finally, new regressors Ω and unknown parameters Θ are defined via the relationship

$$[\Theta_1^{*T}\Omega_1 \;\; \Theta_2^{*T}\Omega_2...\Theta_m^{*T}\Omega_m]^T \triangleq K_1\omega_1 + K_2\omega_2 + K_3 y_\Delta + K_4 r + (I-U)u_\Delta. \tag{4.21}$$

Note that this means that the row vector Θ_i^{*T} contains the i^{th} rows of each K and $I-U$. The regressors are defined as $\Omega_i^T = [\omega^T \;\; u_{\Delta_{i+1}}...u_{\Delta_m}]$. The final form of the error equation is

$$z = W_\Delta SD(u_\Delta - [\Theta_1^{*T}\Omega_1 \;\; \Theta_2^{*T}\Omega_2...\Theta_m^{*T}\Omega_m]^T). \tag{4.22}$$

As the true values of the Θ parameters are unknown, an update law for each of the Θ's is selected to provide an estimate of its value based on measured signals. The current estimated value, denoted by $\hat{\Theta}$, is then used in the control law. Thus, the adaptive delta control law is given by

$$u_\Delta = [\hat{\Theta}_1^T \Omega_1 \;\; \hat{\Theta}_2^T \Omega_2 ... \hat{\Theta}_m^T \Omega_m]^T \tag{4.23}$$

and the full system error is reduced to

$$z = W_\Delta S D[\tilde{\Theta}_1^T \Omega_1 \;\; \tilde{\Theta}_2^T \Omega_2 ... \tilde{\Theta}_m^T \Omega_m]^T \tag{4.24}$$

where $\tilde{\Theta} = \hat{\Theta} - \Theta^*$.

4.1.3 Parameter Update Law Selection

The parameter update laws are now determined via Lyapunov analysis. Consider a Lyapunov function of the form

$$V(z, \Theta) = \frac{1}{2} e^T P e + \frac{1}{2} \sum_{i=1}^{m} \frac{1}{\gamma_i} |d_i| \tilde{\Theta}_i^T \tilde{\Theta}_i > 0. \tag{4.25}$$

Further clarification of the terms is provided subsequently.

- Composite system state error: e

  By combining the state of the delta system x_Δ with the filter states defined in Eqs. (4.10) and (4.11), construct the vector $X_\Delta = [x_\Delta^T \; \omega_1^T \; \omega_2^T]^T$. If a nonminimal realization of $W_\Delta S$ denoted by $C_\Delta (sI - A_\Delta)^{-1} B_\Delta$ is considered that also satisfies $C_\Delta B_\Delta = S$, then the nonminimal realization's state can be similarly defined as X_{Δ_r}. The "state error" is then

$e = X_\Delta - X_{\Delta_r}$, and the dynamics can be stated as

$$\begin{aligned} \dot{e} &= A_\Delta e + B_\Delta D(u_\Delta - [\Theta_1^{*T}\Omega_1 \;\; \Theta_2^{*T}\Omega_2 ... \Theta_m^{*T}\Omega_m]^T) \\ z &= C_\Delta e. \end{aligned} \tag{4.26}$$

- Lyapunov matrix: P

  By requiring that $W_\Delta S$ is SPR there exist matrices $P = P^T > 0$ and $Q = Q^T > 0$ satisfying [8]

$$\begin{aligned} A_\Delta^T P + P A_\Delta &= -2Q \\ P B_\Delta &= C_\Delta^T. \end{aligned} \tag{4.27}$$

  Satisfaction of the SPR requirement can be difficult in general, but by restricting W_Δ to a diagonal, single pole structure it is assured that the $W_\Delta S$ requirement is met [12]. W_Δ is a result of other user-selected items, and as such this simple structure is not infeasible.

- Diagonal entries of D: d_i

  These terms refer to the diagonal entries of the decomposition matrix D. A valid expression for this matrix can be stated as

$$D = \begin{bmatrix} \Delta_1 & 0 & 0 & 0 \\ 0 & \frac{\Delta_2}{\Delta_1} & 0 & 0 \\ & & \ddots & \\ 0 & 0 & 0 & \frac{\Delta_m}{\Delta_{m-1}} \end{bmatrix}. \tag{4.28}$$

  Here Δ_i refers to the i^{th} leading principal minor of K_p. Note that none of the leading principal minors can be zero.

- Learning rate: γ_i

  Each of the m γ_i terms is a user-selected adaptation gain. It is necessary that $\gamma_i > 0$.

Using the fact that $\dot{\tilde{\Theta}}_i = \dot{\hat{\Theta}}_i$ since Θ_i^* is a constant, as well as occasionally taking the transpose of scalar products, the time derivative of the Lyapunov function can be stated as

$$\dot{V} = \frac{1}{2}\dot{e}^T P e + \frac{1}{2} e^T P \dot{e} + \sum_{i=1}^{m} \frac{1}{\gamma_i} |d_i| \tilde{\Theta}_i^T \dot{\hat{\Theta}}_i. \tag{4.29}$$

Consideration of Eq. (4.26) and Eq. (4.27) as well as inclusion of the selected control law bring the derivative to

$$\dot{V} = -e^T Q e + e^T P B_\Delta D[\tilde{\Theta}_1^T \Omega_1 \ \tilde{\Theta}_2^T \Omega_2 ... \tilde{\Theta}_m^T \Omega_m]^T + \sum_{i=1}^{m} \frac{1}{\gamma_i} |d_i| \tilde{\Theta}_i^T \dot{\hat{\Theta}}_i. \tag{4.30}$$

Recall that $PB_\Delta = C_\Delta^T$ and thus $e^T P B_\Delta = e^T C_\Delta^T = z^T$. This relation along with expansion of $z^T D$ leaves

$$\dot{V} = -e^T Q e + \sum_{i=1}^{m} \frac{1}{\gamma_i} |d_i| \tilde{\Theta}_i^T (\gamma_i \text{sign}(d_i) z_i \Omega_i + \dot{\hat{\Theta}}_i). \tag{4.31}$$

The choice of update law is now obvious. For each $i = 1...m$ select

$$\dot{\hat{\Theta}}_i = -\gamma_i \text{sign}(d_i) z_i \Omega_i. \tag{4.32}$$

The derivative is left as

$$\dot{V} = -e^T Q e \leq 0. \tag{4.33}$$

A signal chasing argument permits the conclusion that $e(t)$ and thus $z(t) \to 0$ as $t \to \infty$ as desired for the control law given in Eq. (4.23) and the update laws given in Eq. (4.32).

4.1.4 Nonminimum Phase Adaptation

In the case that the delta partition is nonminimum phase, the derivation shown in the previous section demonstrates that error convergence is not expected. As reviewed in the introduction, however, a handful of techniques do exist for nonminimum phase systems. Here a method is selected that handles the problem by augmenting the system with additional dynamics. The goal is to use the additional dynamics to make the augmented system minimum phase. The addition is made in parallel with the original system, and thus the technique is known as parallel feedforward compensation [19]. The output of the augmented system is the data fed back to the adaptive control law, and the adaptation mechanism only sees minimum phase behavior. However, the output of the true system does not actually include a contribution from the fictitious parallel feedforward compensator (PFC). For best results the PFC should have a small output magnitude so that the augmented system, for which the control is designed, has an output signal similar to that of the true system. Figure 4.1 illustrates the PFC structure used to augment the nonminimum phase delta system. The augmented delta system $G_{\Delta,\text{aug}}$ shown in the diagram replaces the original delta portion of the plant depicted in Figure 3.1.

Traditional PFC designs require that the nonminimum phase system be known in order to select an appropriate compensator. This is not a feasible requirement here since the nonminimum phase delta system is precisely what is unknown. Instead, [62] proposes a PFC procedure that requires only a rough

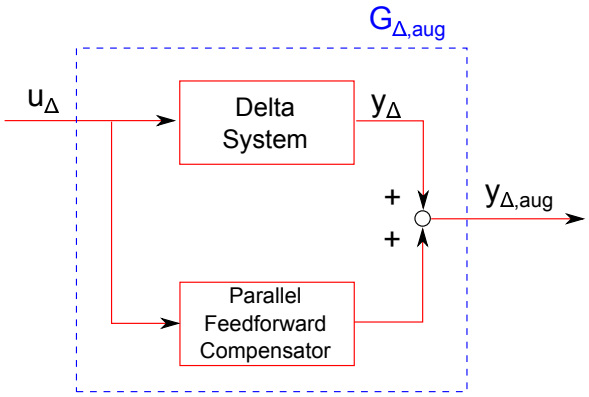

Figure 4.1: Block diagram of augmented delta system, replaces delta portion of the plant in Figure 3.1

estimate of the nonminimum phase system be available. The technique relies on the establishing the almost strictly positive real (ASPR) property for the augmented system. While further discussion on the ASPR property can be found in [63], it is sufficient for the discussion to summarize that a system (A, B, C) is said to be ASPR if there exists a feedback matrix K_{ASPR} such that ($A - BK_{\text{ASPR}}$, B, C) is SPR.

The authors propose calculating a PFC transfer function matrix from the difference between a user-selected ASPR transfer function matrix and the available estimate of the nonminimum phase system. For the structure developed here, this becomes

$$G_{\text{PFC}} = G_{\text{ASPR}} - \hat{G}_{\Delta} \tag{4.34}$$

where $\hat{G}_{\Delta}$ is a delta system estimate. The augmented system will then be

$$G_{\Delta,\text{aug}} = G_{\text{PFC}} + G^{*}_{\Delta} \tag{4.35}$$

where G^*_Δ is the true delta system. Define

$$\Delta = G^{-1}_{\text{ASPR}}(G^*_\Delta - \hat{G}_\Delta) \tag{4.36}$$

and restate the augmented system as

$$G_{\Delta,\text{aug}} = G_{\text{ASPR}}(I + \Delta). \tag{4.37}$$

$G_{\Delta,\text{aug}}$ will then also be ASPR if the following conditions are satisfied:

1. $G_{\text{ASPR}}(s)$ is ASPR
2. $\Delta(s) \in RH_\infty$
3. $||\Delta||_\infty < 1$

A proof for this result can be found in [64]. The augmented delta system then meets all of the necessary requirements, including the minimum phase requirement, for use with the adaptive system described in Sections 4.1.2 and 4.1.3.

4.2 Flexible Aircraft Modeling

The experimental, flexible wing aircraft used in this investigation is a lightweight, high aspect ratio, remotely piloted vehicle. It was built to experience and demonstrate suppress of multiple types of flutter modes within its flight envelope. The aircraft has variety of sensors and a large number of control surfaces available to the controls designer as summarized previously

in Fig. 2.4. Notably, each wing has four flaps along its trailing edge that can be individually actuated. Two flaps at the rear of the body are also available. Accelerometers are distributed over the vehicle with four arranged on the wings and two on the body for measurement feedback.

4.2.1 State Space Model

Linear state space models for the flexible aircraft in steady level flight were provided by NASA Armstrong at an assortment of flight conditions. These state space models were produced using a finite element model along with an aerodynamic model and experimentally identified actuator models. The ZAERO software package [59], employing a rational function approximation, was used to produce the corresponding time domain, state space representation as reviewed in Chapter 2.

The state space models are of the form

$$\begin{aligned} \dot{x} &= A_p x + B_p u \\ y &= C_p x + D_p u. \end{aligned} \tag{4.38}$$

The matrices are defined using block notation as

$$A_p = \begin{bmatrix} A_{rr} & A_{re} & B_{rr} \\ A_{er} & A_{ee} & B_{re} \\ 0 & 0 & A_{act} \end{bmatrix} \quad B_p = \begin{bmatrix} 0 \\ 0 \\ B_{act} \end{bmatrix} \quad C_p = \begin{bmatrix} C_{ae} & D_{ae} \end{bmatrix} \quad D_p = \begin{bmatrix} 0 \end{bmatrix} \tag{4.39}$$

and differ slightly from the form introduced in the background review due to the inclusion of rigid body dynamics. The various subscripts reference the rigid body (r), elastic(e), aeroelastic (ae), and actuator (act) contributions. The

state vector is given as $x = [x_{AS}^T \ x_\xi^T \ x_{act}^T]^T$. The rigid body states are contained in $x_{AS} = [x \ h \ \theta \ u \ \alpha \ q \ y \ \beta \ p \ r \ \phi \ \psi]^T$. The elastic and aerodynamic states are contained in $x_\xi = [x_e \ \dot{x}_e \ x_{lag}]^T$ where x_e and $\dot{x}_e$ corresponds to the flexible body modes and x_{lag} references the unsteady aerodynamic lags. The actuator states in x_{act} correspond to a third order model for each actuator. The result is a 130 state model where x_{AS} is 12 states, x_e and $\dot{x}_e$ are each 14 states, x_{lag} is 60 states, and x_{act} fills the remaining 30 states.

4.2.2 Model Partitioning

Based on the partitioned design shown in Figure 3.1 separate inputs signals are required to be assigned to the nominal and delta models. Both models can share the same outputs. The derivation of the delta control law also makes it clear that both the nominal and delta models must be square. Thus, select m flaps for the nominal partition, m different flaps for the delta partition, and m accelerometers for use as outputs with both partitions.

Referencing the abbreviations shown in Fig. 2.4, wing flaps WF 2L, WF 2R, WF 3L, and WF 3R are selected as inputs for the nominal system. This choice was made to coincide with actuator selections of existing nominal control laws and establishes that $m = 4$. Wing flaps WF 4L and WF 4R as well as body flaps BF R and BF L are selected as inputs for the delta system. Finally, select accelerometers ACC LF, ACC RR, ACC CF, and ACC CR as outputs for moth models. The choice of these particular four sensors will permit detection of the largest number of mode shapes included in the

Table 4.1: Summary of PFC MRAC input and output selections

	Nominal Control System	**Delta Control System**
Inputs	WF 2R & L, WF 3R & L	WF 4R & L, BF R & L
Outputs	ACC CF, ACC CR, ACC LF, ACC RR	ACC CF, ACC CR, ACC LF, ACC RR

state space model generation procedure. Table 4.1 summarizes the input and output selections.

4.2.3 Model Reduction

The state space models produced by ZAERO are typically high order and numerically ill-conditioned. Some type of model conditioning and order reduction is necessary before they can be used for control design. The model treatments used in this paper follow a modified version of the steps presented in [45] where similar flexible aircraft state space models were used.

The reduction procedure is summarized in the following list. Note that two types of model reduction are used here. Model reduction by truncation ensures the reduced model G_r is equivalent to the original model G at infinite frequency, i.e. $G(\infty) = G_r(\infty)$. Model reduction by residualization ensures that the DC gain of the reduced model is equivalent to the DC gain of the original model, i.e. $G(0) = G_r(0)$.

1. Nominal/Delta partitioning

The nominal and delta partitions are constructed from the original model based on the associated input and output selections described in Section 4.2.2.

2. Actuator state residualization

   Most of the acutator states are residualized from both partitions. Two states are retained that significantly improve model accuracy as identified by manually checking for large changes in the frequency response of the reduced model.

3. Unsteady aerodynamic state residualization

   There are three aerodynamic lag states associated with each rigid body and flexible mode. Again, most of these states are residualized from both partitions. Nine states are retained correspond to significant changes in the reduced model's frequency response.

4. Rigid body state truncation

   All rigid body states except pitch rate, roll rate, yaw rate, and angle of attack are truncated as the others do not factor significantly into the aeroelastic dynamics concerned in this investigation.

5. Flexible body state truncation

   The original model contains 14 flexible body modes, ordered by increasing modal frequency. Each mode contributes two states: displacement and velocity. The first 11 flexible body modes are retained in accordance with the results of flutter modal participation analysis omitted here. The

states associated with the remaining three modes are truncated from the model.

6. Balanced realization truncation

   A balancing transformation can be performed on the remaining model [65]. Note that after this point the states no long retain their original physical meaning. All states below a selected threshold for the corresponding Hankel singular values are truncated. For the nominal partition, the threshold is set to 0.5 so as to cut the model off at a existing gap in singular values. The threshold for the delta partition is set to 0.1 for similar reasons.

7. Feedthrough elimination

   Each of the reduction by residualization steps has the potential to result in a reduced state space model with a non-zero D_Δ matrix even when the original model was strictly proper. The adaptive control design will require a strictly proper system, and thus $D_\Delta = 0_{mxm}$ is forced in the final reduced delta model. This step is not strictly necessary for the reduced nominal model. Frequency analysis shows however that feedthrough elimination has little effect on the response of the models used here.

The reduction steps result in two smaller models: a 23-state nominal model and a 26-state delta model. Both of these models have the same accelerometer outputs but different flap inputs. To visualize the accuracy of

the reduced model, look at Bode plots of each of the input/output pairs as compared to their original Bode diagram. Figure 4.2 shows the frequency response comparison for two of the input/output pairs as an example. Figure 4.2(a) illustrates the frequency response of a pair from the nominal model while Figure 4.2(b) illustrates one from the delta model. In all cases, including the ones shown, the reduced model adequately matches the full model up to approximately 11 Hz.

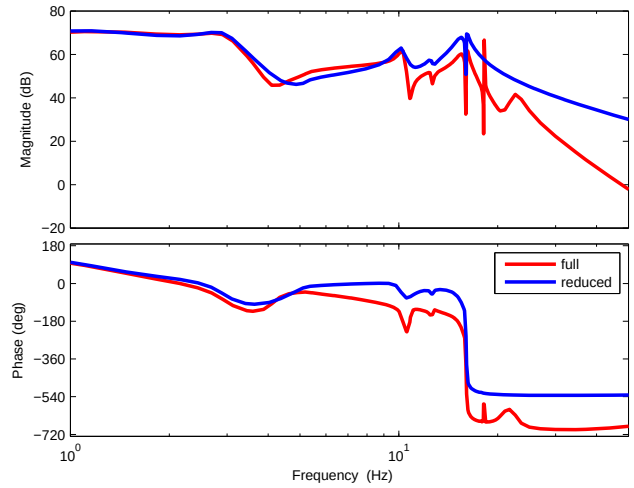

(a) Nominal partition: Wing flap 3 left to right rear accelerometer

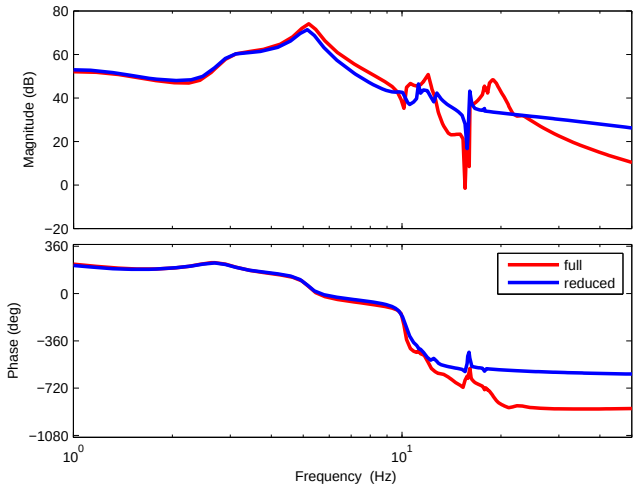

(b) Delta partition: Body flap left to right rear accelerometer

Figure 4.2: Bode plots of truncated system

4.3 Simulation Results

The simulation results presented in this paper were all created using the same reduced state space model. The original model was generated using simulation data of the flexible aircraft at flight conditions just below the flutter boundary via the process outlined in Section 4.2. The model was then reduced via the process outlined in Section 4.2.3. Both the nominal and delta portions of the resulting reduced model are stable but nonminimum phase. For the sake of brevity only two out of the four available output signals is included. Specifically, plots are included for the vertical axis accelerometer located on the trailing edge of the right wing (ACC RR) and the vertical axis accelerometer centered on the front of the body (ACC CF). Both axes on all plots have been normalized by consistent reference values for security purposes.

Figure 4.3 shows the open loop behavior of the reduced system in response to non-zero initial conditions. Although the system is stable at the selected flight conditions, the transient response displays significant oscillation. Figure 4.4 illustrates system performance with only the nominal control law in use. For simplicity, a pole placement controller with tracking is designed using knowledge of the nominal model and serves as the nominal control law. A step function serves as the reference signal for each output. Although tracking is achieved, the transient again leaves much to be desired.

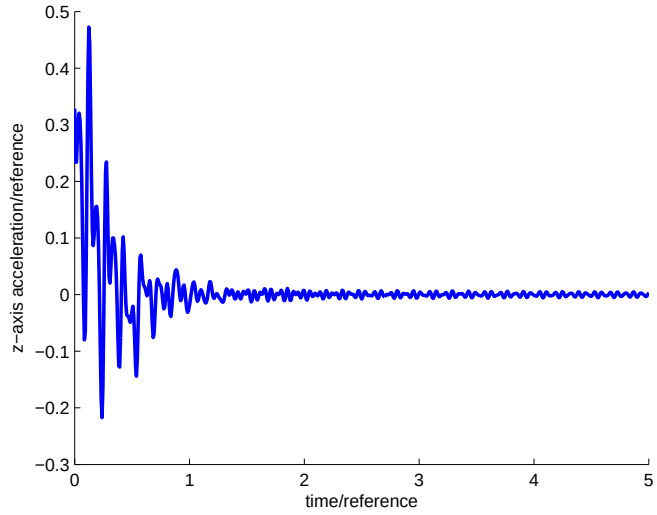

(a) ACC RR

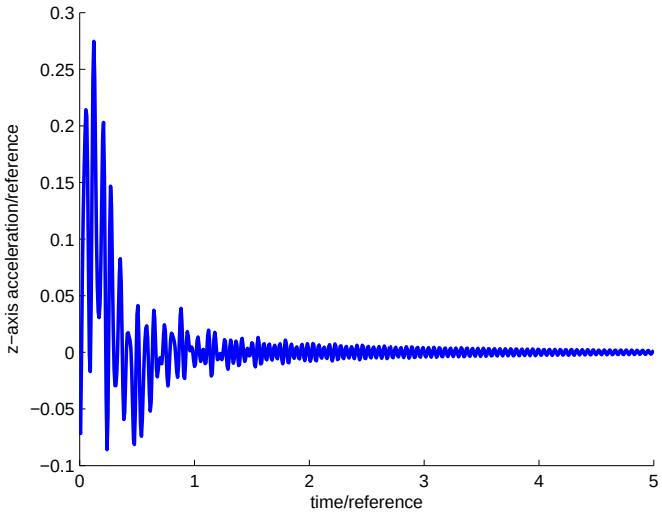

(b) ACC CF

Figure 4.3: Scaled vertical axis accelerometer output, no control

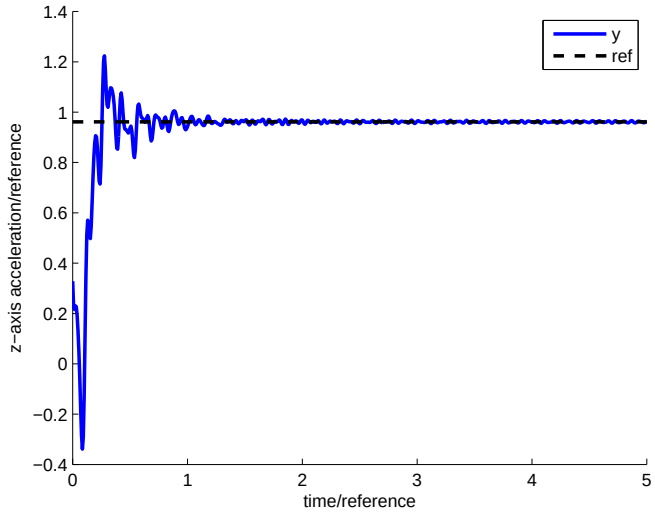

(a) ACC RR

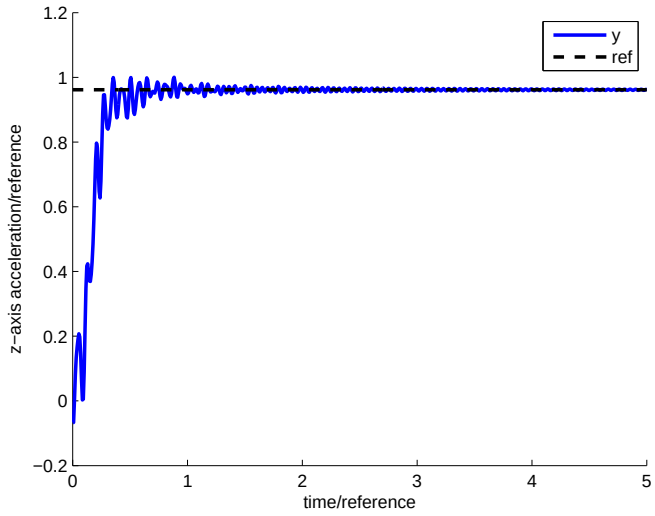

(b) ACC CF

Figure 4.4: Scaled vertical axis accelerometer output, nominal control

In order to implement the delta control law several more design parame-

ters must be selected. First, a reference model must be designed. As described in Chapter 3 the reference model for the full system can be expressed as the controlled nominal model plus the reference model for the delta partition. The delta reference model is yet to be defined. Recall that the delta reference model also has SPR requirements that must be met. Additionally, since the nominal control law already provides acceptable steady-state tracking performance of the reference signal, the output magnitude of the delta reference model should be small. Here $W_\Delta = \frac{0.01}{(s+3)}\mathrm{I}_{4x4}$ has been selected as the delta reference model and added to the controlled nominal model to obtain the full reference model.

Next, a PFC must be designed to augment the nonminimum phase delta partition. Although the delta partition G^*_Δ is an unknown quantity with respect to the adaptive controller, the PFC procedure outlined in Section 4.1.4 requires knowledge of an approximation $\hat{G}_\Delta$. For illustrative purposes take the delta model produced by the model reduction process and reduce it even further by truncating the states below the 0.5 Hankel singular value threshold. This leaves a 21-state model that will serve as the approximation $\hat{G}_\Delta$. G_{ASPR} can now be selected and $\hat{G}_\Delta$ used to generate G_{PFC} in accordance with Eq. (4.34). For this simulation

$$G_{\mathrm{ASPR}} = \begin{pmatrix} \frac{70}{(s+8)} & 0 & 0 & 0 \\ 0 & \frac{25}{(s+8)} & \frac{1}{(s+8)} & 0 \\ \frac{10}{(s+8)} & \frac{0.1}{(s+8)} & \frac{85}{(s+8)} & 0 \\ 0 & 0 & 0 & \frac{50}{(s+8)} \end{pmatrix} \tag{4.40}$$

has been used. The selection was made with the goal of minimizing the output magnitude of $G_{\mathrm{PFC}} = G_{\mathrm{ASPR}} - \hat{G}_\Delta$. Note that the full delta system has not been

used in this choice and will remain unknown to the adaptation mechanism. The actual output of the system does have to be recovered from the output of the augmented system by subtracting off the output component of the PFC before analyzing system performance.

Finally, the adaptive delta control law design is completed by specifying the learning rates (each set to $\gamma = 20$), the required observability index ($\nu = 8$), and the signs of the leading principal minors associated with the delta high frequency gain matrix decomposition (all positive). The deflection of each flap is also set to saturate at $\pm 45^\circ$ to ensure feasibility.

Figure 4.5 provides the results of the nominal and delta control laws working together to make the full augmented system track the output of the full reference model. As expected, the performance of the augmented system exhibits much improved transient properties. However, the augmented system is not the system to be concerned with. The output of the PFC (a known quantity for a given control input) must be subtracted from the output of the augmented system to obtain the output of actual system. Figure 4.6 shows the results after this subtraction and thus contains the true system output in response to nominal and delta control. The plots indicate that the transient behavior is still much more desirable than the nominal-only control case, and tracking of the reference model is quite good.

Ultimately, the preceding results show that good performance can be obtained from the proposed control design when all requirements are met. However it is unlikely that sufficient information about the delta portion of

the plant will be known to facilitate implementation of the delta control law. The need to have a decent estimate of the delta plant portion when the delta system is nonminimum phase is particularly restrictive and negates much of the benefit offered by implementation of an adaptive system. A less restrictive version of the partitioned control design will be pursued moving forward.

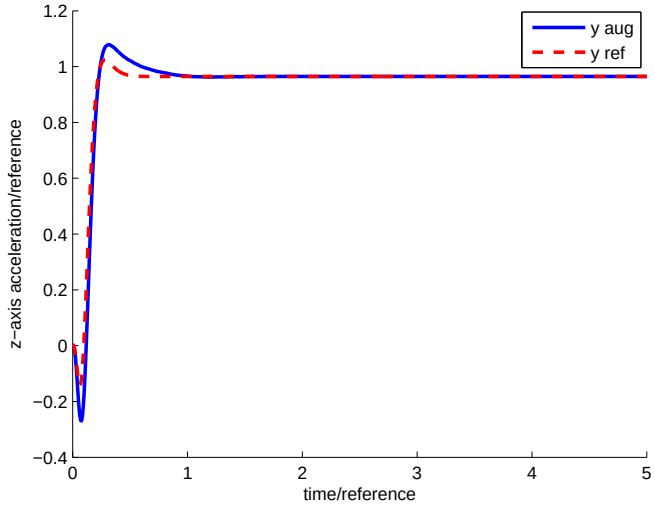

(a) ACC RR

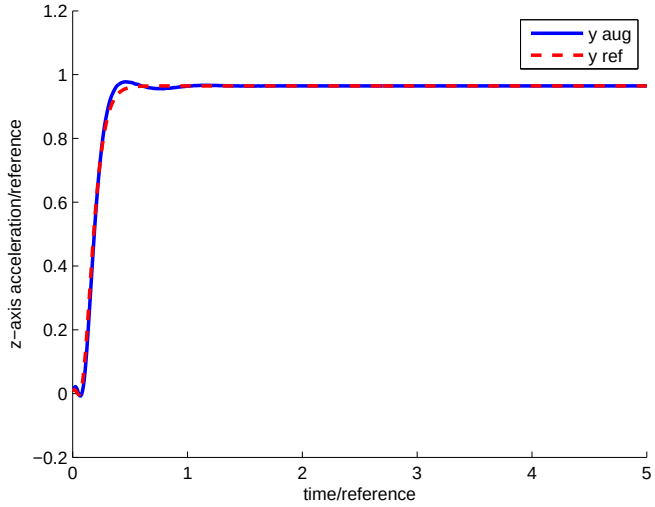

(b) ACC CF

Figure 4.5: Scaled vertical axis accelerometer output, nominal + delta control for augmented system

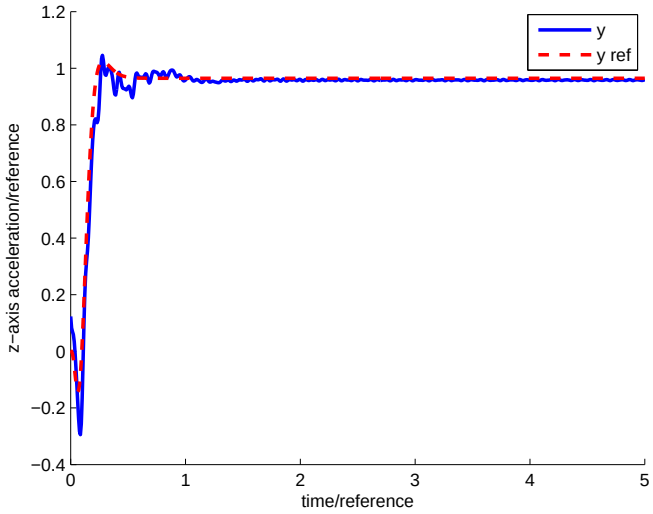

(a) ACC RR

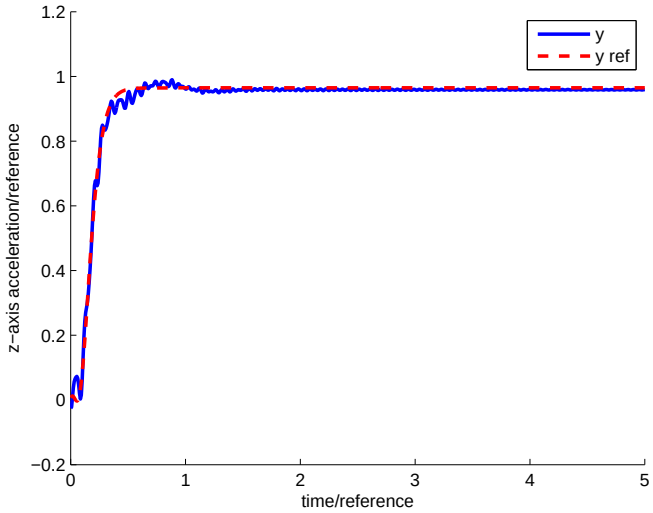

(b) ACC CF

Figure 4.6: Scaled vertical axis accelerometer output, nominal + delta control

Chapter 5

MRAC for Nonminimum Phase Systems

After recognizing the limitations of the PFC approach to accommodating nonminimum phase systems, a more flexible approach was desired. The recent Retrospective Cost Adaptive Control technique seems to be a likely candidate as it can provided adaptive control for nonminimum phase systems by only requiring some additional knowledge about the system [20]. Unfortunately, the technique has only been proven for SISO discrete–time systems. A related continuous–time design, known as surrogate tracking error MRAC, was proposed by Hoagg for both SISO [21] and MIMO [22] nonminimum phase plants. Although the control design is successfully demonstrated in simulation of simple examples, the assumed plant structure is restrictive. Additionally, the tracking error convergence proof is left open.

This chapter modifies the structure of surrogate tracking error MRAC and completes the stability proof left open in [22]. The proof relies on a composite state space description of plant and control scheme, Lyapunov stability techniques, and signal growth analysis. A notable feature of the proof is establishment of the regressor's boundedness despite the presence of nonminimum phase zeros throughout the design. The results do however require that

nonminimum phase zero information from the pant be known.

The surrogate tracking error MRAC design is simulated using the linear version of an aircraft wing's aeroelastic pitch and plunge dynamics. In particular this paper utilizes the physical 2–input model built by Texas A&M University to determine realistic values for simulation [38]. The model is MIMO, unstable, and nonminimum phase at certain freestream velocities and thus fully stresses the control design. A version of this work appeared as [66].

5.1 Problem Description

The plant transfer function from control input $u(t) \in \mathbb{R}^l$ to output $y(t) \in \mathbb{R}^l$ is given by

$$G(s) = \beta_p(s)\alpha_p^{-1}(s) \tag{5.1}$$

where $\beta_p(s) = \beta_{du}(s)\beta_s(s)$. Note that $\alpha_p(s)$ is a monic $l \times l$ polynomial matrix of degree $n > 0$, $\beta_{du}(s)$ is an $l \times l$ polynomial matrix with degree n_u, and $\beta_s(s)$ is an $l \times l$ monic polynomial matrix with degree $n - n_u - d$.

Plant Assumptions

P1. Relative degree $d \geq 1$ is known.

P2. Upper bound on the degree of $\alpha_p(s)$ is known (i.e. $\bar{n} \geq n$).

P3. $\alpha_p(s)$ and $\beta_p(s)$ are right coprime.

P4. $\beta_{du}(s)$ has the known decomposition

$$\beta_{du}(s) = \sum_{i=1}^{l} \beta_{d_i}\beta_u(s)e^i \tag{5.2}$$

where $\beta_u(s)$ is an $l \times l$ monic polynomial matrix and each $\beta_{d_i} \in \mathbb{R}^{l \times l}$. Here e^i indicates the i^{th} column of the $l \times l$ identity matrix. Additionally, if $\zeta \in \mathbb{C}$ and $\text{Re}[\zeta] \geq 0$ then $\det\beta_u(\zeta) = 0$ and $\det\beta_s(\zeta) \neq 0$. Note that this assumption implies that knowledge of the nonminimum phase zeros (and and some structural information in the MIMO case) is necessary. Also note that $\beta_{du}(s) = \beta_p(s)$ and $\beta_s(s) = I$ is one valid choice that will accommodate any plant.

The reference model transfer function from a bounded and piecewise continuous reference input $r(t) \in \mathbb{R}^l$ to reference output $y_m(t) \in \mathbb{R}^l$ is given by

$$W_m(s) = \alpha_m^{-1}(s)\beta_m(s). \tag{5.3}$$

Here $\alpha_m(s)$ is a monic, asymptotically stable polynomial of degree $n_m > 0$. The model's relative degree is denoted as d_m, and thus $\beta_m(s)$ is an $l \times l$ polynomial matrix of degree $n_m - d_m$.

Reference Model Assumptions

M1. Relative degree $d_m > d$.

M2. $\alpha_m(s)$ and $\beta_m(s)$ are left coprime.

M3. $\beta_m(s)$ can be decomposed as

$$\beta_m(s) = \beta_{d_m}\beta_{du}(s)\beta_r(s) \tag{5.4}$$

so that the reference model contains at least the same nonminimum phase zero information as the plant. Any additional zeros to be included

in the reference model appear in the monic $l \times l$ polynomial matrix $\beta_r(s)$ of degree $n_m - d_m - n_u$. Note that $\beta_{d_m} \in \mathbb{R}^{l \times l}$.

M4. There exists an $N^* \in \mathbb{R}^{l \times l}$ such that the gain matching condition $\beta_{du}(s)N^* = \beta_{d_m}\beta_{du}(s)$ can be satisfied.

The goal is to use the control signal to ensure that the output tracking error, $z(t)$, goes to zero:

$$\lim_{t \to +\infty} z(t) = \lim_{t \to +\infty} \big(y(t) - y_m(t)\big) = 0. \tag{5.5}$$

The main user choices are the reference model itself, the polynomials $a_f(s)$ and $b_f(s)$, the polynomial matrix $C_f(s)$, and the degree of $a_f(s)$—denoted as n_c. Further details of the problem description can be found in [22].

5.2 Surrogate Tracking Error MRAC Design

In the reference paper [22] the control law was designed as

$$u(t) = \sum_{i=1}^{n_c} L_i(t)\bar{y}_i(t) + \sum_{i=1}^{n_c} M_i(t)\bar{u}_i(t) + N(t)r_f(t). \tag{5.6}$$

Here the updated parameters are $L_i, M_i, N : [0, \infty) \to \mathbb{R}^{l \times l}$ for $i = 1 \dots n_c$. The signals $\bar{y}_i$ and $\bar{u}_i$ are filtered quantities generated from y_p and u using

$$G_{a_{f,i}} = \frac{s^{n_c - i}}{a_f(s)} I_l. \tag{5.7}$$

The filtered quantity r_f is generated from r using

$$G_{a_f}(s) = \frac{b_f(s)\beta_r(s)}{a_f(s)}. \tag{5.8}$$

The parameter n_c is user choice. However it is subject to the requirement

$$n_c \geq \max(\bar{n}l, n_m - n_u - d). \tag{5.9}$$

The asymptotically stable, monic polynomial $a_f(s)$ of degree n_c is also user choice—as is the asymptotically stable, monic polynomial $b_f(s)$ of degree $n_c + n_u + d - n_m$. The control law can be equivalently written as

$$u(t) = \theta^T(t)\phi(t) \tag{5.10}$$

where

$$\theta(t) = \begin{bmatrix} L_1(t) \dots L_{n_c}(t) & M_1(t) \dots M_{n_c}(t) & N(t) \end{bmatrix}^T \tag{5.11}$$

$$\phi(t) = \begin{bmatrix} \bar{y}_1^T(t) \dots \bar{y}_{n_c}^T(t) & \bar{u}_1^T(t) \dots \bar{u}_{n_c}^T(t) & r_f^T(t) \end{bmatrix}^T. \tag{5.12}$$

Finally, the control law can be restated in a more useful form as

$$u(t) = \Psi^T(t)\Theta(t) \tag{5.13}$$

where $\Theta(t) = \operatorname{vec} \theta^T(t) \in \mathbb{R}^{(2n_c+1)l^2}$, and Ψ is defined using the Kronecker product as $\Psi(t) = \phi(t) \otimes I_l \in \mathbb{R}^{(2n_c+1)l^2 \times l}$.

Before prescribing the update law, define the filters

$$G_{C_{f,1}}(s) = \alpha_m(s) b_f(s) C_f^{-1}(s) \tag{5.14}$$

$$G_{C_{f,2}}(s) = a_f(s) C_f^{-1}(s) \beta_{du}(s), \tag{5.15}$$

and note that both depend on the user–selected, asymptotically stable, monic $l \times l$ polynomial matrix $C_f(s)$ of degree $n_c + n_u + d$. The filtered control, $u_f(t) \in \mathbb{R}^l$, is obtained by

$$u_f = G_{C_{f,2}}(s) u \tag{5.16}$$

The transpose of the filtered regressor, $\Phi^T(t) \in \mathbb{R}^{l\times(2n_c+1)l^2}$, is obtained by passing each column of the rearranged regressor, $\Psi^T(t)$, through $G_{C_{f,2}}(s)$ also and is denoted as

$$\Phi^T = G_{C_{f,2}}(s)\Psi^T. \tag{5.17}$$

The filtered tracking error, $z_f(t) \in \mathbb{R}^l$, is obtained by

$$z_f = G_{C_{f,1}}(s)z. \tag{5.18}$$

The update law is given by

$$\dot{\Theta}(t) = -P(t)\Phi(t)\Omega^{-2}(t)z_s(t) \tag{5.19}$$

where $P(t) \in \mathbb{R}^{(2n_c+1)l^2\times(2n_c+1)l^2}$ is updated as

$$\dot{P}(t) = -P(t)\Phi(t)\Omega^{-2}(t)\Phi^T(t)P(t). \tag{5.20}$$

A resetting procedure is utilized to prevent P from becoming too small and slowing adaptation. This work uses the method suggested in [7]: For some $c_P > 0$, $P(t_r^+) = P(0)$ where $t_r = \{t|\lambda_{\min}(P(t)) \leq c_P\}$. The quantity z_s in the update law for Θ is known as the surrogate tracking error and is given by

$$\begin{aligned} z_s(t) &= z_f(t) + \Phi^T(t)\Theta(t) - u_f(t) \\ &= G_{C_{f,1}}(s)\left[z\right] + G_{C_{f,2}}(s)\left[\Psi^T\right]\Theta - G_{C_{f,2}}(s)\left[\Psi^T\Theta\right]. \end{aligned} \tag{5.21}$$

The normalizing matrix $\Omega^2 \in \mathbb{R}^{l\times l}$ is given by

$$\Omega^2(t) = I_l + \eta\Phi^T(t)\Phi(t) \tag{5.22}$$

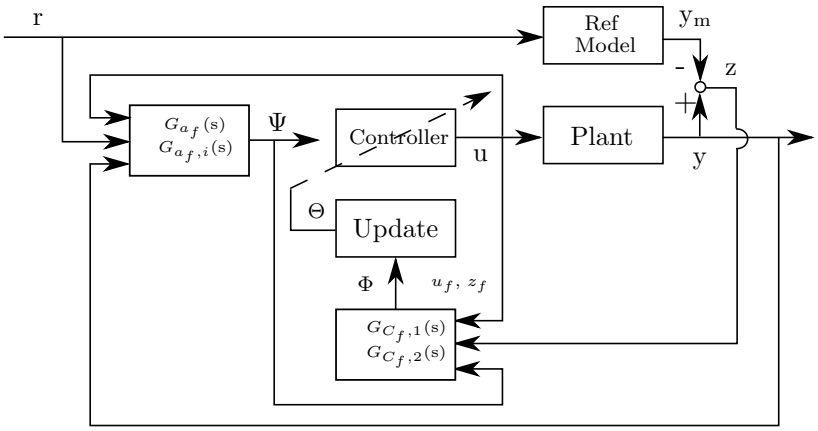

Figure 5.1: Block diagram of existing control design

where $\eta \in (0, \infty)$.

In [22], Lemma 1 demonstrated that an equivalent expression for z_f is

$$z_f(t) = G_{C_{f,2}}(s)\left(\Psi^T \tilde{\Theta}\right). \tag{5.23}$$

while Lemma 2 establishes that and equivalent expression for z_s is

$$z_s(t) = \Phi^T(t)\tilde{\Theta}(t). \tag{5.24}$$

Note that these expressions will be used for analysis only as they are dependent on the true, unknown parameter values. Additionally, define the normalized surrogate tracking error to be ϵ through the relationship

$$z_s(t) = \Omega^2(t)\epsilon(t) \tag{5.25}$$

A block diagram of the control design is given in Fig. 5.1.

5.3 Ideal Fixed-gain Controller

This section shows that there exists an ideal fixed-gain controller $u^*(t) = \Psi^T(t)\Theta^*$ that causes the plant to match the reference model. To begin, consider the control law proposed in [22] composed of the ideal parameters:

$$u^*(t) = \sum_{i=1}^{n_c} L_i^* \bar{y}_i(t) + \sum_{i=1}^{n_c} M_i^* \bar{u}_i(t) + N^* r_f(t) + \varepsilon(t). \tag{5.26}$$

This is equivalently expressed as $u^*(t) = \Psi^T(t)\Theta^* + \varepsilon(t)$. $\varepsilon(t)$ is an arbitrary signal used in the development of the surrogate tracking error and is not used explicitly in this paper. A block diagram of the system utilizing the ideal control law is given in Fig. 5.2.

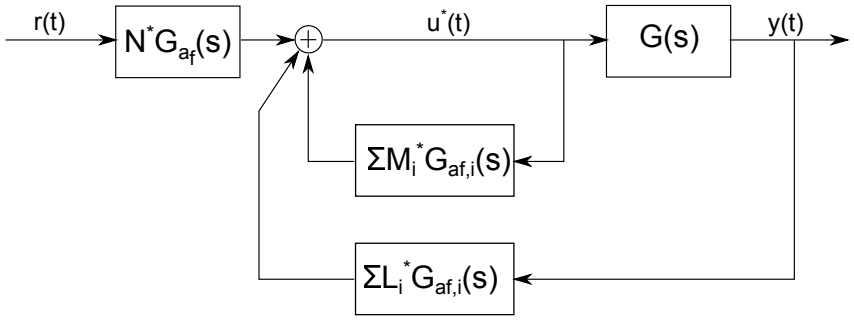

Figure 5.2: Block diagram for controlled plant using ideal parameter values

Manipulation of the block diagram gives the closed–loop transfer function from r to y as

$$G_{\rm cl}(s) = \beta_{du}(s)\beta_s(s)[a_f(s)\alpha_p(s) - M^*(s)\alpha_p(s) - L^*(s)\beta_{du}(s)\beta_s(s)]^{-1} N^* b_f(s)\beta_r(s). \tag{5.27}$$

where the definitions $L^*(s) = \sum_{i=1}^{n_c} L_i^* s^{n_c - i}$ and $M^*(s) = \sum_{i=1}^{n_c} M_i^* s^{n_c - i}$ have been used for simplicity. The goal is to have Eq. (5.27) match the reference

model transfer function $W_m(s) = \alpha_m^{-1}(s)\beta_{dm}\beta_{du}(s)\beta_r(s)$. Using this expression the $G_{\text{cl}}(s) = W_m(s)$ matching condition is

$$\beta_s(s)[a_f(s)\alpha_p(s) - M^*(s)\alpha_p(s) - L^*(s)\beta_{du}(s)\beta_s(s)]^{-1}b_f(s) = \alpha_m^{-1}(s)I_l. \quad (5.28)$$

This statement assumes $\beta_{dm} = N^* = kI_l$ (with $k \in \mathbb{R}$) so that assumption **M4** is satisfied. Rearranging, the matching condition is stated concisely as

$$\left[a_f(s)I_l - M^*(s)\right]\alpha_p(s) - L^*(s)\beta_{du}(s)\beta_s(s) = b_f(s)\alpha_m(s)\beta_s(s). \quad (5.29)$$

From the previous two expressions it is clear that, due to the inclusion of $\beta_{du}(s)$ in the reference model, any pole/zero cancellations that must occur in $G_{\text{cl}}(s)$ will be in the left half plane.

All that remains is to show that there exists an $L^*(s)$ and $M^*(s)$ such that the matching condition is satisfied. Note that a similar requirement arises in the establishment of an ideal fixed-gain controller in Theorem 2 of [22], and is omitted here.

5.4 Composite System Construction

Now write the dynamics of the plant in state space as

$$\begin{aligned} \dot{x}_p &= A_p x_p + B_p u \\ y &= C_p x_p, \end{aligned} \quad (5.30)$$

also denoted as the triple (A_p, B_p, C_p) with state $x_p \in \mathbb{R}^{nl}$. Create a composite system by selecting the new composite state vector $Y_c \in \mathbb{R}^{nl+(2n_c+1)n_cl}$ as

$$Y_c = \begin{pmatrix} x_p^T & x_{\bar{y}_1}^T & \dots & x_{\bar{y}_{nc}}^T & x_{\bar{u}_1}^T & \dots & x_{\bar{u}_{nc}}^T & x_{r_f}^T \end{pmatrix}^T \quad (5.31)$$

where $x_{\bar{y}_i}, x_{\bar{u}_i}, x_{r_f} \in \mathbb{R}^{n_c l}$ are state vectors arising from the filtering of the y, u, and r signals respectively. Specifically,

$$\bar{y}_i(t) = G_{a_{f,i}}(s)y(t) = \frac{s^{n_c-i}}{a_f(s)} I_l \, y(t) \tag{5.32}$$

which can also be represented by an appropriately selected state space system (A, B, C_i) with state $x_{\bar{y}_i}$. Similarly, $\bar{u}_i(t)$ is generated using $G_{a_{f,i}}(s)$ and can be represented by (A, B, C_i) with state $x_{\bar{u}_i}$. Finally,

$$r_f(t) = G_{a_f}(s)r(t) = \frac{b_f(s)\beta_r(s)}{a_f(s)} r(t) \tag{5.33}$$

which can be represented as (A, B, C_{r_f}) with state x_{r_f}.

Note that for each of these state space representations both A and B remain the same. This is permissible when selecting each representation to be in controller canonical form and noting that each filter has the same denominator structure. Also note that C_i is the same between the input and output filters due to their identical structures. While these consistencies are not necessary (i.e. other representations could be selected), the choice will simplify subsequent notation.

The corresponding composite state equations can be written as

$$\begin{aligned} \dot{Y}_c &= A_0 Y_c + B_c u + B_{cr} r \\ y &= C_c Y_c \end{aligned} \tag{5.34}$$

where the matrices are given by

$$A_0 = \begin{pmatrix} A_p & \boldsymbol{0}^T & \dots & \boldsymbol{0}^T & \boldsymbol{0}^T & \dots & \boldsymbol{0}^T & \boldsymbol{0}^T \\ BC_p & A & \dots & \mathbf{0} & \mathbf{0} & \dots & \mathbf{0} & \mathbf{0} \\ & & \ddots & & & & & \\ BC_p & \mathbf{0} & \dots & A & \mathbf{0} & \dots & \mathbf{0} & \mathbf{0} \\ \boldsymbol{0} & \mathbf{0} & \dots & \mathbf{0} & A & \dots & \mathbf{0} & \mathbf{0} \\ & & & & & \ddots & & \\ \boldsymbol{0} & \mathbf{0} & \dots & \mathbf{0} & \mathbf{0} & \dots & A & \mathbf{0} \\ \boldsymbol{0} & \mathbf{0} & \dots & \mathbf{0} & \mathbf{0} & \dots & \mathbf{0} & A \end{pmatrix}$$

$$B_c = \begin{pmatrix} B_p^T & 0^T & \dots & 0^T & B^T & \dots & B^T & 0^T \end{pmatrix}^T$$

$$B_{cr} = \begin{pmatrix} \mathit{0}^T & 0^T & \dots & 0^T & 0^T & \dots & 0^T & B^T \end{pmatrix}^T$$

$$C_c = \begin{pmatrix} C_p & 0^T & \dots & 0^T & 0^T & \dots & 0^T & 0^T \end{pmatrix}. \tag{5.35}$$

Here, zero matrices in A_0 are denoted as either $\mathbf{0} \in \mathbb{R}^{n_c l \times n_c l}$ or $\boldsymbol{0} \in \mathbb{R}^{n_c l \times nl}$. Zero matrices in the other terms are denoted as either $\mathit{0} \in \mathbb{R}^{nl \times l}$ or $0 \in \mathbb{R}^{n_c l \times l}$.

5.4.1 Ideal Parameter Case

Using the control signal $u^* = \Psi^T \Theta^*$ composed of the ideal parameter values, state the composite system dynamics as

$$\begin{aligned} \dot{Y}_c &= A_c Y_c + B_{cr} r \\ y &= C_c Y_c. \end{aligned} \tag{5.36}$$

Here the $B_c u^*$ term has been absorbed into A_0 to create A_c. However, an r to y transfer function expression already exists in Eq. (5.27). The supporting

discussion established that the matching condition causes the plant transfer function to equal that of the reference model when using the ideal control:

$$\begin{aligned} C_c(sI - A_c)^{-1}B_{cr} &= \beta_{du}(s)\beta_s(s)[a_f(s)\alpha_p(s) - M^*(s)\alpha_p(s) \\ &\quad - L^*(s)\beta_{du}(s)\beta_s(s)]^{-1}N^*b_f(s)\beta_r(s) \\ &= W_m(s). \end{aligned} \tag{5.37}$$

From this statement it is clear that (A_c, B_{cr}, C_c) can be used to express the dynamics of the reference model. Thus, the system

$$\begin{aligned} \dot{Y}_m &= A_c Y_m + B_{cr} r \\ y_m &= C_c Y_m \end{aligned} \tag{5.38}$$

is a permissible nonminimal representation for the reference model dynamics.

Before moving on note that the set of eigenvalues of A_c will be a subset of $\left\{S \in \mathbb{C} : \det\left[b_f(s)\alpha_m(s)\beta_s(s)\right] = 0\right\}$ because of the matching condition. This expression establishes that all eigenvalues of A_c will be stable due to the structure of $b_f(s)$, $\alpha_m(s)$, and $\beta_s(s)$. Since A_c is stable and r is bounded it is permissible to conclude that Y_m is also bounded.

5.4.2 Unknown Parameter Case

Next return to the composite system dynamics of Eq. (5.34) where the control is yet to be specified. Add and subtract $B_c\Psi^T\Theta^*$ from the $\dot{Y}_c$ equation to arrive at

$$\begin{aligned} \dot{Y}_c &= A_c Y_c + B_c(u - \Psi^T\Theta^*) + B_{cr} r \\ y &= C_c Y_c \end{aligned} \tag{5.39}$$

where A_c is the same as in the ideal parameter case. Defining $e = Y_c - Y_m$ and $z = y - y_m$ then selecting the control containing the updated parameter estimates $u = \Psi^T \Theta$ gives

$$\begin{aligned} \dot{e} &= A_c e + B_c(\Psi^T \tilde{\Theta}) \\ z &= C_c e. \end{aligned} \tag{5.40}$$

This composite error dynamics relationship will be used to facilitate stability analysis in the subsequent section.

5.5 Stability Analysis

To show that z goes to zero, define the Lyapunov-like function

$$V = \gamma \tilde{\Theta}^T(t) P^{-1}(t) \tilde{\Theta}(t) + \frac{1}{2} e(t)^T P_c e(t) + \frac{\gamma}{\epsilon} S(t) \tag{5.41}$$

where $P_c = P_c^T > 0$ and γ and ϵ are positive constants. Define the scalar quantity $S(t)$ and prescribe its evolution as

$$\dot{S}(t) = -S(t) \left(\tilde{\Theta}^T(t) \Psi(t) \Psi^T(t) \tilde{\Theta}(t) + c_s \right) + \epsilon w^2(t) \tag{5.42}$$

with $S(0) > 0$ and some constant $c_s > 0$. $S(t)$ will be shown to remain positive subsequently. Note that w is any bounded and persistently exciting scalar signal. Also note that since

$$\frac{d}{dt} \left[P(t) P^{-1}(t) \right] = \dot{P}(t) P^{-1}(t) + P(t) \frac{d}{dt} \left[P^{-1}(t) \right] = 0 \tag{5.43}$$

the derivative of P^{-1} becomes

$$\frac{d}{dt} \left[P^{-1}(t) \right] = -P^{-1}(t) \dot{P}(t) P^{-1}(t) = \Phi(t) \Omega^{-2}(t) \Phi^T(t) \tag{5.44}$$

after recalling Eq. (5.20). Since $P(0) > 0$ and the resetting procedure keeps P^{-1} bounded, both P and P^{-1} remain positive definite and bounded for all $t \geq 0$.

Taking the derivative of V and omitting function arguments where possible,

$$\dot{V} = 2\gamma\tilde{\Theta}^T P^{-1}\left[-P\Phi\Omega^{-2}z_s\right] + \gamma\tilde{\Theta}^T\left[\Phi\Omega^{-2}\Phi^T\right]\tilde{\Theta} + \frac{d}{dt}\left[\frac{1}{2}e^T P_c e\right] + \frac{\gamma}{\epsilon}\left[-S\left(\tilde{\Theta}^T\Psi\Psi^T\tilde{\Theta} + c_s\right) + \epsilon w^2\right]. \quad (5.45)$$

The alternate definition for z_s in Eq. (5.24) which permits the simplification

$$\dot{V} = -\gamma\|\Omega^{-1}\Phi^T\tilde{\Theta}\|^2 + \frac{d}{dt}\left[\frac{1}{2}e^T P_c e\right] - \frac{\gamma}{\epsilon}\|\Psi^T\tilde{\Theta}\|^2 S - \frac{\gamma c_s}{\epsilon}S + \gamma w^2. \quad (5.46)$$

Next establish the fact that $S(t)$ is positive. Using the same approach as in Eq. (5.43) and Eq. (5.44) it follows that

$$\frac{d}{dt}\left[S^{-1}\right] = \left(\tilde{\Theta}^T\Psi\Psi^T\tilde{\Theta} + c_s\right)S^{-1} - S^{-1}\left(\epsilon w^2\right)S^{-1}. \quad (5.47)$$

Note that $\Psi^T\tilde{\Theta}$ is assured to remain bounded through separate signal growth analysis summarized presented in Section 5.6. This result along with the persistently exciting signal w and $S(0) > 0$ makes leads to a familiar structure that ensures $S^{-1}(t)$ remains bounded and positive for $t \geq 0$ (see, for example, Chapter 4.3 in [8]). Equivalently, $S \geq \epsilon$. Utilizing this result, bounding the persistently exciting signal as $w_{\max} = \max_{t\geq 0} w^2(t)$, and selecting $c_s = w_{\max}$ gives

$$\dot{V} \leq -\gamma\|\Omega^{-1}\Phi^T\tilde{\Theta}\|^2 + \frac{d}{dt}\left[\frac{1}{2}e^T(t)P_c e(t)\right] - \gamma\|\Psi^T\tilde{\Theta}\|^2. \quad (5.48)$$

Now substitute the error dynamics for the composite system with $u(t) = \Psi^T(t)\Theta(t)$:

$$\dot{V} \leq -\gamma\|\Omega^{-1}\Phi^T\tilde{\Theta}\|^2 + \frac{1}{2}e^T(t)\left[P_cA_c + A_c^TP_c\right]e(t) + e^T(t)P_cB_c\Psi^T(t)\tilde{\Theta}(t) - \gamma\|\Psi^T\tilde{\Theta}\|^2. \tag{5.49}$$

Select $P_c = P_c^T > 0$ to be the matrix satisfying the Lyapunov equation

$$P_cA_c + A_c^TP_c = -Q_c \tag{5.50}$$

where $Q_c = Q_c^T > 0$. Note that it will be possible to find such a P_c and Q_c since A_c is stable. $\dot{V}$ becomes

$$\dot{V} \leq -\gamma\|\Omega^{-1}\Phi^T\tilde{\Theta}\|^2 - \frac{1}{2}e^T(t)Q_ce(t) + e^T(t)P_cB_c\Psi^T(t)\tilde{\Theta}(t) - \gamma\|\Psi^T\tilde{\Theta}\|^2. \tag{5.51}$$

Recall the eigenvalue relationship for quadratic forms

$$\lambda_{\min}(Q_c)\|e\|^2 \leq e^T(t)Q_ce(t) \leq \lambda_{\max}(Q_c)\|e\|^2 \tag{5.52}$$

and also note that

$$e^T(t)P_cB_c\Psi^T(t)\tilde{\Theta}(t) \leq c\|e\|\|\Psi^T\tilde{\Theta}\| \tag{5.53}$$

so long as $\|P_cB_c\| \leq c$. The derivative can then be bounded by

$$\dot{V} \leq -\gamma\|\Omega^{-1}\Phi^T\tilde{\Theta}\|^2 - \frac{1}{2}\lambda_{\min}(Q_c)\|e\|^2 + c\|e\|\|\Psi^T\tilde{\Theta}\| - \gamma\|\Psi^T\tilde{\Theta}\|^2. \tag{5.54}$$

Next complete the square to arrive at

$$\dot{V} \leq -\gamma\|\Omega^{-1}\Phi^T\tilde{\Theta}\|^2 - \frac{\gamma}{2}\|\Psi^T\tilde{\Theta}\|^2 - \frac{\gamma}{2}\left(\|\Psi^T\tilde{\Theta}\| - \frac{c}{\gamma}\|e\|\right)^2 - \left(\frac{\lambda_{\min}(Q_c)}{2} - \frac{c^2}{2\gamma}\right)\|e\|^2. \tag{5.55}$$

So long as $\gamma > \frac{c^2}{\lambda_{\min}(Q_c)}$ the coefficient of the last term will remain negative. $\dot{V}$ can then be bounded as

$$\dot{V} \leq -\gamma \|\Omega^{-1}\Phi^T\tilde{\Theta}\|^2 - \frac{\gamma}{2}\|\Psi^T\tilde{\Theta}\|^2 - \left(\frac{\lambda_{\min}(Q_c)}{2} - \frac{c^2}{2\gamma}\right)\|e\|^2. \tag{5.56}$$

The expression now permits the desirable conclusion $\dot{V} \leq 0$.

Since $V > 0$ and $\dot{V} \leq 0$, note that $\tilde{\Theta} \in \mathcal{L}_\infty$, $e \in \mathcal{L}_\infty$, and $S \in \mathcal{L}_\infty$. Additionally, observe that V_∞ exists such that $-\int_0^\infty \dot{V}(t)dt = V_0 - V_\infty \leq V_0$. From here conclude that $\Omega^{-1}\Phi^T\tilde{\Theta} \in \mathcal{L}_2$, $\Psi^T\tilde{\Theta} \in \mathcal{L}_2$, and $e \in \mathcal{L}_2$.

Next return to the error dynamics Eq. (5.40) to establish boundedness of $\dot{e}$. For this result note that since $e = Y_c - Y_m$ and Y_m is bounded due to the stability of A_c, Y_c is also bounded. The boundedness of Y_c's entries ensures that $\bar{y}_i$, $\bar{u}_i$, r_f, and thus Ψ are bounded. Therefore, $\dot{e} \in \mathcal{L}_\infty$ by Eq. (5.40).

Finally, the constant relationship between e and z permits the claims $\dot{z} \in \mathcal{L}_\infty$ and $z \in \mathcal{L}_\infty \cap \mathcal{L}_2$. The corollary to Barbalat's Lemma permits the conclusion that

$$\lim_{t\to+\infty} z(t) = \lim_{t\to+\infty} \big(y(t) - y_m(t)\big) = 0 \tag{5.57}$$

as desired.

5.6 $\Psi^T\tilde{\Theta}$ Boundedness

The mathematical results provided here establish boundedness of the regressor Ψ and related quantity $\Psi^T\tilde{\Theta}$ in surrogate tracking error MRAC error convergence proof. The procedure given is a modified version of that presented

in [9]. First several signal properties are established. Next, the growth rate of some signals when assuming unbounded behavior is shown to contradict the actual growth rates, establishing boundedness of all signals.

Theorem 5.6.1. *Let* $\Theta(t) \in \mathbb{R}^m$ *and* $\Phi(t) \in \mathbb{R}^{m\times l}$. *For the update laws in Eqs.* (5.19) *and* (5.20) *with covariance resetting, the surrogate tracking error definition in Eq.* (5.24)*, and the normalized version in Eq.* (5.25)*, the following results can be obtained:*

i Θ, $\tilde{\Theta} \in \mathcal{L}_\infty$

ii $\dot{\Theta} \in \mathcal{L}_2$

iii $\Omega^{-1} z_s \in \mathcal{L}_2$

iv ϵ, $\Phi\epsilon \in \mathcal{L}_2$.

Proof. Begin with the Lyapunov function

$$V_1(\tilde{\Theta}(t), P(t)) = \tilde{\Theta}^T(t) P^{-1}(t) \tilde{\Theta}(t). \tag{5.58}$$

Taking the derivative of V_1 and omitting function arguments where possible

$$\begin{aligned}
\dot{V}_1 &= 2\dot{\tilde{\Theta}}^T P^{-1}\tilde{\Theta} + \tilde{\Theta}^T \frac{d}{dt}\left[P^{-1}\right]\tilde{\Theta} \\
&= -2\tilde{\Theta}^T \Phi\Omega^{-2} z_s + \tilde{\Theta}^T \Phi\Omega^{-2}\Phi^T\tilde{\Theta} \\
&= -\tilde{\Theta}^T \Phi\Omega^{-2} z_s \\
&= -z_s\Omega^{-2} z_s.
\end{aligned} \tag{5.59}$$

Since $V_1 > 0$ and $\dot{V}_1 < 0$, $V_1(\infty)$ exists and is bounded. Thus $\tilde{\Theta}$ and therefore Θ are bounded demonstrating *(i)*. Additionally, integrating both sides demonstrates

$$V_1(0) - V_1(\infty) = \int_0^\infty z_s \Omega^{-2} z_s \, dt < \infty \tag{5.60}$$

and thus $\Omega^{-1} z_s \in \mathcal{L}_2$ establishing *(iii)*.

Since

$$\begin{aligned} z_s &= \Omega^2 \epsilon \\ &= \left(I_l + \eta \Phi^T \Phi \right) \epsilon \end{aligned} \tag{5.61}$$

the derivative of the Lyapunov function can also be stated as

$$\begin{aligned} \dot{V}_1 &= -z_s \Omega^{-2} z_s \\ &= -\epsilon^2 \Omega^2 \epsilon \\ &= -\epsilon^T \left(I_l + \eta \Phi^T \Phi \right) \epsilon \\ &= -\epsilon^T \epsilon - \eta \epsilon^T \Phi^T \Phi \epsilon. \end{aligned} \tag{5.62}$$

Integrating both sides,

$$V_1(0) - V_1(\infty) = \int_0^\infty \epsilon^T \epsilon \, dt + \eta \int_0^\infty \epsilon^T \Phi^T \Phi \epsilon \, dt < \infty \tag{5.63}$$

and ϵ, $\Phi\epsilon \in \mathcal{L}_2$ verifying *(iv)*.

Now turning to $\dot{\Theta}$, note that the norm of vector can be written as

$$\begin{aligned}
\|\dot{\Theta}\|_2^2 &= z_s^T \Omega^{-2} \Phi^T P^2 \Phi \Omega^{-2} z_s \\
&\leq \|\Omega^{-1} \Phi^T P^2 \Phi \Omega^{-1}\|_2 \|\Omega^{-1} z_s\|_2^2 \\
&\leq \lambda_{\max}^2(P) \|\Omega^{-1} \Phi^T \Phi \Omega^{-1}\|_2 \|\Omega^{-1} z_s\|_2^2 \\
&= \lambda_{\max}^2(P) \|\Phi \Omega^{-2} \Phi^T\|_2 \|\Omega^{-1} z_s\|_2^2 \\
&= \lambda_{\max}^2(P) \|\Phi \left[I_l + \Phi^T \Phi \right]^{-1} \Phi^T\|_2 \|\Omega^{-1} z_s\|_2^2
\end{aligned} \tag{5.64}$$

where the middle portion must be shown to be finite. Recall the matrix inversion result

$$(I + AB)^{-1} = I - A(I + BA)^{-1} B \tag{5.65}$$

and apply the equality to the inverted quantity

$$(I_l + \Phi^T \Phi)^{-1} = I_l - \Phi^T (I_m + \Phi \Phi^T)^{-1} \Phi. \tag{5.66}$$

Note that this can be rewritten as

$$\Phi^T (I_l + \Phi^T \Phi)^{-1} \Phi = I_l - (I_l + \Phi \Phi^T)^{-1}. \tag{5.67}$$

Also note that a similar application of Eq. (5.65) permits the statement

$$(I_m + \Phi \Phi^T)^{-1} = I_m - \Phi (I_l + \Phi^T \Phi)^{-1} \Phi^T \tag{5.68}$$

or equivalently

$$\Phi (I_l + \Phi^T \Phi)^{-1} \Phi^T = I_m - (I_m + \Phi \Phi^T)^{-1}. \tag{5.69}$$

Using these results

$$\begin{aligned}\|\Phi(I_l + \Phi^T\Phi)^{-1}\Phi^T\|_2 &= \|I_m - (I_m + \Phi\Phi^T)^{-1}\|_2 \\ &\leq 1 + \|(I_m + \Phi\Phi^T)^{-1}\|_2 \end{aligned} \tag{5.70}$$

Since $I_m + \Phi\Phi^T > 0$ and therefore $(I_m + \Phi\Phi^T)^{-1} > 0$ also, the statement can be made that

$$\begin{aligned}\|(I_m + \Phi\Phi^T)^{-1}\|_2 &\leq \frac{1}{\lambda_{\min}(I_m + \Phi\Phi^T)} \\ &\leq 1 \end{aligned} \tag{5.71}$$

where the fact that $\lambda(I + A) = 1 + \lambda(A) \geq 1$ if $A \geq 0$ was used for the last line.

Now going back to Eq. (5.70),

$$\begin{aligned}\|\Phi(I_l + \Phi^T\Phi)^{-1}\Phi^T\|_2 &\leq 1 + \|(I_m + \Phi\Phi^T)^{-1}\|_2 \\ &\leq 2. \end{aligned} \tag{5.72}$$

Finally, this result along with $\Omega^{-1}z_s \in \mathcal{L}_2$ and the fact that P remains bounded by the resetting procedure gives

$$\begin{aligned}\|\dot{\Theta}\|_2^2 &\leq \lambda_{\max}^2(P)\|\Phi\left[I_l + \Phi^T\Phi\right]^{-1}\Phi^T\|_2\|\Omega^{-1}z_s\|_2^2 \\ &\leq \infty \end{aligned} \tag{5.73}$$

and $\dot{\Theta} \in \mathcal{L}_2$ verifying *(ii)*. □

Theorem 5.6.2. *For the problem description in Section 5.1 and adaptive system in Section 5.2, the results of Theorem 5.6.1 can be used to show that*

$$\|z(t)\| = o\left[\sup_{\tau \leq t}\|\Psi(\tau)\|\right]. \tag{5.74}$$

Proof. Define $\bar{z} = z_s - z_f$ and then manipulate the filtered tracking error expression to obtain

$$\begin{aligned} z_f &= z_s - \bar{z} \\ G_{C_{f,1}}(s)\left[z\right] &= z_s - \bar{z} \\ z &= G_{C_{f,1}}^{-1}(s)\left[z_s - \bar{z}\right] \\ z &= G_{C_{f,1}}^{-1}(s)\left[\Omega^2\epsilon - \bar{z}\right]. \end{aligned} \tag{5.75}$$

Recall the definition for Ω to arrive at

$$z = G_{C_{f,1}}^{-1}(s)\left[\epsilon + \eta\Phi^T\Phi\epsilon - \bar{z}\right]. \tag{5.76}$$

Given that $G_{C_{f,1}}^{-1}(s)$ is an asymptotically stable, proper transfer function matrix of the form in Theorem 2.3.6, a more useful expression for the right side of Eq. (5.76) can be obtained. First, use the theorem and the fact that $\Omega^{-1}z_s \in \mathcal{L}_2$ to state

$$\begin{aligned} G_{C_{f,1}}^{-1}(s)\left[\epsilon\right] &= G_{C_{f,1}}^{-1}(s)\left[\Omega^{-2}z_s\right] \\ &= o\left[\sup_{\tau\leq t}\|\Omega^{-1}(\tau)\|\right]. \end{aligned} \tag{5.77}$$

Use Theorem 2.3.6 again, $\Phi\epsilon \in \mathcal{L}_2$, and the stable filter relationship between Φ and Ψ to reach

$$\begin{aligned} G_{C_{f,1}}^{-1}(s)\left[\Phi^T\Phi\epsilon\right] &= o\left[\sup_{\tau\leq t}\|\Phi(\tau)\|\right] \\ &= o\left[\sup_{\tau\leq t}\|\Psi(\tau)\|\right]. \end{aligned} \tag{5.78}$$

Treatment of the $\bar{z}$ term requires use of the swapping lemma Theorem 2.2.7 to state that

$$\begin{aligned}\bar{z} &= G_{C_{f,2}}(s)\left[\Psi^T\right]\Theta - G_{C_{f,2}}(s)\left[\Psi^T\Theta\right] \\ &= G_{C_{f,2C}}(s)\left[G_{C_{f,2B}}(s)\left[\Psi^T\right]\dot{\Theta}\right] \\ &= G_{C_{f,2C}}(s)\left[Q_B^T\dot{\Theta}\right] \end{aligned} \tag{5.79}$$

where $Q_B^T \triangleq G_{C_{f,2B}}(s)[\Psi^T]$. Recalling that $\dot{\Theta} \in \mathcal{L}_2$ permits the use of Theorem 2.3.6 to obtain

$$\begin{aligned} G_{C_{f,1}}^{-1}(s)\left[\bar{z}\right] &= G_{C_{f,1}}^{-1}(s)G_{C_{f,2C}}(s)\left[Q_B^T\dot{\Theta}\right] \\ &= o\left[\sup_{\tau\leq t}\|Q_B(\tau)\|\right]. \end{aligned} \tag{5.80}$$

The further claim

$$G_{C_{f,1}}^{-1}(s)\left[\bar{z}\right] = o\left[\sup_{\tau\leq t}\|\Psi(\tau)\|\right]. \tag{5.81}$$

can be made by noting that $G_{cf,2_B}(s)$ is an asymptotically stable transfer function.

Using the previous statements, Eq. (5.76) can be rewritten as

$$\|z(t)\| = o\left[\sup_{\tau\leq t}\|\Omega^{-1}(\tau)\|\right] + o\left[\sup_{\tau\leq t}\|\Psi(\tau)\|\right]. \tag{5.82}$$

The first term of the right side is uniformly bounded and can be dropped to obtain

$$\|z(t)\| = o\left[\sup_{\tau\leq t}\|\Psi(\tau)\|\right]. \tag{5.83}$$

□

Theorem 5.6.3. *For the problem description in Section 5.1 and adaptive system in Section 5.2, if the signals of the system grow in an unbounded fashion (i.e.* $\lim_{t\to\infty} \sup_{\tau\leq t} \|x(\tau)\| = \infty$*) then it follows that*

$$\|\Psi(t)\| = \mathcal{O}\left[\sup_{\tau\leq t} \|z(\tau)\|\right]. \tag{5.84}$$

Proof. Consider two transfer functions, $G_{C_{f,2}}(s)$ and $F(s)$, arranged in series. $G_{C_{f,2}}(s)$ is defined by Eq. (5.15) and $F(s)$ is user-choice subject to requirements specified subsequently. The composite system is given the input $\Psi^T\tilde{\Theta}$ and is depicted in Fig. 5.3. Note that the output of $G_{C_{f,2}}(s)$ is z_f according to Eq. (5.23).

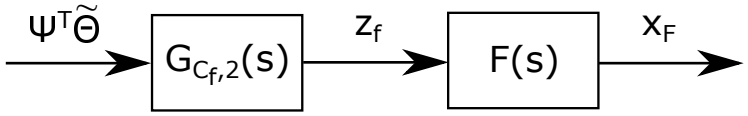

Figure 5.3: Composite system used in Theorem 5.6.3

A minimal state space representation of the $G_{C_{f,2}}(s)$ portion of the system is given by

$$\begin{aligned} \dot{x}_G &= A_G x_G + B_G \Psi^T \tilde{\Theta} \\ z_f &= C_G x_G. \end{aligned} \tag{5.85}$$

A state space representation for the $F(s)$ portion of the system is given by

$$\dot{x}_F = A_F x_F + B_F z_f. \tag{5.86}$$

The composite system can be represented by

$$\dot{\bar{x}} = \bar{A}\bar{x} + \bar{B}\Psi^T\tilde{\Theta} \tag{5.87}$$

where

$$\bar{x} = \begin{bmatrix} x_F \\ x_G \end{bmatrix}, \quad \bar{A} = \begin{bmatrix} A_F & B_F C_G \\ 0 & A_G \end{bmatrix}, \quad \bar{B} = \begin{bmatrix} 0 \\ B_G \end{bmatrix}. \tag{5.88}$$

$F(s)$ and its state space representation must be chosen so that it is exponentially stable, $(A_F, B_F C_G)$ is controllable, and $(\bar{A}, \bar{B})$ is controllable.[1]

According to the process outlined in Appendix C of [9], note that Ψ is the effective state of the adaptive system and satisfies

$$\|\dot{\Psi}(t)\| \leq c\|\Psi(t)\| + c \tag{5.89}$$

where c is a finite positive constant. Accordingly, $\Psi^T\tilde{\Theta} \in \epsilon$ since $\tilde{\Theta}$ is bounded. Thus, it is permissible to apply Theorem 2.3.5 to the system in Eq. (5.88) to obtain

$$\sup_{\tau \leq t} \|\Psi^T(\tau)\tilde{\Theta}(\tau)\| = \mathcal{O}\left[\sup_{\tau \leq t} \|\bar{x}(\tau)\|\right]. \tag{5.90}$$

Next, since (A_G, B_G) is controllable and $\Psi^T\tilde{\Theta} \in \epsilon$, application of Theorem 2.3.5 to the system in Eq. (5.85) yields

$$\sup_{\tau \leq t} \|\Psi^T(\tau)\tilde{\Theta}(\tau)\| = \mathcal{O}\left[\sup_{\tau \leq t} \|x_G(\tau)\|\right] \tag{5.91}$$

or correspondingly

$$\|\Psi^T(t)\tilde{\Theta}(t)\| = \mathcal{O}\left[\sup_{\tau \leq t} \|x_G(\tau)\|\right]. \tag{5.92}$$

[1]This is always possible. For example, consider $F(s) = \frac{1}{s+\alpha} I_l$ and use the rank test in [67]. Also, $(A_F, B_F C_G)$ controllability is assured by $(\bar{A}, \bar{B})$ controllability [68].

However since the same system also leads to

$$\|\dot{x}_G\| \leq c\|x_G\| + c\|\Psi^T\tilde{\Theta}\|, \tag{5.93}$$

it follows that

$$\|\dot{x}_G\| \leq c \sup_{\tau \leq t} \|x_G(\tau)\| + c \tag{5.94}$$

and thus $x_G \in \epsilon$.

Use $z_f = C_G x_G$ to rewrite the $F(s)$ system in Eq. (5.86) as

$$\dot{x}_F = A_F x_F + B_F C_G x_G. \tag{5.95}$$

A final application of Theorem 2.3.5 to this system is now possible since $(A_F, B_F C_G)$ is controllable and $x_G \in \epsilon$ and results in

$$\sup_{\tau \leq t} \|x_G(\tau)\| = \mathcal{O}\left[\sup_{\tau \leq t} \|x_F(\tau)\|\right]. \tag{5.96}$$

Also note that Theorem 2.3.3 can be used with the original $F(s)$ dynamics in Eq. (5.86) to claim that

$$\sup_{\tau \leq t} \|x_F(\tau)\| = \mathcal{O}\left[\sup_{\tau \leq t} \|z_f(\tau)\|\right]. \tag{5.97}$$

since A_F is exponentially stable.

Now consider the state vector of the composite system $\bar{x} = [x_F^T \; x_G^T]^T$. Since Eq. (5.96) bounds the growth of x_G with that of x_F, Theorem 2.3.2 can be used to claim that

$$\sup_{\tau \leq t} \|\bar{x}(\tau)\| \sim \sup_{\tau \leq t} \|x_F(\tau)\|. \tag{5.98}$$

Subsequent use of Eq. (5.97) provides the additional result that

$$\sup_{\tau \leq t} \|\bar{x}(\tau)\| = \mathcal{O}\left[\sup_{\tau \leq t} \|z_f(\tau)\|\right]. \tag{5.99}$$

Finally, combination of Eqs. (5.90) and (5.99) results in

$$\sup_{\tau \leq t} \|\Psi^T(\tau)\tilde{\Theta}(\tau)\| = \mathcal{O}\left[\sup_{\tau \leq t} \|z_f(\tau)\|\right]. \tag{5.100}$$

Dropping the supremum on the left side and recalling that $\tilde{\Theta}$ is bounded gives

$$\|\Psi(t)\| = \mathcal{O}\left[\sup_{\tau \leq t} \|z_f(\tau)\|\right]. \tag{5.101}$$

The stable, minimum phase, proper transfer function $G_{C_{f,1}}(s)$ that relates input z to output z_f permits use of Corollary 2.3.4 to state that

$$\sup_{\tau \leq t} \|z(\tau)\| \sim \sup_{\tau \leq t} \|z_f(\tau)\|. \tag{5.102}$$

Use of this result in Eq. (5.101) established the theorem's claim that

$$\|\Psi(t)\| = \mathcal{O}\left[\sup_{\tau \leq t} \|z(\tau)\|\right]. \tag{5.103}$$

□

The result of Theorem 5.6.2 contradicts the result of Theorem 5.6.3 obtained when it is assumed that signals in the system grow unbounded (see Theorem 2.3.7). Therefore, all signals in the feedback system are uniformly bounded including the regressor Ψ. The quantity in question $\Psi^T\tilde{\Theta}$ will be bounded as well due to previously established boundedness of $\tilde{\Theta}$.

5.7 Estimated Zero Location Modification

One important disturbance source that must be considered is the possibility of error in the required knowledge of the plant's nonminimum phase zero structure $\beta_{du}(s)$. If this structure is not perfectly known then the previous error convergence proof no longer holds. However, some robustness to zero error is expected even though it is not mathematically demonstrated [20].

Zero error will be considered in each of the simulations presented in the dissertation. The error is incorporated by replacing $\beta_u(s)$ in Eq. (5.2) with an estimate. Assuming that the user-known estimate of the necessary zeros is given by the $l \times l$ polynomial matrix $\beta'_u(s)$ and the error of that estimate is given by the $l \times l$ polynomial matrix $\Delta(s)$, the following expression for $\beta_{du}(s)$ can be formed:

$$\begin{aligned}\beta_{du}(s) &= \sum_{i=1}^{l} \beta_{d_i} \left[\beta'_u(s) + \Delta(s)\right] e^i \\ &= \sum_{i=1}^{l} \beta_{d_i}\beta'_u(s)e^i + \sum_{i=1}^{l} \beta_{d_i}\Delta(s)e^i \\ &= \beta'_{du}(s) + \beta_{du,\Delta}(s). \end{aligned} \tag{5.104}$$

Here $\beta'_{du}(s)$ serves as the known estimate of $\beta_{du}(s)$, and $\beta_{du,\Delta}(s)$ represents the error of the estimate. Thus, only $\beta'_{du}(s)$ can be used for implementation. The reference model is then given by

$$W_m(s) = \alpha_m^{-1}(s)\beta_{d_m}\beta'_{du}(s)\beta_r(s) \tag{5.105}$$

and the $G_{C_{f,2}}(s)$ filter by

$$G_{C_{f,2}}(s) = a_f(s)C_f^{-1}(s)\beta'_{du}(s) \tag{5.106}$$

in the zero error case. The rest of the implementation remains the same.

5.8 Aeroelastic Pitch and Plunge Model

Consider the MIMO and potentially nonminimum phase, unstable plant dynamics given by the aeroelastic response of an aircraft wing model described in [38]. Although relatively simple, this system has many of the features necessary to demonstrate the output tracking capability of the surrogate tracking error MRAC design and will be used in subsequent simulations. The system has two inputs, leading-edge control surface deflection δ and trailing-edge control surface deflection ζ, and two outputs, pitch angle α and plunge displacement h. A cross-sectional view is given in Fig. 5.4.

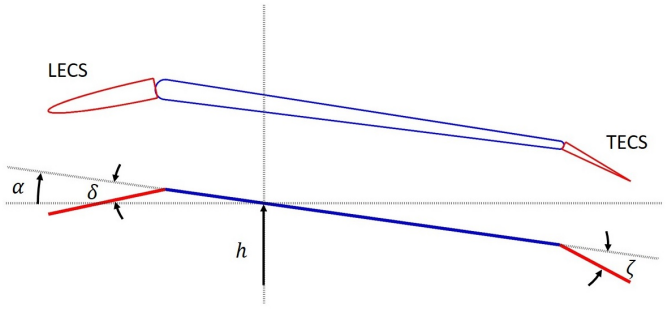

Figure 5.4: Pitch and plunge wing model

The equations of motion for the wing are given by

$$\begin{bmatrix} I_\alpha & m_W x_\alpha b \\ m_W x_\alpha b & m_t \end{bmatrix} \begin{Bmatrix} \ddot{\alpha} \\ \ddot{h} \end{Bmatrix} + \begin{bmatrix} c_\alpha & 0 \\ 0 & c_h \end{bmatrix} \begin{Bmatrix} \dot{\alpha} \\ \dot{h} \end{Bmatrix} + \begin{bmatrix} k_\alpha(\alpha) & 0 \\ 0 & k_h \end{bmatrix} \begin{Bmatrix} \alpha \\ h \end{Bmatrix} = \begin{Bmatrix} M(t) \\ -L(t) \end{Bmatrix}. \quad (5.107)$$

The lift L and moment M are given by

$$L = \rho U^2 b s C_{l_\alpha} \left[\alpha + \left(\frac{\dot{h}}{U} \right) + \left(\frac{1}{2} - a \right) b \left(\frac{\dot{\alpha}}{U} \right) \right] + \rho U^2 b s C_{l_\zeta} \zeta + \rho U^2 b s C_{l_\delta} \delta \quad (5.108)$$

$$M = \rho U^2 b^2 s C_{m_{\alpha-\text{eff}}} \left[\alpha + \left(\frac{\dot{h}}{U} \right) + \left(\frac{1}{2} - a \right) b \left(\frac{\dot{\alpha}}{U} \right) \right] + \rho U^2 b^2 s C_{m_{\zeta-\text{eff}}} \zeta + \rho U^2 b^2 s C_{m_{\delta-\text{eff}}} \delta \quad (5.109)$$

where $C_{m_{\alpha-\text{eff}}} = \left(\frac{1}{2} + a\right) C_{l_\alpha} + 2C_{m_\alpha}$, $C_{m_{\zeta-\text{eff}}} = \left(\frac{1}{2} + a\right) C_{l_\zeta} + 2C_{m_\zeta}$, and $C_{m_{\delta-\text{eff}}} = \left(\frac{1}{2} + a\right) C_{l_\delta} + 2C_{m_\delta}$. The polynomial nonlinearity $k_\alpha(\alpha)$ is of the form described in [41] and is given by $k_\alpha(\alpha) = k_{\alpha_0} + k_{\alpha_1}\alpha + k_{\alpha_2}\alpha^2$. The equations of motion can be restated more conveniently using the state vector $\mathbf{x} = [\alpha \;\; h \;\; \dot{\alpha} \;\; \dot{h}]^T$ as

$$\begin{aligned} \dot{\mathbf{x}} &= \begin{bmatrix} 0_{2\times2} & I_{2\times2} \\ A_1 & A_2 \end{bmatrix} \mathbf{x} + \begin{bmatrix} 0_{2\times1} \\ g \end{bmatrix} k_{n_\alpha}(\alpha) + \begin{bmatrix} 0_{2\times2} \\ B \end{bmatrix} \begin{Bmatrix} \zeta \\ \delta \end{Bmatrix} \\ y &= \begin{bmatrix} I_{2\times2} & 0_{2\times2} \end{bmatrix} \mathbf{x} \end{aligned} \quad (5.110)$$

where $k_{n_\alpha}(\alpha) = \alpha(k_{\alpha_1}\alpha + k_{\alpha_2}\alpha^2)$. A_i, g, and B are all constant matrices whose structures can be derived from the equation of motion. Notice that the system is nonlinear due to the $k_{n_\alpha}(\alpha)$ term, and thus for the current investigation only

the linear portion of the system is considered:

$$\dot{\mathbf{x}} = \begin{bmatrix} 0_{2\times2} & I_{2\times2} \\ A_1 & A_2 \end{bmatrix} \mathbf{x} + \begin{bmatrix} 0_{2\times2} \\ B \end{bmatrix} \begin{Bmatrix} \zeta \\ \delta \end{Bmatrix}$$
$$y = \begin{bmatrix} I_{2\times2} & 0_{2\times2} \end{bmatrix} \mathbf{x}. \tag{5.111}$$

Relevant parameter values are shown in [41], also summarized in Table 5.1, where the freestream velocity U is variable.

Table 5.1: Parameter values for wing pitch and plunge simulation

Parameter	**Value**
U	variable
ρ	1.225 kg/m^3
a	-0.6719
b	0.1905 m
r_{cg}	$-b(0.0998 + a)$
x_α	r_{cg}/b
s_p	0.5945 m
c_h	27.43 kg/s
c_α	0.0360 kg·m^2/s
m_{wing}	4.340 kg
m_W	5.230 kg
m_t	15.57 kg
I_{cam}	0.04697 kg·m^2
I_{cg}	0.04342 kg·m^2
I_α	$I_{\text{cam}}+I_{\text{cg}}+m_{\text{wing}}r_{\text{cg}}^2$
$C_{l\alpha}$	6.757
$C_{l\beta}$	3.774
$C_{l\gamma}$	-0.1566
$C_{m\alpha}$	0
$C_{m\beta}$	-0.6719
$C_{m\gamma}$	-0.1005
k_h	2844
k_{α_0}	12.77
k_{α_1}	53.47
k_{α_2}	1003

5.8.1 Surrogate Tracking Error MRAC Simulation

The surrogate tracking error MRAC design presented earlier in the chapter is now applied to control of the linear version of the pitch and plunge dynamics. Selecting the freestream velocity $U = 11.5$ m/s makes the linear sys-

tem's dynamics unstable with poles at 0.3077±12.7954i and -1.8107±12.3545i and gives transmission zeros at -1.8137±12.3550i and 0.3105±12.7943i. Note that for this choice $\alpha_p(s) = (s^4+3.006s^3+317.5s^2+497.3s+25541)I_2$. Selecting $\beta_s(s) = I_2$ means that $\beta_{du}(s)$ decomposes as

$$\beta_u(s) = \begin{bmatrix} s^2 + 3.522s + 287.2 & s^2 + 2.2s + 155.7 \\ s^2 - 1.551s + 49.1 & s^2 + 2.432s + 166.9 \end{bmatrix} \tag{5.112}$$

$$\beta_{d,1}(s) = \begin{bmatrix} -37.4813 & 0 \\ 0 & -3.1840 \end{bmatrix} \tag{5.113}$$

$$\beta_{d,2}(s) = \begin{bmatrix} -6.0386 & 0 \\ 0 & 0.4101 \end{bmatrix} \tag{5.114}$$

according to Eq. (5.2). For the reference model choose $\alpha_m(s) = (s + 9)^5$, $\beta_{d_m}(s) = 10 \cdot I_2$, and $\beta_r(s) = I_2$. For the filters select $n_c = 9$, $a_f(s) = (s + 3.1)^{n_c}$, $b_f(s) = (s+3)^{n_c+n_u+d-n_m}$, and $C_f(s) = b_f(s)\alpha_m(s)I_2$. The normalizing quantity is constructed using $\eta = 1$. The reference signal is $r = [-1 \;\; 10]^T$. For the simulation select $\mathbf{x}(0) \neq 0$ and $P(0) = 1 \cdot 10^{15} I_{2n_c+1}$. P is reset to its initial value when $\lambda_{\min}(P(t)) \leq 0.01$. All other initial conditions are zero.

The output tracking performance is shown in Fig. 5.5 for the control law given by Eq. (5.13), the update laws given by Eqs. (5.19) and (5.20), and the settings described. The commanded control surface deflections are given in Fig. 5.6. The control is able to bring the both outputs of the plant to match the outputs of the reference model asymptotically.

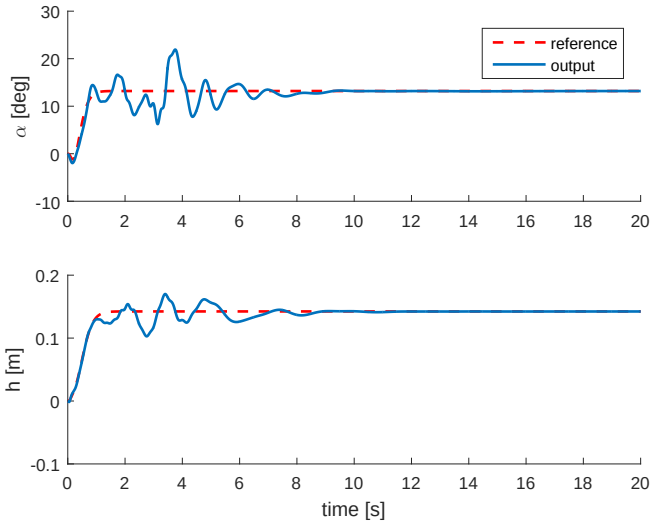

Figure 5.5: (Top) Pitch angle α and (Bottom) plunge displacement h of the controlled plant and reference model

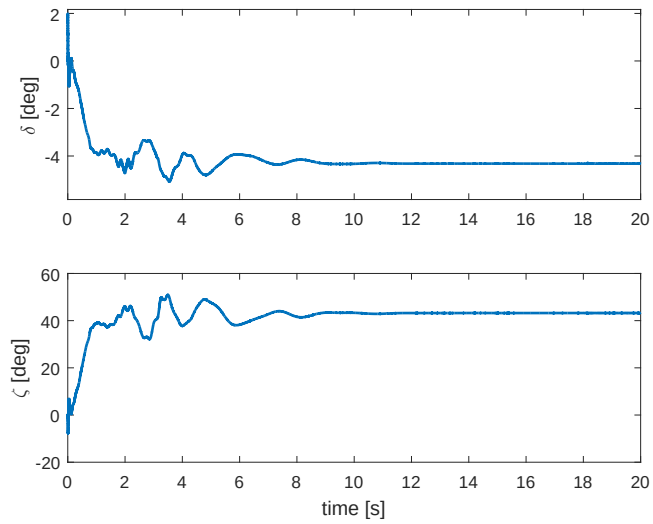

Figure 5.6: (Top) Leading edge control surface deflection δ and (Bottom) trailing edge control surface deflection ζ

Next consider the same simulation but with error in knowledge of the zeros contained in $\beta_{du}(s)$. As an example, assume that that $\beta_u(s)$ is unknown and instead a known estimate is given by

$$\beta'_u(s) = \begin{bmatrix} s^2 - 6.478s + 287.2 & s^2 - 0.7996s + 140.7 \\ s^2 - 6.551s + 49.1 & s^2 + 2.432s + 216.9 \end{bmatrix}. \tag{5.115}$$

This error of the estimate is therefore

$$\Delta(s) = \begin{bmatrix} 10s & 3s + 15 \\ 5s & -50 \end{bmatrix} \tag{5.116}$$

Leaving $\beta_{d,1}(s)$ and $\beta_{d,2}(s)$ the same, $\beta'_{du}(s)$ is constructed according to Eq. (5.104) and used in the reference model and $G_{C_{f,2}}(s)$ instead of $\beta_{du}(s)$. The original $\beta_{du}(s)$ is still used to simulate the plant. All other parameters remain the same.

The output tracking performance for this instance of zero error is given in Fig. 5.7. It is clear that the adaptive system is still able to track the desired reference trajectory despite the imperfect zero knowledge, although transient performance is degraded. The commanded control surface deflections are shown in Fig. 5.8 and display a similarly increased demands in the transient.

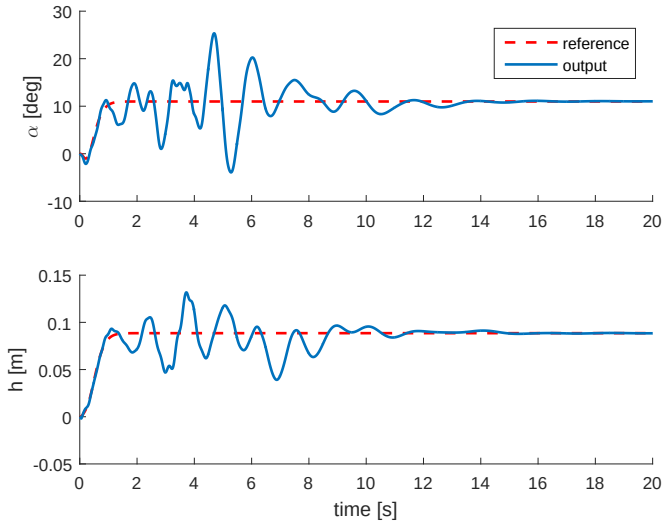

Figure 5.7: (Top) Pitch angle α and (Bottom) plunge displacement h of the controlled plant and reference model, acceptable error in zero knowledge

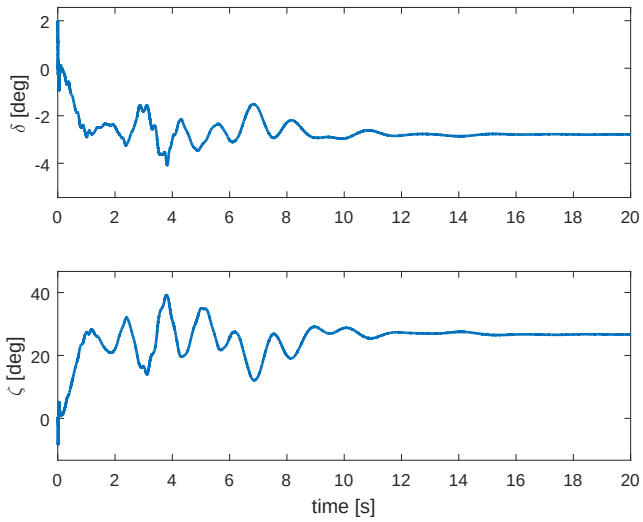

Figure 5.8: (Top) Leading edge control surface deflection δ and (Bottom) trailing edge control surface deflection ζ, acceptable error in zero knowledge

While the previous example demonstrates that the control design is robust to some error in zero location knowledge, the next example illustrates that this is not universally true. Consider again the same simulation now with an estimate for $\beta_u(s)$ that does not have the same number of zeros in each entry, such as

$$\beta_u'(s) = \begin{bmatrix} -6.478s + 287.2 & s^2 - 0.7996s + 140.7 \\ s^2 - 6.551s + 49.1 & s^2 + 2.432s + 216.9 \end{bmatrix}. \tag{5.117}$$

Here the (1,1) entry has only one root instead of the two actually contained in the plant dynamics. The error of the estimate is given by

$$\Delta(s) = \begin{bmatrix} s^2 + 10s & 3s + 15 \\ 5s & -50 \end{bmatrix}. \tag{5.118}$$

Note that this type of zero error will be particularly relevant to applications involving aircraft in changing flight conditions explored in the dissertation's later chapters. The output tracking performance and control signals are provided in Figs. 5.9 and 5.10. However, the adaptive system is unable to stabilize the plant.

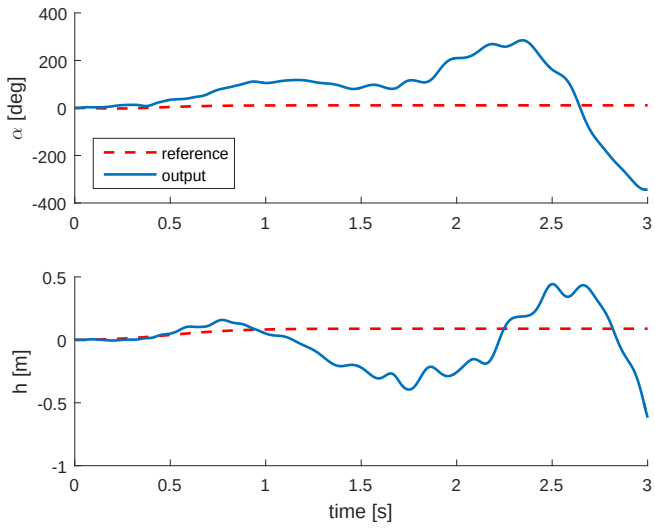

Figure 5.9: (Top) Pitch angle α and (Bottom) plunge displacement h of the controlled plant and reference model, unacceptable error in zero knowledge

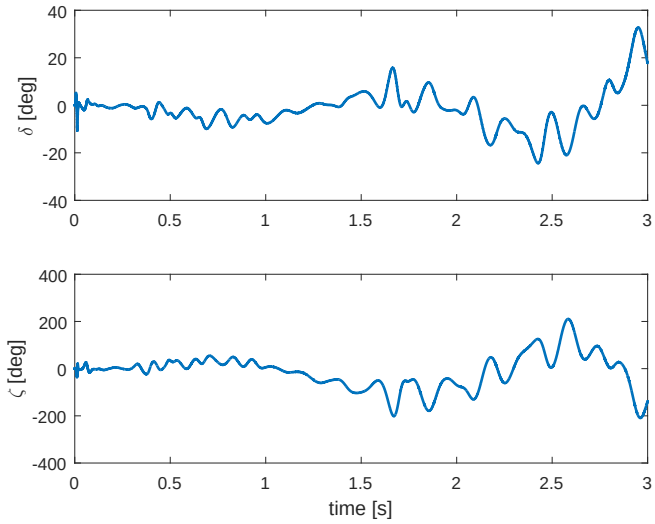

Figure 5.10: (Top) Leading edge control surface deflection δ and (Bottom) trailing edge control surface deflection ζ, unacceptable error in zero knowledge

The adaptive system fails similarly anytime a $\beta'_{du}(s)$ is used that contains a different number of zeros in a given entry than $\beta_{du}(s)$. However, the adaptive system may successfully control the system, provide residual set convergence, or fail if the zero location estimates are simply incorrect. Generally speaking, performance is sensitive to estimating zero locations to be further left than they actually are and estimating nonminimum phase zeros as minimum phase. The safest scenario appears to be using a $\beta'_{du}(s)$ that contains the correct number of zeros in each entry and, if not fully known, estimating their locations to be safely to the right of where they might feasibly reside.

5.8.2 Nonlinear Dynamics Comparison

Later in the dissertation dynamic simulations of a full flexible wing aircraft based on linear models will be presented. However, in reality the flexible aircraft is influenced by nonlinear effects such as control surface dynamics and limitations, nonuniform stiffness effects, and aerodynamic nonlinearities as flight conditions approach transonic [69]. As a nonlinear dynamic model would be difficult to generate for even a small aspect of the full system and very little flight data is currently available, the state-of-the-art analysis methods for highly flexible aircraft rely on creation of many linear models to represent the aircraft's behavior over a range of flight conditions. The appropriate model is selected and swapped out as necessary for the conditions currently being simulated.

The validity of the linear model approach is a topic that merits at least

brief discussion. Due to the aforementioned issues, quantifying the inaccuracy of linear model use for the flexible aircraft configuration is difficult. However, a nonlinear description does exit for the aeroelastic wing pitch and plunge model presented in [38] and used for simulation in Chapter 5. The model will be used to justify linear model use for the aircraft in the absence of any other suitable options.

First consider the nonlinear equations of motion for the pitch and plunge model stated in Eq. (5.110) as well as the linear versions given in Eq. (5.111) and the parameter values stated in Table 5.1. A small initial pitch displacement and velocity of $\alpha = 0.05$ rad and $\dot{\alpha} = 0.1$ rad/sec are provided to the model at a freestream velocity $U = 10$ m/s (comfortably below a freestream velocity resulting in limit cycle oscillations). The results of the corresponding linear and nonlinear simulations are compared in Fig. 5.11 and are largely similar.

However, it is also necessary to explore the validity of linear model use as the flight condition deviates from the flight condition used to generate the linear model. This comparison is accomplished by holding the linear model constant and comparing its performance to the nonlinear dynamics at various other freestream velocities. Figure 5.12 presents such a comparison where the linear model used in all panels is that generated at $U = 10$ m/s. The nonlinear dynamics used in the top panels are also those associated with $U = 10$ m/s while the nonlinear dynamics in the middle panels are from $U = 9$ m/s and the bottom panels are from $U = 5$ m/s. While the performance of the linear model

is still reasonably close to that nonlinear dynamics in the $U = 9$ m/s case, the deviation between the two is notable in the $U = 5$ m/s case. This helps establish a general limit on the range of flight conditions that can be covered by a single linear model before another linear model should be utilized.

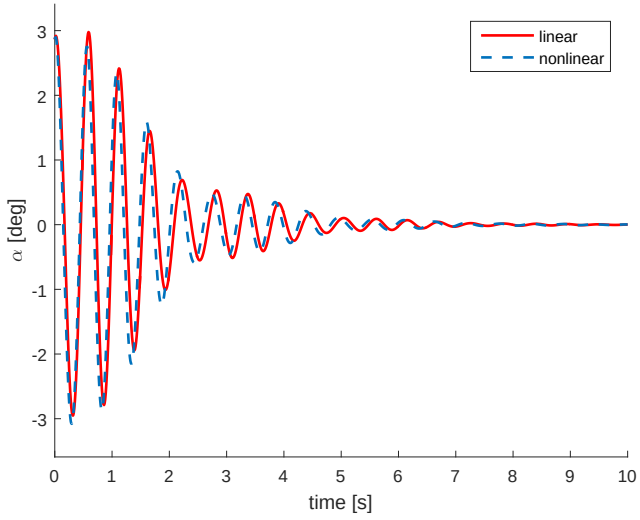

(a) α

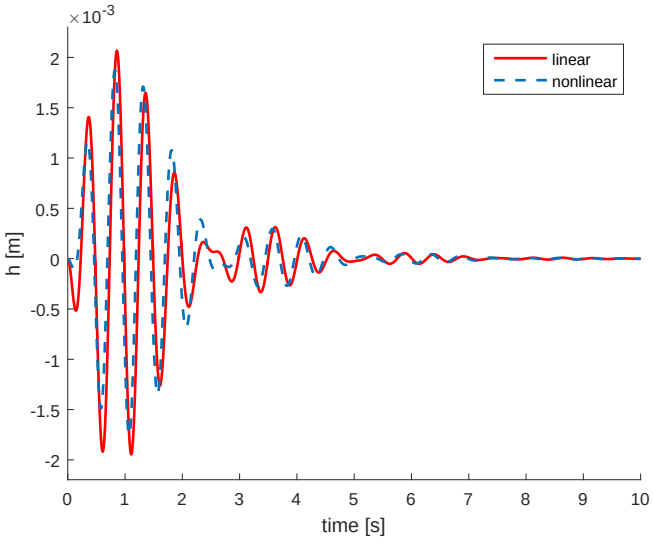

(b) h

Figure 5.11: Comparison of linear and nonlinear versions of pitch and plunge aeroelastic wing dynamics at freestream velocity $U = 10$ m/s

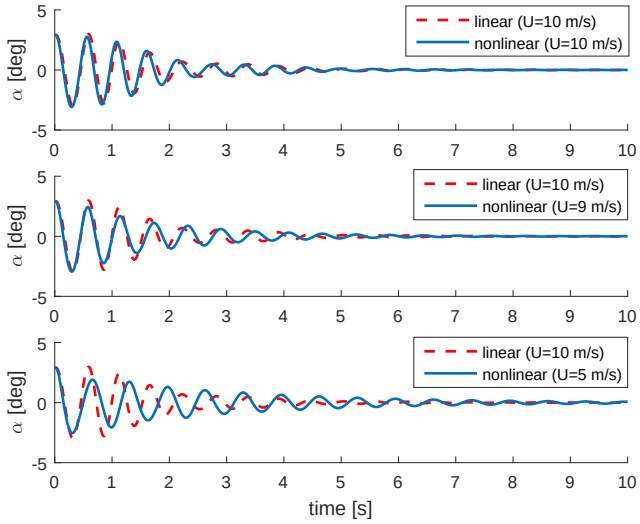

(a) α

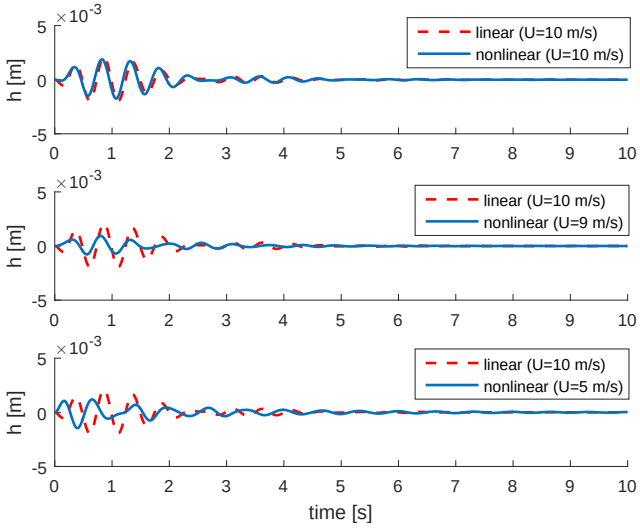

(b) h

Figure 5.12: Comparison of linear version of pitch and plunge aeroelastic wing dynamics at freestream velocity $U = 10$ m/s and nonlinear version various freestream velocities

Chapter 6

Flexible Aircraft Flight Control

The surrogate tracking error MRAC approach is now applied to flight control of the same flexible aircraft used to demonstrate the PFC version of MRAC in Chapter 3. After developing the aircraft–specific implementations of the nominal and delta laws, the partitioned control design is used to demonstrate flight path angle command tracking much improved over the performance of the aircraft's existing nonadaptive control law. Robustness to nonminimum phase zero error and nominal model inaccuracy is also considered.

6.1 Control Law Input/Output Assignment

As mentioned previously, the input and output assignments for the nominal and delta control laws are a critical implementation decision. In this paper the goal is use the two control laws to track the desired flight path angle γ. The throttle, all wing flaps, and both body flaps are available as control inputs. For the nominal law, an existing nonadaptive control law utilizing the eight wing flap and throttle as inputs is used. Outputs are the total velocity, bank angle, pitch rate, roll rate, and six accelerometers shown in Fig. 2.4. As

Table 6.1: Surrogate tracking error MRAC input and output assignments for flight path angle tracking

	Nominal Control System	**Delta Control System**
Inputs	all WFs, throttle	BF R & BF L
Outputs	γ, all accelerometers, velocity bank angle, pitch & roll rates	γ

the goal is to provide desirable flight path angle tracking, the delta control law uses the two body flaps that remain as inputs and only γ as output. A summary of the input and output assignments is provided in Table 6.1.

The body flaps, however, are treated as a single unit for the purposes of the delta control implementation by sending the same command to each flap. This signal copying behavior is accomplished by taking the delta system to be the sum of transfer functions from BF L to γ and BF R to γ. The delta system thus becomes a SISO implementation instead of MIMO, and only a scalar u_Δ signal is computed. The signal is then sent to both BF L and BF R. This structure seeks to prevent roll coupling and is appropriate for the γ command tracking goal.

Prior to this study the body flaps remained unused in control designs for the aircraft. Flight data suggests that their impact on flight dynamics is currently poorly modeled. The desire to design a secondary, adaptive control law stems largely from this modeling uncertainty. Rather than ignoring the body flaps as available control surfaces or attempting to design a control law

for them using unsatisfactory models, they are assigned as control inputs for an adaptive law. With an adaptive law there is less need for an accurate model beforehand, making body flap portion of the system a useful candidate for such an implementation.

Note that the proposed input and output selection leaves some of the system outputs unmanaged by the delta control law. For example, the accelerometers are only used by the nominal control law. Although the delta law does not use the accelerometers, its operation still impacts them. Important but delta–unmanaged quantities such as these must be monitored for unacceptable performance changes when the two control laws are used together.

6.2 State Space Modeling

The linear state space aircraft models used for control design and simulation were generated for a grid of flight conditions that cover speeds ranging from 50 to 150 KEAS and fuel weight ranging from 0 to 80 lbs. This range comfortably covers boundaries for various types of flutter. Each of the models, generated primarily using a finite element model of the aircraft and the ZAERO aeroservoelastic modeling software package, are linear. The models include rigid body dynamics, flexible mode dynamics, unsteady aerodynamic force approximations, and actuator dynamics.

The raw ZAERO models are often not appropriate for control design purposes. Specifically, they can be high order depending on the number of

modes included and the accuracy desired in the unsteady aerodynamic forces rational function approximation. They can also be numerically ill-conditioned due to the selected speed of the actuator dynamics. Careful consideration must be given to the choices made when creating these models for the purpose of control design to keep the order and condition number sufficiently small. Additional model reduction steps involving the removal of certain states can also be undertaken as were discussed in Chapter 3.

In this paper the performance of the control law is demonstrated in simulation using the reduced linear models. The reduced models are split into the nominal and delta partitions based on the input and output assignments discussed in Section 6.1. Initially, the reduced nominal model is assumed to be known exactly for the purposes of determining $\bar{y}_n$. Later, error in this knowledge of the nominal partition is introduced to assess robustness. The delta partition is always composed of the reduced delta model which remains unknown to the control system.

6.3 Aircraft Control Implementation

The nominal law was designed using an modern control methodology where the objective of the flight control laws was to stabilize multiple unstable flutter modes while providing reasonably good tracking performance. The design is not detailed here for security reasons. However, similar control methodologies can be found in [37, 70–73].

While the nominal law does provide acceptable performance, some is-

sues are not fully addressed by the nominal controller. Notably, the inaccurate modeling of the body flaps made it difficult to incorporate them into the nominal control design. Subsequently, the body flaps remained unused in previous control implementations for the vehicle. Additionally, the aggressively unstable Phugoid mode requires a balance to be struck between nominal law stability margins and tracking performance. The γ tracking response in particular has room for improvement due to its extended settling time.

The delta law utilizes the partitioned adaptive control design described in Chapter 3 along with the SISO structure discussed in Section 6.1. The first task is to design the delta reference model and then use it to recover the full reference model. The delta reference model is formed by choosing $\beta_u(s)$ to contain the two nonminimum phase zeros seen in the transfer function resulting from the addition of transfer functions from BF L to γ and BF R to γ. The gain β_d is also recovered from this model. No additional zeros are to be included and thus $\beta_r(s) = 1$. The order of the delta reference model is selected to satisfy assumption **M1** and poles are clustered near $s = -6.5$. β_{dm} is set to 20 and, considering the nominal design, causes $y_{\Delta,r}$ to constitute about 30% of the total γ value to be tracked. The selections are then used to construct $W_\Delta(s)$.

The portion of the closed loop nominal system from the γ command to the output γ is acquired by closing the nominal loop and setting all other reference commands to zero. The resulting expression is taken to be $W_n(s)$ and, in this paper, will first be used directly as the estimated nominal system $\bar{W}_n(s)$

and then perturbed before being used as $\bar{W}_n(s)$. Finally, the full reference model for the combined body flaps to γ is obtained from $W_r(s) = \bar{W}_n(s) + W_\Delta(s)$. The output of $W_r(s)$ is what the entire control system attempts to track.

6.4 Simulation Results

To demonstrate the performance of the proposed design, the control law is simulated in use with a linear model of the aircraft dynamics at a selected speed and weight case just past the body freedom flutter boundary. Flight path angle tracking performance is compared as various uncertainties are introduced. The polynomials used in the filter designs are $a_f(s) = (s+2)^{n_c}$, $b_f(s) = (s+3)^{n_c+n_u+d-n_m}$, and $C_f(s) = (s+4)^{n_c+n_u+d}$. The filter degree n_c is selected according to Eq. (5.9). Initial conditions for all filters are zero. P_0 is set to $1e17I$ and reset to P_0 when $\lambda_{\min}(P(t)) \leq 0.01$. The factor $\eta = 1$ is used to construct $\Omega(t)$. For all simulations shown, the plant is given a nonzero initial displacement. Also note that all signals have been scaled by reference values for security purposes. The same reference value for a given type of signal is used for all results (i.e. every γ plot uses the same γ_{ref} scaling factor).

6.4.1 Perfect Knowledge Case

Figure 6.1 demonstrates the command tracking ability of the control design with perfect knowledge of all information required. For this simulation the nominal portion of the plant is used directly as the nominal model. The

nonminimum phase zeros of the delta portion of the plant are known and used in the delta reference model. The rest of the delta portion is unknown but linear. No disturbances or uncertainties are considered. Figure 6.1(a) shows the flight path angle output when controlled by the nominal law alone versus the nominal and delta laws together. The original doublet command that the nominal law tracks is also shown along with the implied command generated by the full reference model that the nominal + delta system tracks. Figure 6.1(b) shows the surface deflection of the body flaps in response to the delta control signal.

For the quick doublet command considered here, the delta law is able to offer improved tracking performance over the nominal law alone. The output is closer to the command during the doublet maneuver and the settling time is faster. The delta control signal also has neither unreasonably large magnitude nor rate of change. Figure 6.2 shows some of the outputs unmanaged by the delta control law. Recall that the in this situation the delta law has the potential to disrupt their behavior provided by the nominal law. However the resulting performance of these outputs, while degraded by use of the delta law, is not undesirable.

Before introducing error, the percentage of the tracking task allocated to the delta system should be investigated. As mentioned the preceding results were obtained by setting the delta system to be 30% of the total. In other words, design parameters were chosen such that $y_{\Delta,r}$ is 30% of y_r and $\bar{y}_n$ is 70%. The split can be adjusted by altering the gains of the closed-loop nom-

inal model and delta reference model while ensuring that the total tracking value y_r does not change. Figure 6.3 shows a comparison of such an allocation variation. Three cases are presented: 10% allocated to the delta system, 30%, and 50%. All signals are scaled by the same reference values used in the previously considered 30% case. Figure 6.3(a) demonstrates that, in the perfect knowledge case, marginally better performance is obtained with 50% delta allocation. However, Fig. 6.3(b) shows a significant increase the maximum delta control surface deflection for the high percentage case while the low percentage case experiences a more substantial transient after the doublet command. The body flaps used by the delta law also have target deflection limits that must be kept in mind when selecting the control authority distribution. The insignificant performance gain of the 50% case does not merit the increased commanded deflection. The 30% delta allocation is therefore retained for the remainder of the paper.

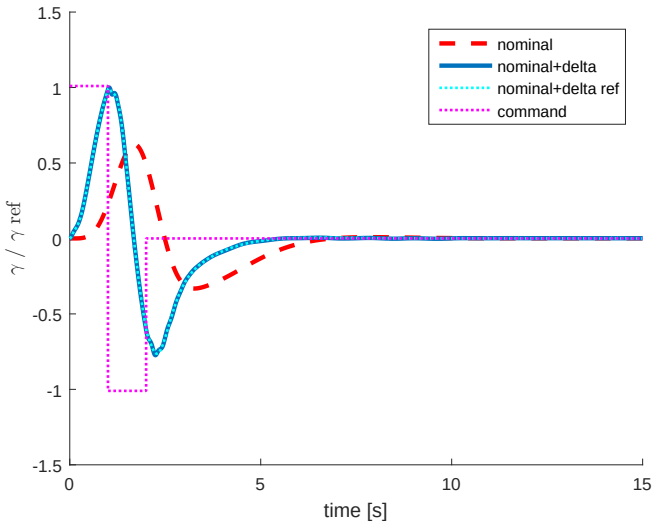

(a) γ

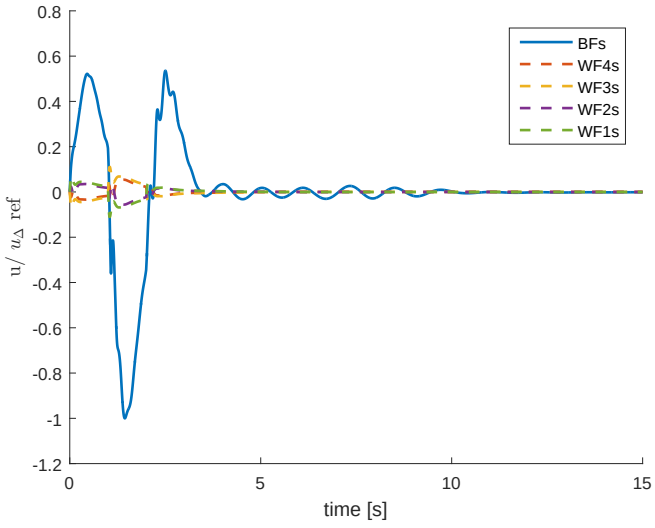

(b) u_Δ

Figure 6.1: Flight path angle doublet command tracking performance using perfect nominal model and nonminimum phase zero knowledge

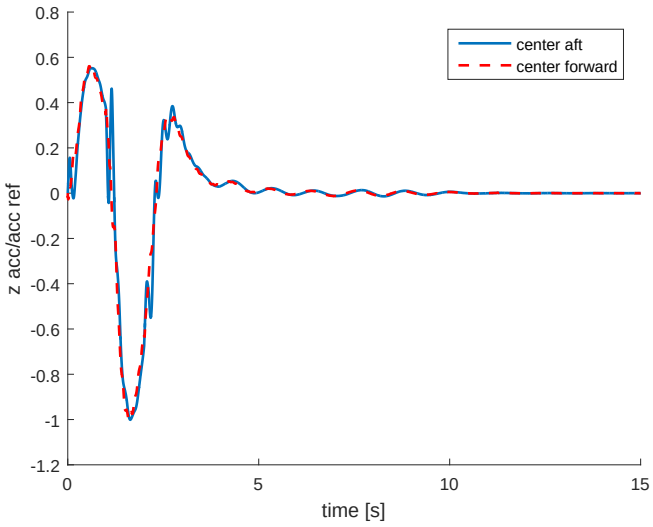

(a) Center body accelerometer signals

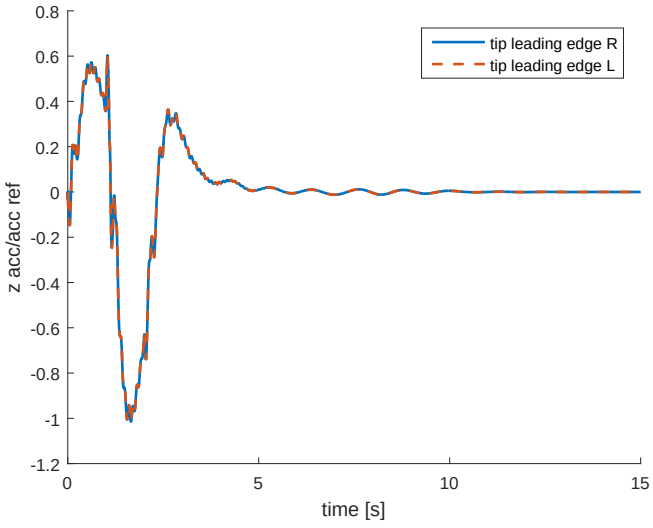

(b) Tip leading edge accelerometer signals

Figure 6.2: Response of output signals unmanaged by the delta control law when both laws in use, perfect knowledge case

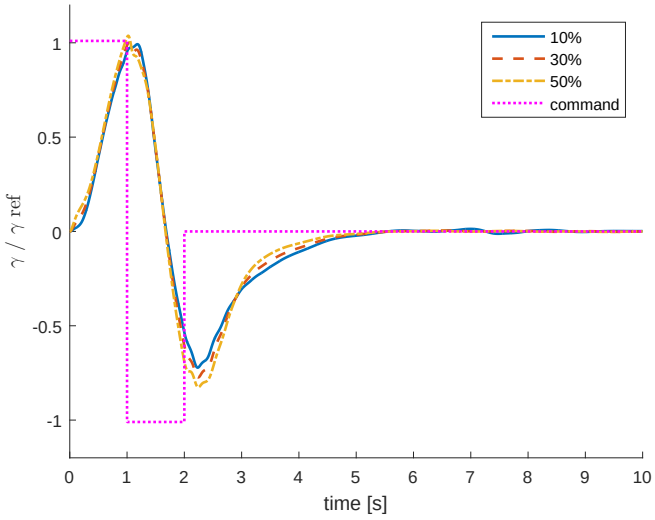

(a) γ

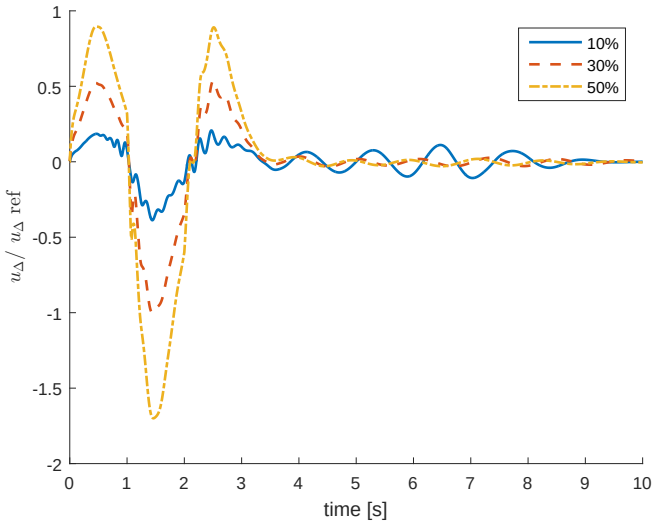

(b) u_Δ

Figure 6.3: Performance comparison of tracking task percentage allocated to delta system, perfect knowledge case

6.4.2 Estimated Nonminimum Phase Zeros

The same simulation is repeated now with error in the knowledge of the delta portion's nonminimum phase zeros. All other aspects of the simulation remain the same. Here, the estimated location of these zeros is set to halfway between the zeros from the speed and weight case used for aircraft simulation and the zeros from an adjacent case. However, only adjacent cases with the same number of nonminimum phase zeros can be used. Attempting to use a $\beta'_{du}(s)$ with more or less zeros than the real $\beta_{du}(s)$ results in divergence. Figures 6.4 and 6.5 shows the results of moving the nonminimum phase zeros halfway to the next mass case (10 lbs more fuel than the perfect case), halfway to the previous mass case (10 lbs less fuel), and halfway to the next speed case (10 KEAS faster). The case using nonminimum phase zeros shifted towards a slower speed are not included as this changes the number of nonminimum phase zeros and is below the flutter boundary. Results for perfect knowledge of the nonminimum phase zeros is also included for comparison. Note that shifting the nonminimum phase zeros towards those at a faster speed case or lower mass case has the effect of pushing them further into the right half plane than the true nonminimum phase zeros, i.e. the estimates are "more" unstable than the truth.

Figure 6.4(a) shows the tracking performance with the nonminimum phase zero error in response to the same doublet command used in the previous simulation. Similar tracking of the doublet is observed, but some small oscillation is noted as the signal settles for the shifted mass case. Much more

significant oscillation is seen with the shifted speed zeros, though the error ultimately converges. Figure 6.4(b) contains the body flap command for each case. Similar behavior is seen with the shifted mass cases having slightly larger oscillation and the shifted speed case having significantly larger oscillation. However, all cases remain within reasonable flap deflection limits. Figure 6.5 shows some of the unmanaged outputs which also display corresponding decaying oscillations.

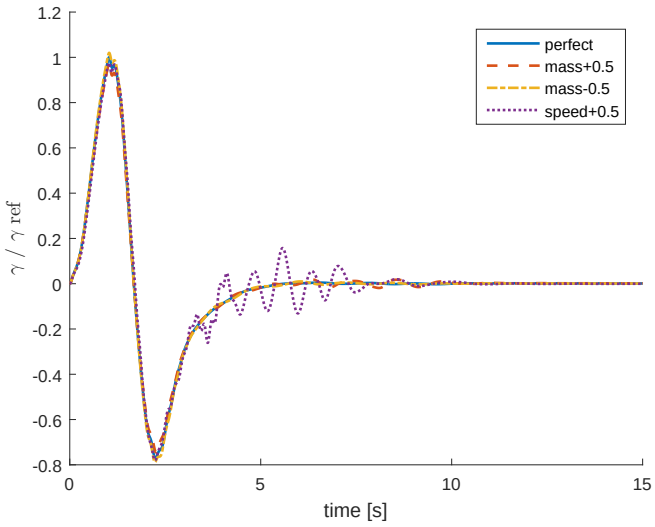

(a) γ

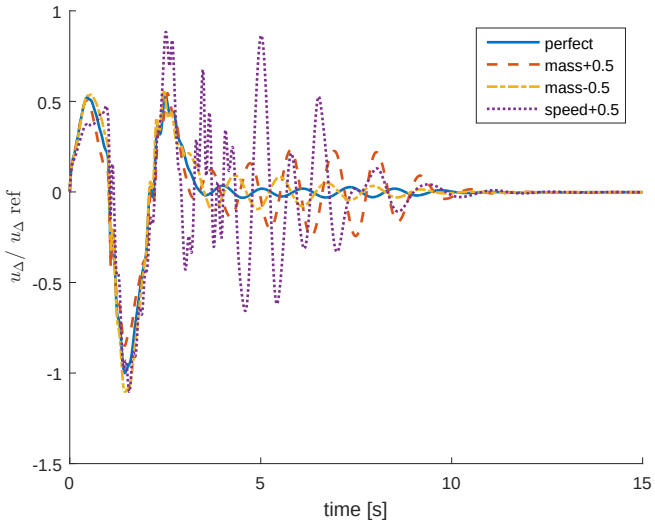

(b) u_Δ

Figure 6.4: Flight path angle doublet command tracking performance using perfect nominal model and estimated nonminimum phase zero locations

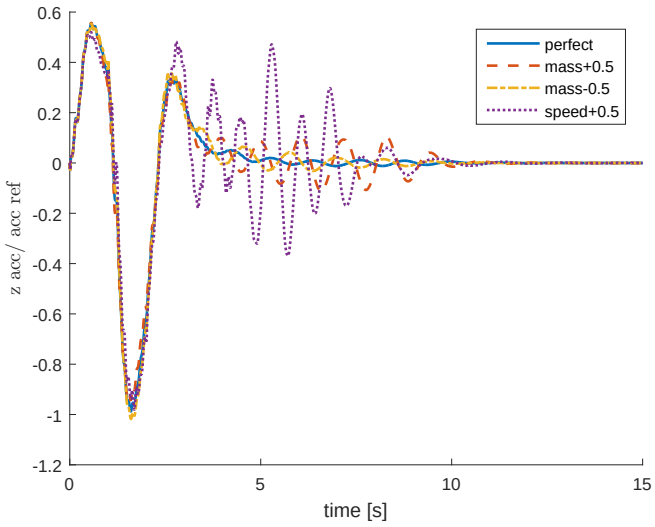

(a) Center body accelerometer signals

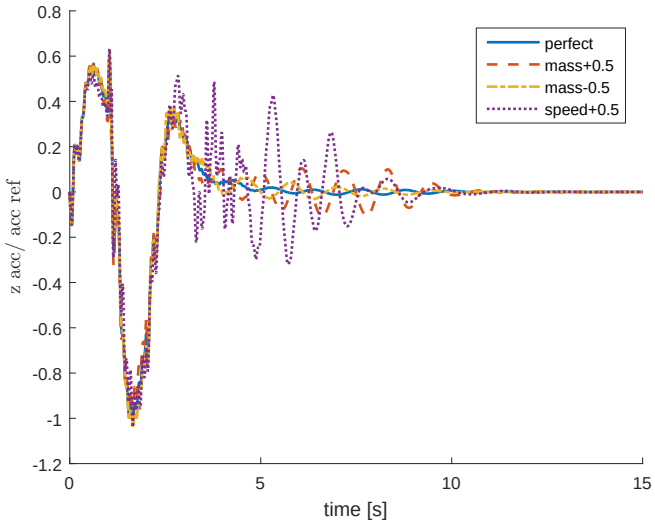

(b) Tip leading edge accelerometer signals

Figure 6.5: Response of output signals unmanaged by the delta control law when both laws in use, estimated nonminimum phase zero case

6.4.3 Estimated Nonminimum Phase Zeros and Incorrect Nominal Model

Finally, the simulation is again repeated with nonminimum phase zero error in addition to a nominal model that does not match the nominal portion of the plant. Here, the aircraft simulation is executed using the model from the same speed and weight condition as the previous two simulations. Estimated nonminimum phase zeros used in the control implementation are taken to be those shifted halfway to the next speed case (the worst case shown in Fig. 6.4). Nominal models from three different adjacent cases are then used including the next mass case (10 lbs more fuel), previous mass case (10 lbs less fuel), and next speed case (10 KEAS faster). Figures 6.6 and 6.7 display the results of each estimated zero, incorrect nominal model case compared to the case with only the estimated nonminimum phase zeros.

Figure 6.6(a) shows the tracking performance in response to the same doublet command with the various incorrect nominal models and consistent nonminimum phase zero error included. Command tracking using lower mass and higher speed nominal models is comparable to or better than using the correct nominal model. Use of a nominal model from the higher mass case, which is closer to the flutter boundary than the case used for aircraft simulation, results in significantly worse tracking performance. Similar trends are seen for the delta control signal in Fig. 6.6(b) with the control signal from the higher mass case becoming uncomfortably large. Figure 6.7 shows the unmanaged outputs which demonstrate the same performance trends.

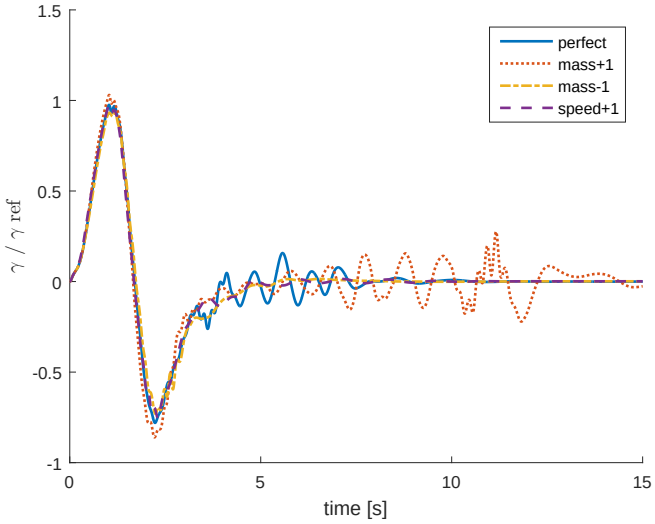

(a) γ

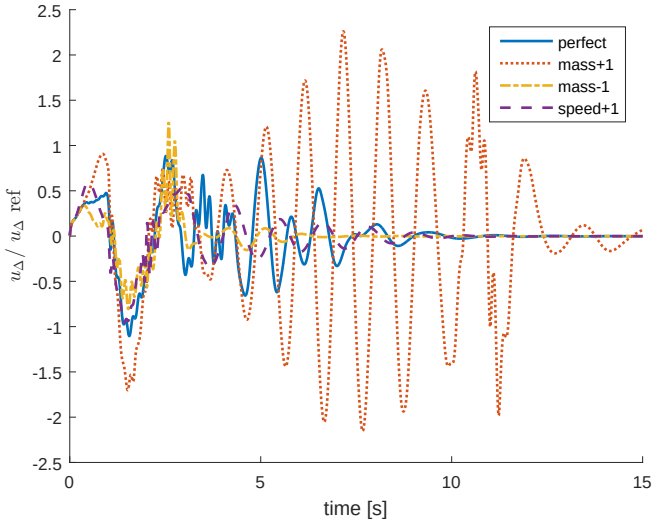

(b) u_Δ

Figure 6.6: Flight path angle doublet command tracking performance using various incorrect nominal models and consistent estimated nonminimum phase zero locations

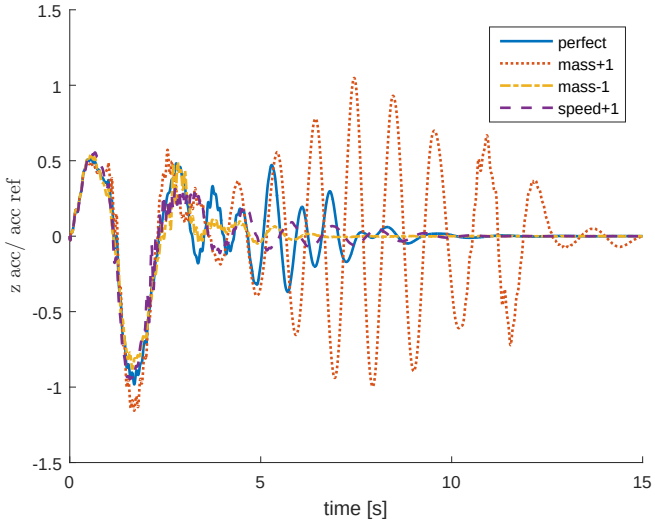

(a) Center body accelerometer signals

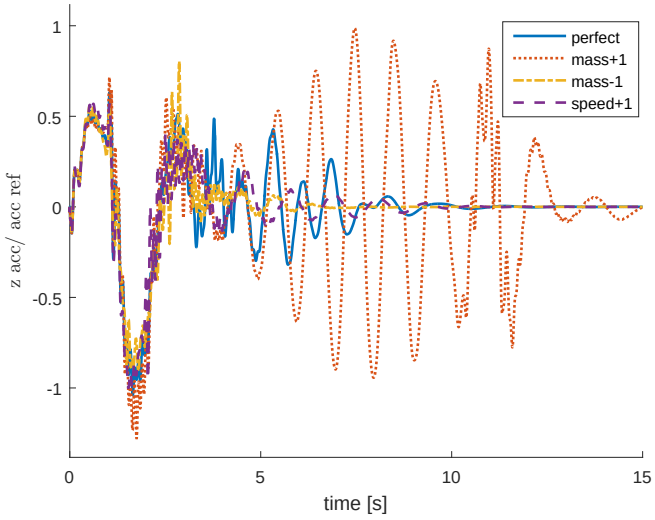

(b) Tip leading edge accelerometer signals

Figure 6.7: Response of output signals unmanaged by the delta control law when both laws in use, incorrect nominal model and estimated nonminimum phase zero case

Chapter 7

Flexible Aircraft Aeroservoelastic Control

The partitioned surrogate tracking error MRAC design is finally investigated for flexible motion stabilization of the same experimental aircraft. To accomplish this implementation, a simplified model of the aircraft wing is created to assist in the input assignment decision. The simple wing is then used to test various input combinations for the nominal and delta laws and systematically establish an intelligent input arrangement. The selected design is then ported back to the full aircraft for performance analysis. Simulations are performed to assess the benefits offered by the partitioned design compared to those offered by the existing nonadaptive control law. Nonminimum phase zero and nominal model error are progressively included as for the flight control implementation.

7.1 Simple Wing Model

A simple model of the flexible aircraft's wing is created to investigate control surface assignments for the nominal and delta laws. The simple wing is modeled as a thin rectangular plate with four flaps. No body flap is included in the simple model nor will the body flap on the aircraft be used for flexible

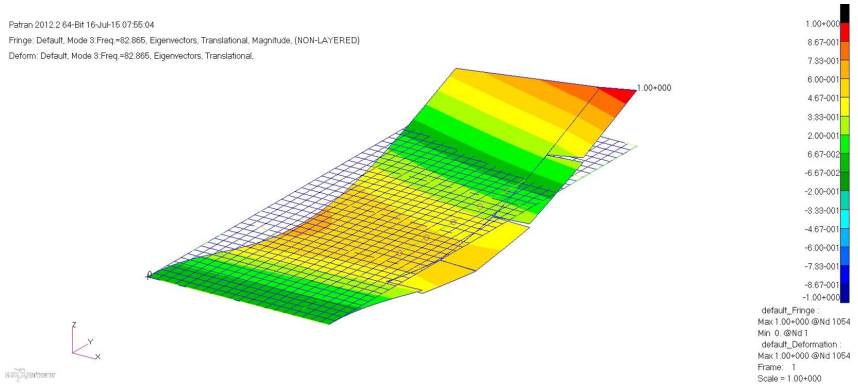

Figure 7.1: Finite element model for simple wing with four control surfaces

motion control. The simple wing model is similar to the physical wing model utilized in the experimental investigation of [74] save for the presence of the control surfaces. Characteristics of the simple wing will be compared to the experimental wing to ensure that the simulated results are realistic.

First, a finite element model of the simple wing is constructed to match the shape and properties of the experimental wing. The simple wing is modeled to be much smaller than the aircraft wing at 11.5 in x 4.56 in x 0.065 in and is made of aluminum. The "body" edge of the model is held fixed. Four rectangular 2 in x 0.912 in portions are separated from the trailing edge of the wing and are reattached with two torsional springs each to serve as the flaps. The resulting model is shown in Fig. 7.1.

Next, the finite element model is used to create aeroservoelastic state space models of the simple wing at various flight conditions. This is accomplished using the aeroelastic design software ZAERO and requires the user to specify further details about the model's sensing and actuating capabilities.

Rotation about the hinge line of each flap defines the model's control inputs. Third-order actuator dynamics are specified to create realistic command execution. The actuator dynamics are chosen to be four times faster than the flutter frequency of the wing. Accelerometers are included at various locations by selecting availability of acceleration measurement in the vertical axis at chosen finite element grid points. The sensor and actuator arrangement used for the simple wing is summarized in Fig. 7.2.

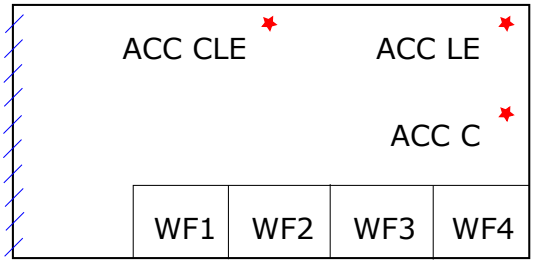

Figure 7.2: Input and output diagram for simple wing including flap and accelerometer abbreviations

Additional choices regarding flexible motion representation of the wing can be made to adjust the fidelity of the resulting state space models. However, fidelity must be balanced with system order and numerical conditioning as the ultimate goal is to use the models for simulation and control design. To help control the system order, only the first five mode shapes are included. Figure 7.3 illustrates these modes and provides their frequencies. Additionally, 2% damping is included on each mode. The unsteady aerodynamic forces are incorporated using a rational function approximation based on Roger's formula [75] with a third-order approximation used for each of the modes

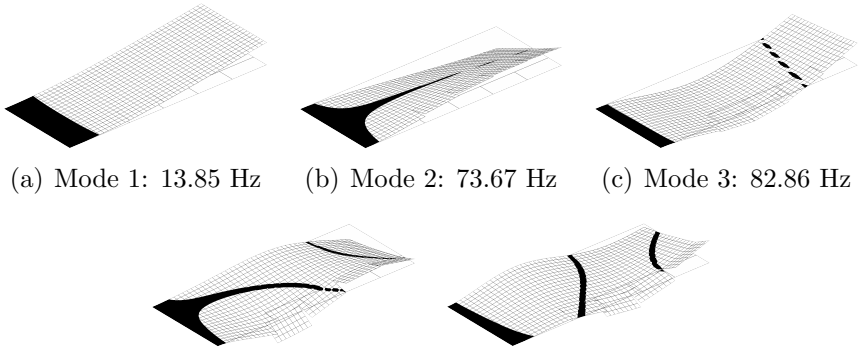

(a) Mode 1: 13.85 Hz (b) Mode 2: 73.67 Hz (c) Mode 3: 82.86 Hz

(d) Mode 4: 214.2 Hz (e) Mode 5: 225.3 Hz

Figure 7.3: First five mode shapes of simple wing

included.

Finally, several state space models are created to emulate the range of flight conditions explored with the experimental wing. In [74], behavior of the experimental wing over a wide flow velocity range is analyzed in a wind tunnel at sea level using freon as the medium. Correspondingly, ZAERO is used to generate aeroservoelastic state space models of the simple wing for Mach numbers M=0.1 to M=0.9 also at sea level in the same freon medium. Each of the resulting models has 10 modal displacement and velocity states, 15 aero lag states, and 12 actuator states. Rigid body dynamics are not included.

The flutter characteristics of the simple wing are summarized in the speed vs. damping and speed vs. frequency plots shown in Fig. 7.4. The line of squares indicates that there is one flutter mode at 208.7 KEAS and 39 Hz. The line of circles indicates divergence at 245.1 KEAS. Note that the experimental wing with no control surfaces exhibits a flutter mode at 217 KEAS and 35.5 Hz as well as divergence at 263.6 KEAS. The flexible motion

characteristics of the simple wing model seem reasonable in comparison to the experimental wing given the addition of the flaps.

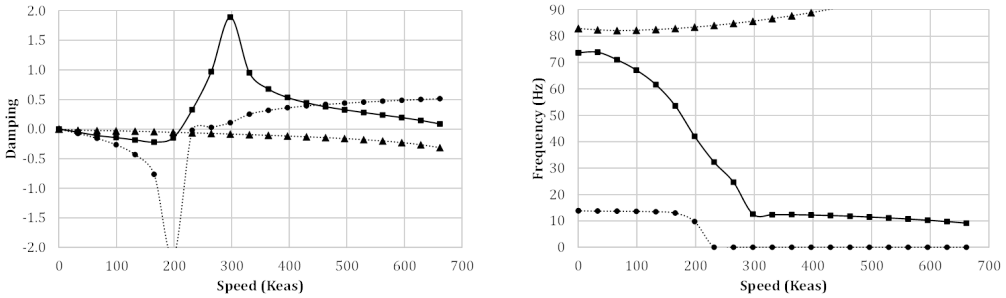

(a) Speed vs. damping

(b) Speed vs. frequency

Figure 7.4: Simple wing flutter analysis plots

With a physically reasonable wing model the next step is to investigate control surface assignments for the nominal control law. All possible combinations of control surfaces WF 3, WF 2, and WF 1 are considered as inputs for the nominal law. Use of WF 4 is preemptively reserved for the delta law as it is likely the most effective surface for flutter suppression and aids in reducing the number of nominal input options. Accelerometers ACC LE, ACC C, and/or ACC CLE are used for feedback depending on how many control surfaces are used such that the nominal system is square.

The goal is to determine sensible input assignments for the nominal law to suppress vibratory motion. Simulations utilizing each possible input combination are compared to select an effective nominal input arrangement before the delta law is considered. The model generated for M=0.714, which lies on the flutter boundary for the experimental wing and is just past the

flutter boundary for the simple wing, is used to test each configuration. A similar pole placement design acts as the nominal controller in each case to establish a fair comparison. Every input combination tested has two unstable poles which are moved to s=-1 and s=-1.2. The remaining poles are left at their original stable locations. The same nonzero initial displacement is given to the wing in each simulation.

Figure 7.5 shows the results of assigning each possible combination of WF 1, WF 2, and WF 3 to the nominal law. In Figure 7.5(a) the resulting error magnitude of the ACC LE accelerometer signal is shown. Figure 7.5(b) shows the total control effort required. The top panel in each graphic provides the results of using each of the three flaps on their own. The middle panel shows the results from each combination of two flaps. The last panel gives the result for use of all three flaps together. The error plot for single control use demonstrates an unacceptably large transient making use of any single control surface infeasible. The plots for dual surface use demonstrate a much improved result with the WF 3 and WF 2 combination having slightly smaller error and control effort need than the other combinations. Use of all three surfaces produces results similar to the dual surface results making it unnecessary to use three flaps instead of just two for the nominal implementation. Therefore, WF 3 and WF 2 will serve as inputs for the nominal control law and WF 1 will left available for the delta control law in addition to the already reserved WF 4.

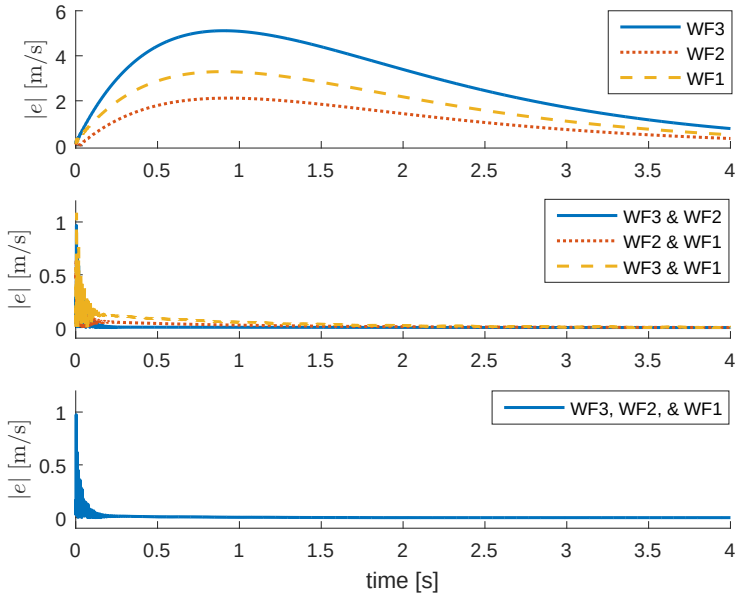

(a) Error magnitude at ACC LE

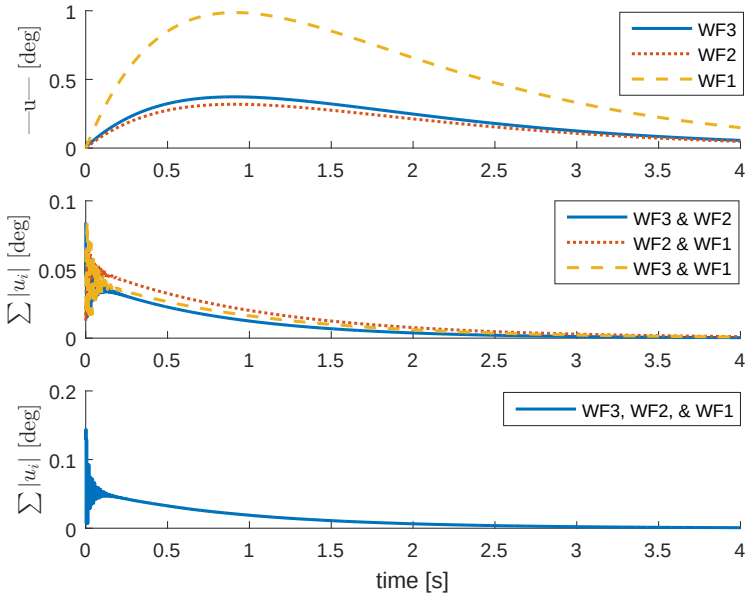

(b) Total control effort

Figure 7.5: Nominal law control surface assignment comparison

Now, the surrogate tracking error MRAC design is used for the delta law and is added to the pole placement nominal law using WF 3 and WF 2. The delta law can use WF 4, WF 1, or both as inputs. Each possibility is simulated at the same M=0.714 condition. Accelerometer ACC LE is used for delta law feedback when one surface is used. ACC LE and ACC C are used when both surfaces are involved.

The delta reference model is defined in a similar way regardless of input choice. The required structure $\beta_{du}(s)$ is set to contain all zeros from the wing's delta portion. No additional zeros are included so $\beta_r(s) = I_2$. The gain matrix is chosen to be $\beta_{dm} = 1e-13I_2$. The order n_c is chosen according to Eq. (5.9), and the roots of $\alpha_m(s)$ are distributed evenly between $s = -4$ and $s = -6$. The filters are specified by placing the roots of the user-choice items: $a_f(s)$ at $s = -2$, $b_f(s)$ at $s = -3$, and $C_f(s)$ at $s = -4$. The full reference model can be recovered by adding the closed loop nominal system to the delta reference model if needed, though only the delta reference model is actually used.

The implementation is completed by specifying a few remaining settings. P_0 is set to $5e8I$ and reset to P_0 when $\lambda_{\min}(P(t)) \leq 0.01$. All filters use zero initial conditions. The plant initial condition is brought down to near zero to make the steady state behavior clearly visible.

The results of the three control surface possibilities are given in Fig. 7.6. At this level of inspection it is clear that even though the nominal law does provide stabilization it does not completely eliminate oscillation. This behavior is seen unless a nominal law commanding high gains is implemented.

Addition of the delta law, however, is able offer full oscillation suppression in this test without resorting to high gains. The first panel shows that addition of the delta law using only WF 1 eliminates the oscillation around 3 s. The middle panel demonstrates that the delta law using WF 4 accomplishes the same around 2 s. The last panel shows the same behavior occurring near 1.5 s when using both WF 1 and WF 4, and it is clear that use of both control surfaces in delta system is preferable.

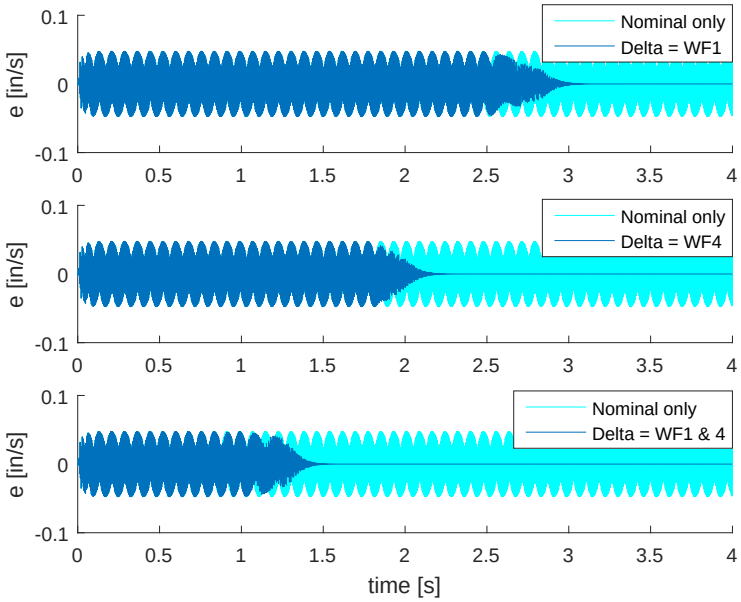

Figure 7.6: Simple wing delta control input comparison

7.2 Aircraft Implementation

The surface assignment information gained from analysis of the simple wing is now transfered to the flexible aircraft. The partitioned MRAC design,

using the previously established input and output choices for both control laws, is implemented on the vehicle and used to stabilize flexible motion of the wing in response to a gust disturbance. Details of the implementation specific to the aircraft are discussed subsequently.

7.2.1 Input/Output Assignment

Similar input and output assignments for the two control laws are made for the aircraft as were made for the simple wing. Some output assignment modifications are made for the transition to a full vehicle with rigid body dynamics that the fixed simple wing obviously lacked. Further, matching wing flaps on either side of the aircraft are actuated symmetrically. For example, only one command for the WF 1's is calculated and then issued identically to WF 1L and WF 1R. The signal copying behavior attempts to prevent roll coupling and is appropriate the level flight flexible motion stabilization task under investigation. The aircraft's existing nominal law is therefore modified to use the inner wing flaps WF 2L & R and WF 3L & R. Measurement of total velocity, bank angle, pitch rate, roll rate, and the six accelerometers shown in Fig. 2.4 are used for feedback. The delta law uses the outer wing flaps WF 1L & R and WF 4L & R, but output assignment for the delta portion is less straightforward.

In this investigation the partitioned control design is used for stabilization of the wings at flight conditions just past the body freedom flutter boundary. This type of flutter causes a known vibratory shape of the vehicle,

Table 7.1: Surrogate tracking error MRAC input and output assignments for flexible motion control

	Nominal Control System	**Delta Control System**
Inputs	WF 2R & WF 2L, WF 3R & WF 3L, throttle	WF 1R & WF 1L, WF 4R & WF 4L
Outputs	all accelerometers, velocity, bank angle, pitch & roll rates, flight path angle	ACC CF + ACC CR, ACC RF + ACC LF

and knowledge of that shape can use used to determine which accelerometers are most useful for delta system feedback. The delta system is still restricted to be square, and the signal copying means that although the delta system has control authority over four physical wing flaps only two control signals are calculated. The two-input delta system can therefore have only two outputs assigned. The solution proposed is to use two composite accelerometer signals that emphasize the flutter mode. Specifically, the two body accelerometer measurements ACC CF and ACC CR are added to created one output while the two forward wing tip accelerometers ACC RF and ACC LF are added to create the other. The delta portion is thus a 2×2 MIMO system. A summary of the input and output assignments is provided in Table 7.1.

It is important to highlight that the output selection described results in some aspects of the system being unmanaged by the delta law. Notably, only information from the accelerometers is utilized by the delta controller even though actuation of the delta control surfaces certainly impacts other quantities of interest such as fight path angle and pitch rate. Important but

unmanaged signals like these should be monitored to ensure that their behavior does not become unacceptable once use of the delta law is added.

7.2.2 Modeling

Linear, time-invariant state space models, each corresponding to a single flight condition, are used for control design and simulation in this study. Models are generated over a grid of conditions using airspeeds ranging from 50 to 150 KEAS and fuel weight from 0 to 80 lbs. so that the body freedom flutter boundary is amply covered. ZAERO is used create aeroservoelastic models from a finite element model of the aircraft along with sensor and actuator definitions. The resulting models describe the rigid body dynamics, modal dynamics, unsteady aerodynamic forces, and actuator dynamics.

As with the simple wing, reduced order and numerically suitable models are obtained using ZAERO by making appropriate choices in the model generation process. The number of included modes is limited to reasonably small number. The order of the unsteady dynamic force approximation is reduced below what is typically used in aeroelastic studies. The actuator speed is limited to what is strictly necessary to suppress the flutter mode considered. Additional model reduction steps including state removal and truncation are also pursued after the models have been generated as discussed in Chapter 3.

Performance of the control design will be simulated using the reduced order linear models. The aircraft model for the flight condition considered is split into the nominal and delta portions according the input and output

assignments established in Section 7.2.1. At first the nominal portion will be assumed to be known perfectly and used directly as the nominal model to calculate $\bar{y}_n$. Subsequently, a disturbed version of the nominal portion will be used to obtain $\bar{y}_n$ in an effort to investigate robustness. The same delta portion of the model will be used throughout. The delta portion remains unknown aside from the nonminimum phase zero structure. Similar to the nominal model, perfect knowledge of the nonminimum phase zero structure will be used initially and then error introduced.

7.2.3 Control Laws

The nominal law was designed using modern control techniques with the objective of stabilizing multiple unstable flutter modes while providing reasonable tracking performance. The nominal control design is not detailed here for security reasons but ultimately adheres to the structure outlined in Section 3.1. However, similar control methodologies can be found in [37, 70–73]. The closed-loop nominal system $\bar{W}_n(s)$ is obtained by using the existing nominal control law to close the loop around a model of the nominal system and extracting a selection that relates WF 2L & R and WF 3L & R to ACC CF +ACC CR and ACC RF + ACC LF.

The partitioned control design with surrogate tracking error MRAC is used for the delta law. The aircraft implementation is a 2×2 MIMO system according the previous described input and output assignments. To implement the adaptive design the delta reference model $W_\Delta(s)$ must be designed

using knowledge of the delta plant matrix $\beta_{du}(s)$. For the flexible aircraft implementation all zeros will be included in $\beta_{du}(s)$ and $\beta_s(s) = I_2$ for simplicity. No extra zeros are included in the delta reference model resulting in $\beta_r(s) = I_2$. The delta reference model order is chosen to make its relative degree one higher than the relative degree of the plant, and its poles are then all placed at $s = -3$. Finally, the gain matrix β_{dm} is chosen to be $1e5I_2$. Although the gain matrix can be varied to change the control authority division between the nominal and delta systems, it is left at the stated value for the duration of the paper. The adaptive design for the delta system is completed by specifying the various filters. The same filter polynomials used for the simple wing are again chosen here by placing the poles of $a_f(s)$ at s=-2, $b_f(s)$ at s=-3, and $C_f(s)$ at s=-4. The parameter n_c is chosen as the minimum value that satisfies Eq. (5.9).

7.3 Simulation Results

The performance of the partitioned control design is next demonstrated in simulation. The reduced order, linear aircraft model generated at a speed and weight case slightly beyond the body freedom flutter boundary is used for the plant dynamics. Stabilization of flexible motion in response to a gust disturbance applied directly to the body is compared when using the partitioned design and when using the nominal law only. Various errors are systematically introduced. For each case considered, the plant and reference model are each given a small, nonzero initial condition. All filter states begin at zero. P_0 is

set to $1e3I$ and reset to P_0 when $\lambda_{\min}(P(t)) \leq 0.01$. $\Omega(t)$ is constructed using $\eta = 1$. Signals in the following plots are scaled by consistent reference values for security purposes.

7.3.1 Perfect Knowledge

Figures 7.7 to 7.9 demonstrate the flexible motion control ability of the partitioned design with perfect knowledge of all information required. For this simulation the nominal portion of the plant is used directly as the nominal model. The zero information of the delta portion contained in $\beta_{du}(s)$ is known and used in the delta reference model and filter. The rest of the delta portion is unknown but linear. No disturbances or uncertainties are considered. Figures 7.7(a) and 7.7(b) show the vertical accelerometer measurement at two locations in response to the doublet gust-like disturbance that is applied to the body of the aircraft. The graphs compare the output when the system is controlled by the nominal law alone versus the nominal and delta laws together. While no significant improvement is seen (or even needed) at the body accelerometer location in Fig. 7.7(a), notable improvement is seen in the amplitude of oscillation at wing tip accelerometer location shown in Fig. 7.7(b). Note that the same scaling value has been used in both plots.

The commanded surfaces deflections resulting from both the nominal and delta laws are shown in Fig. 7.8. Control surfaces associated with the nominal law are denoted by dashed lines and surfaces associated with the delta law are solid. The various update law settings selected for the delta law ensure

that the nominal law provides the primary response for initial conditions. The delta law is then the primary responder for the disturbance since feedback in the nominal system is based on signals obtained from an undisturbed model. Note that the surface deflections associated with the delta law are reasonable in magnitude, especially when compared to the nominal surface deflections, despite the adaptive nature of the delta system.

Finally, Fig. 7.9 shows the aircraft's flight path angle, one of the outputs unmanaged by the delta law that is particularly susceptible to the gust disturbance considered. The dashed line shows the output when only the nominal law is in use. The solid line shows the output when both laws are in use. In the perfect knowledge case addition of the delta law does not significantly alter the performance of this output. However this signal will be monitored as errors are introduced to ensure that use of the delta law is not causing undesirable effects.

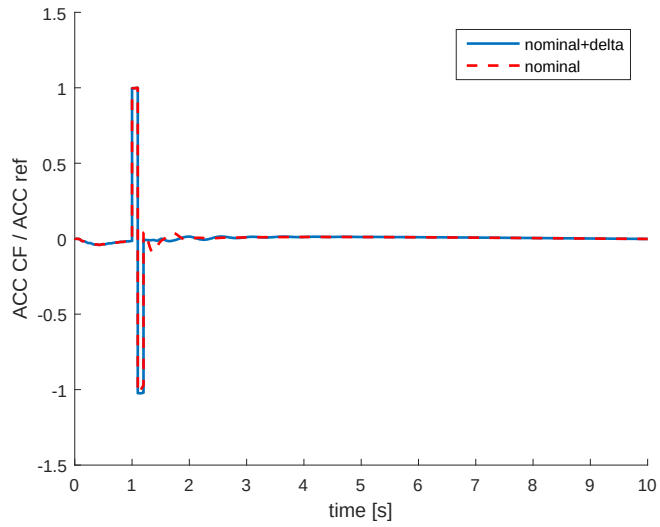

(a) Forward body accelerometer

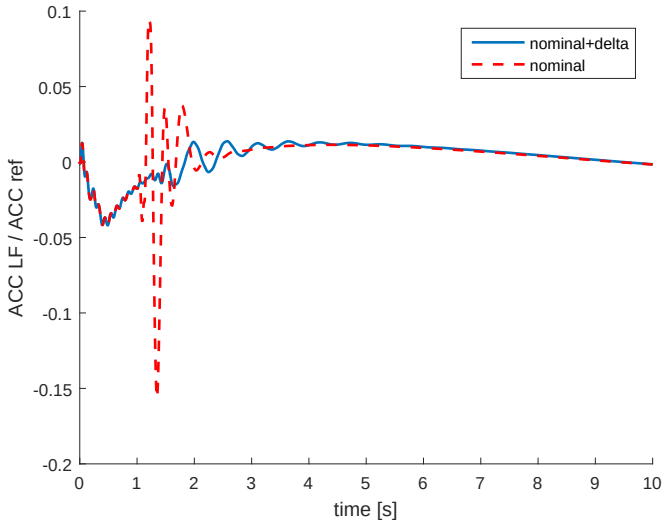

(b) Forward wing tip accelerometer

Figure 7.7: Accelerometer gust disturbance response, perfect knowledge

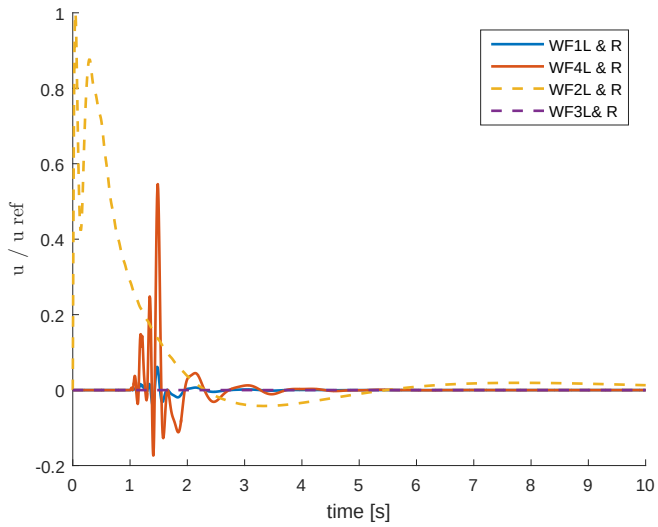

Figure 7.8: Delta control surface deflections for gust disturbance response, perfect knowledge

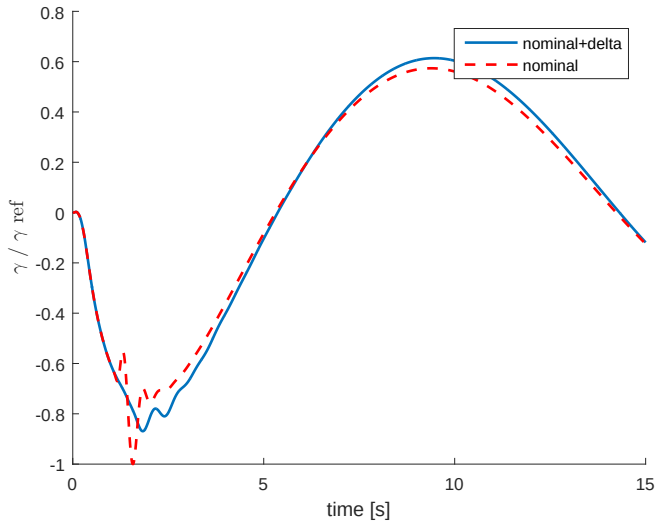

Figure 7.9: Flight path angle for gust disturbance response, perfect knowledge

7.3.2 Estimated Nonminimum Phase Zeros

Figures 7.10 to 7.12 contain the results of the same simulation but now with error in the zero information used in the adaptive implementation. The delta portion of the plant contains the actual zero structure $\beta_{du}(s)$ for the speed and weight case simulated. The delta reference model and filter $G_{cf,2}(s)$ however use an incorrect estimate of the zero structure $\beta'_{du}(s)$. Similar to the command tracking discussion in the previous chapter, various estimates of the zero structure are used. However since the entire numerator structure of the plant is being used in $\beta_{du}(s)$, the simulation is not restricted to using a $\beta'_{du}(s)$ that contains the same number of nonminimum phase zeros and instead must simply have the same number of zeros. This turns out to be a much less restrictive requirement as the number of zeros is consistent across the range of flight conditions investigated while the number of nonminimum phase zeros is not. Although, the lesser restriction comes at the expense of greater knowledge of the plant. Four estimated zero cases are compared to the perfect zero knowledge case in the plots. For each estimated zero simulation the zeros are shifted halfway to zeros of the next case including the ± 10 lbs cases and ± 10 KEAS cases. Note that when going from a slower speed case to a faster one or a heavier mass case to a lighter one the nonminimum phase zeros tend to move further into the right half plane. The simulations in these cases uses a "more unstable" zero structure for the adaptive implementation than the actual zero structure of the plant.

The same assortment of plots is shown for the zero error simulation as

for the perfect knowledge simulation. Note that the some plots only show a portion of the time axis to provide make detail visible. Figures 7.10(a) and 7.10(b) give two accelerometer signals used for delta law feedback. Little difference is seen among the perfect zero case and estimated zero cases. Although, moving to a faster case appears to produce the most notable deviation out of the results shown with the shift to a lower mass case close behind. Figure 7.11 compares the commanded control surface deflections again with only small differences between the perfect and estimated cases. The unmanaged flight path angle measurement is shown in Fig. 7.12. Here it is again apparent that the zeros from the higher speed and lower mass cases cause the most notable deviations, but overall introduction of zero error does not significantly degrade performance of the partitioned design for the conditions considered.

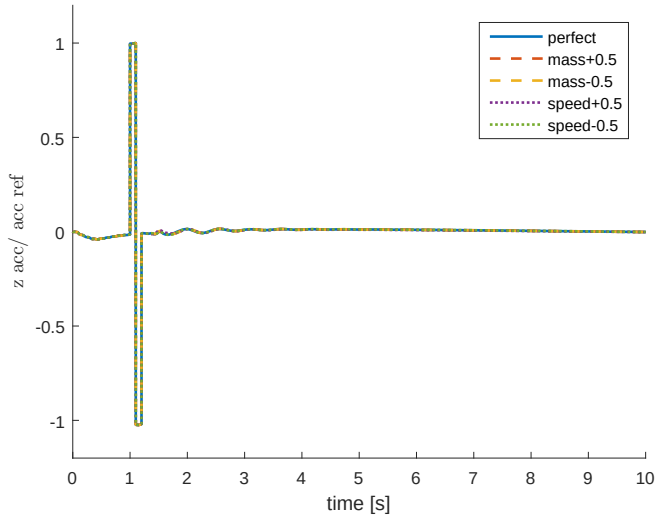

(a) Forward body accelerometer

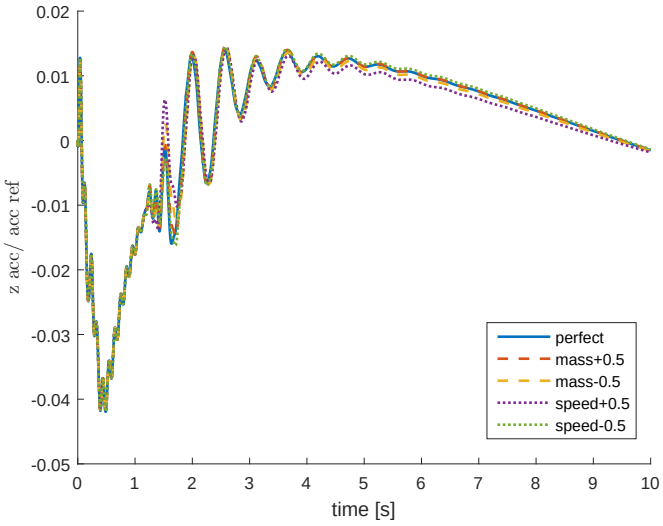

(b) Forward wing tip accelerometer

Figure 7.10: Accelerometer gust disturbance response, zero error

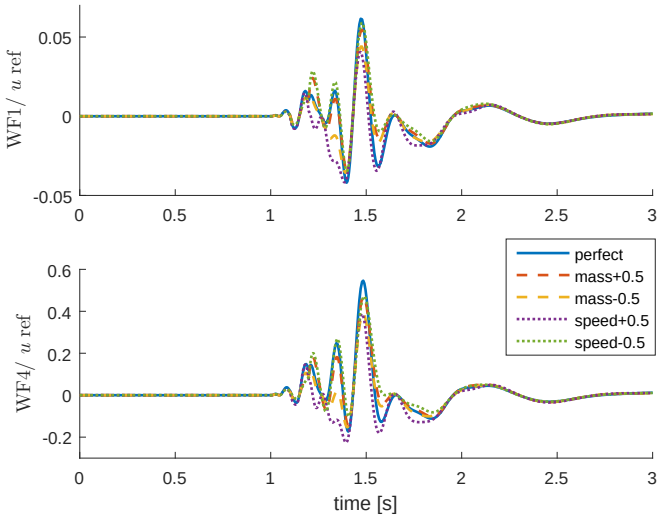

Figure 7.11: Delta control surface deflections for gust disturbance response, zero error

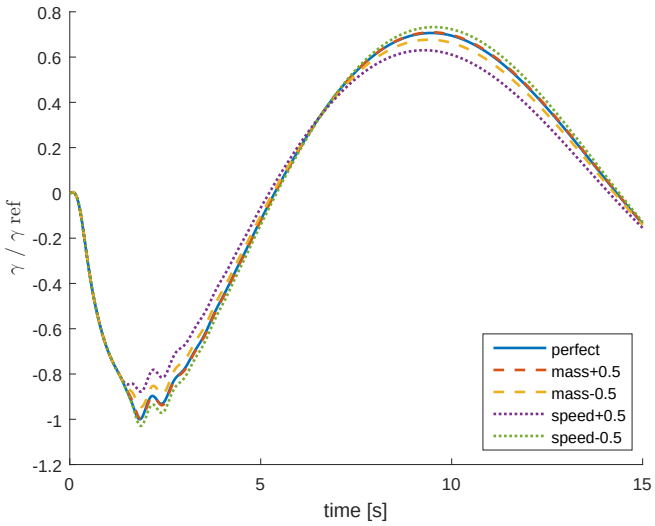

Figure 7.12: Flight path angle for gust disturbance response, zero error

7.3.3 Estimated Nonminimum Phase Zeros and Incorrect Nominal Model

The same simulation is repeated a third time now with an incorrect nominal model in addition to zero error. The nominal portion of the actual plant is from the speed and weight case considered in the previous simulations. The nominal model used to calculate $\bar{y}_n$ however is varied among those from adjacent cases at ± 10 KEAS and ± 10 lbs. The worst case zero estimate from the previous section where the zeros are moved halfway to the +10 KEAS case is used at all times for the reference model and filter.

Figures 7.13 to 7.15 provide the results of the nominal model and zero error simulation. Partitioned design performance changes are still a considerable improvement compared to the nominal only design. Figure 7.13(b) demonstrates that mass–related model inaccuracies result in larger degradation of transient performance than speed–related model inaccuracies. Figure 7.14 shows the nominal model error results in insignificant changes to the delta control commands calculated. Figure 7.15 however highlights that the sensitivity to mass–related model changes established by the wing tip accelerometer plot also holds for flight path angle stabilization.

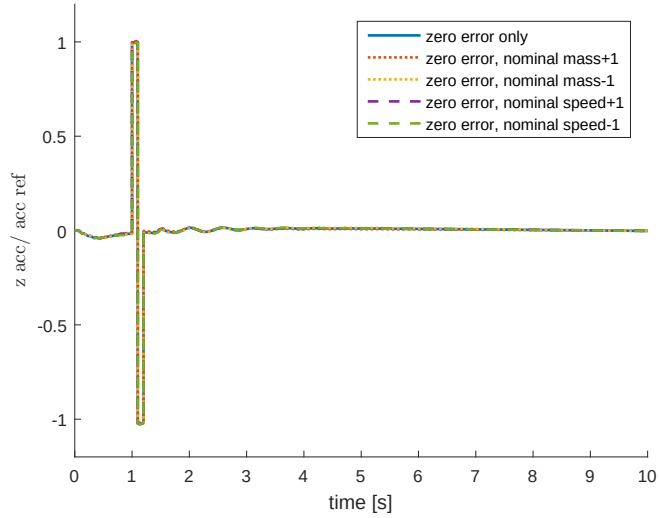

(a) Forward body accelerometer

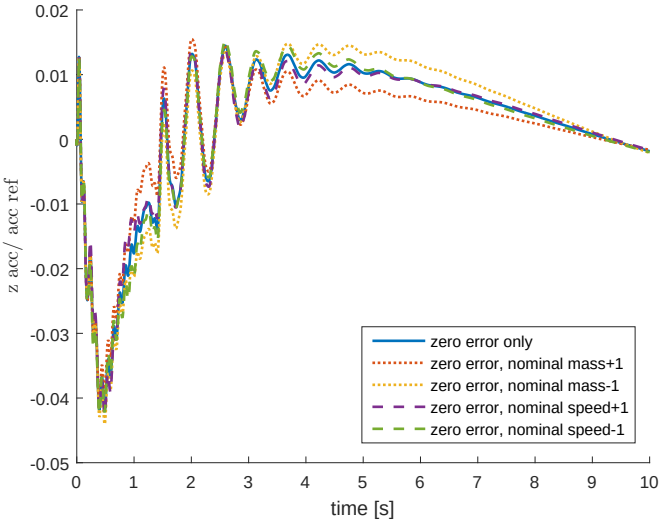

(b) Forward wing tip accelerometer

Figure 7.13: Accelerometer gust disturbance response, zero and nominal model error

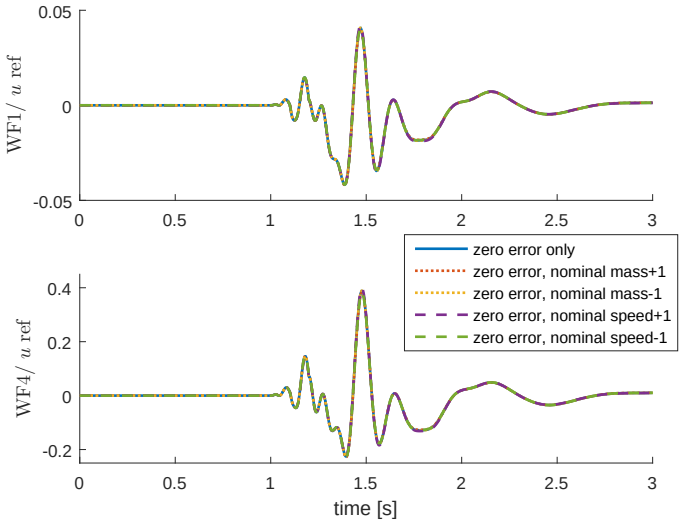

Figure 7.14: Delta control surface deflections for gust disturbance response, zero and nominal model error

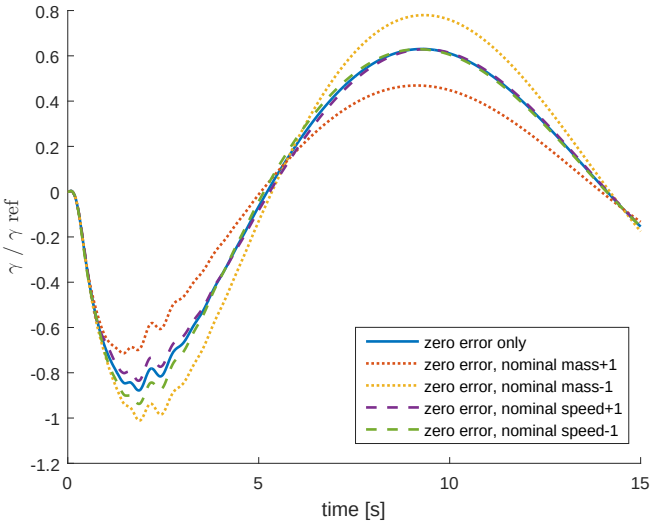

Figure 7.15: Flight path angle for gust disturbance response, zero and nominal model error

Chapter 8

Conclusion

8.1 Summary of Contributions

The main research contributions described in the dissertation can be summarized as follows:

1. Strongly motivated by complex aircraft control applications, a partitioned framework was created to combine use of a nonadaptive control law with an MRAC–based control law to control a multi–input, linear system. The design utilizes separate control surfaces for each law to prevent competition. The required structure of the nonadaptive portion is not restrictive and can accommodate a wide range of control techniques. The adaptive portion can be any version of MRAC.

2. A tracking error convergence proof for MRAC applied to continuous–time, nonminimum phase systems was provided. The proof requires knowledge of the nonminimum phase zeros and includes a new argument for demonstrating regressor boundedness.

3. The partitioned design was demonstrated in simulation using models of an experimental flexible wing aircraft for the purpose of flight path

angle command tracking. The partitioned control design was shown to offer better tracking performance than that obtained when using the aircraft's existing nonadaptive control law alone. Similar results were shown despite the introduction of various modeling errors.

4. The partitioned design was also used to demonstrate flexible motion control and gust alleviation of the same aircraft. An aeroservoelastic model of the aircraft's wing was created to establish appropriate choices of several design parameters and inform the full aircraft implementation. The partitioned design was shown to provide improved suppression of oscillatory motion over the the nonadaptive–only implementation. Favorable results were still demonstrated after the inclusion of modeling error.

8.2 Future Work

Future research related to the work contained in the dissertation falls into two categories. First, several extensions and refinements of the partitioned design are still outstanding. Simulated use of the partitioned design using higher fidelity models and nonlinear effects would be a worthwhile investigation of its performance capabilities. Analysis of performance across changing conditions or with a time–varying plant would also provide insight to the design robustness. An alternate version of the partitioned design could also be developed for the experimental aircraft that uses the adaptive law for flexible motion control and the nonadaptive law for command tracking.

The second category of extensions relates to manipulation of the surrogate tracking error MRAC design. Performance characterization of the design when there is error in the user knowledge of the nonminimum phase zeros remains an open problem. Changes to the design could be attempted to permit accommodation of nonlinear plants. Another possible modification would be to permit the reference model to be time varying. Since the reference model need to contain the the user's best knowledge of the nonminimum phase zeros, it would be beneficial to try and update their potentially incorrect assumed location using output information from the plant. This would require the design to permit variation in reference system and would necessitate another update law. Inclusion of full time–varying reference model could also be pursued as a way to accommodate a gain–scheduled nominal system in the context of the partitioned design ultimately facilitating a unified design over a wide range of operating conditions.

Appendices

Appendix A

Dual Swapping Lemmas

Here it is demonstrated how the dual swapping lemma approach used in Chapter 6 of [8] fails for a restricted version of the nonminimum phase MRAC variant stated in Chapter 5 of the dissertation. For this approach the plant must have a diagonal $\beta_{du}(s)$ and no zeros at the origin. The general procedure is to establish a normalizing signal m_f and then demonstrate that the exponentially weighted norms of the adaptive system's normalized signals are each bounded. The quantity $\Psi^T\tilde{\Theta}$ is then given an upper bound in terms of m_f through the use of two nested swapping lemmas. The normalizing signal itself can then be bounded by the $\Psi^T\tilde{\Theta}$ bound, also containing m_f, and the Bellman–Gronwall Lemma used to conclude that m_f is bounded. The result is that all signals of the adaptive system are bounded as their normalized versions were previously established as bounded. Definitions and theorems relevant to the procedure and stated here are taken from Chapter 3 of [8]. MIMO extensions of these items are taken from [49].

Theorem A.0.1 (Bellman-Gronwall Lemma)**.** *For any nonnegative, piecewise continuous function $\lambda(t)$, $g(t)$, and $k(t)$, if the function $y(t)$ satisfies*

$$y(t) \leq \lambda(t) + g(t)\int_{t_0}^{t} k(s)y(s)ds \quad \forall t \geq t_0 \geq 0 \tag{A.1}$$

then

$$y(t) \leq \lambda(t) + g(t) \int_{t_0}^{t} \lambda(s)k(s) \left[exp\left(\int_{s}^{t} k(\tau)g(\tau)d\tau \right) \right] ds \quad \forall t \geq t_0 \geq 0. \tag{A.2}$$

Additionally, in the case $\lambda(t) = \lambda$ *and* $g(t) = 1$ *the result becomes*

$$y(t) \leq \lambda exp\left(\int_{t_0}^{t} k(s)ds \right) \quad \forall t \geq t_0 \geq 0. \tag{A.3}$$

Definition A.0.1. The exponentially weighted $\mathcal{L}_2$ norm is given by

$$\|x_t\|_{2\delta} \triangleq \left(\int_{0}^{t} e^{-\delta(t-\tau)} x^T(\tau)x(\tau)d\tau \right)^{1/2} \tag{A.4}$$

for $\delta \geq 0$.

System properties related to this norm are stated in the following theorem.

Theorem A.0.2. *If* $H(s)$ *is proper and analytic in* $Re[s] \geq \frac{-\delta}{2}$ *for some* $\delta \geq 0$ *and* $u \in \mathcal{L}_2$ *then*

i

$$\|y_t\|_{2\delta} \leq \|H(s)\|_{\infty\delta} \|u_t\|_{2\delta} \tag{A.5}$$

where

$$\|H(s)\|_{\infty\delta} \triangleq \sup_{\omega} \left| H(j\omega - \frac{\delta}{2}) \right|. \tag{A.6}$$

ii When $H(s)$ *is strictly proper*

$$\|y(t)\|_2 \leq \|H(s)\|_{2\delta} \|u_t\|_{2\delta} \tag{A.7}$$

where

$$\|H(s)\|_{2\delta} \triangleq \frac{1}{\sqrt{2\pi}} \left[\int_{-\infty}^{\infty} \left| H\left(j\omega - \frac{\delta}{2}\right) \right|^2 d\omega \right]^{\frac{1}{2}}. \tag{A.8}$$

Next, define a fictitious normalizing signal

$$m_f^2 \triangleq 1 + \|u_t\|_{2\delta}^2 + \|y_t\|_{2\delta}^2. \tag{A.9}$$

Normalized versions of signals in the adaptive system are shown to be bounded in the following theorem.

Theorem A.0.3. *Consider the adaptive system defined in Chapter 5 and normalizing signal in Eq.* (A.9)*. When* $\Theta \in \mathcal{L}_\infty$ *and for some* $\delta > 0$ *the following hold:*

i $\frac{\bar{y}_i}{m_f}, \frac{\bar{u}_i}{m_f} \in \mathcal{L}_\infty$ *for* $i = 1...n_c$ *and* $\frac{r_f}{m_f} \in \mathcal{L}_\infty$

ii $\frac{\Psi}{m_f}, \frac{u}{m_f}, \frac{y}{m_f} \in \mathcal{L}_\infty$

iii $\frac{\Phi}{m_f} \in \mathcal{L}_\infty$

iv If $\dot{r} \in \mathcal{L}_\infty$ *then* $\frac{\|\dot{y}\|_{2\delta}}{m_f}, \frac{\|\dot{\Psi}\|_{2\delta}}{m_f} \in \mathcal{L}_\infty$.

Proof. (i) $\frac{\bar{y}_i}{m_f}, \frac{\bar{u}_i}{m_f} \in \mathcal{L}_\infty$ follow directly from the filter structure used to generate each $\bar{y}_i$ and $\bar{u}_i$, the definition of m_f, and Theorem A.0.2. Since r is bounded the r_f filter definition gives $r_f \in \mathcal{L}_\infty$ and thus $\frac{r_f}{m_f} \in \mathcal{L}_\infty$ as well.

(ii) $\frac{\Psi}{m_f} \in \mathcal{L}_\infty$ is apparent from $\frac{\bar{y}_i}{m_f}, \frac{\bar{u}_i}{m_f}, \frac{r_f}{m_f} \in \mathcal{L}_\infty$. Then, since $u = \Psi^T \Theta$ and $\Theta \in \mathcal{L}_\infty$, $\frac{u}{m_f} \in \mathcal{L}_\infty$ as well.

To establish a similar result for the output, note that the structure of Ψ and Θ permit the expression

$$\begin{aligned}
\|\Psi^T\Theta\|_2^2 &= \sum_{i=1}^{m}\left(\sum_{j=1}^{m}\phi_j\theta_{ij}\right)^2 \\
&\leq \left(\sum_{k=1}^{m}\phi_k^2\right)\left(\sum_{i=1}^{m}\sum_{j=1}^{m}\theta_{ij}^2\right) \\
&= \left(\sum_{k=1}^{m}\phi_k^2\right)\|\Theta\|_2^2 \\
&\leq c\left(\sum_{k=1}^{m}\phi_k^2\right) \qquad \text{(A.10)}
\end{aligned}$$

since $\Theta \in \mathcal{L}_\infty$. Here c is used to represent a finite constant and $m = (2n_c+1)l^2$. Then the exponentially weighted version can be written as

$$\begin{aligned}
\|\Psi^T\Theta_t\|_{2\delta}^2 &= \int_0^t e^{-\delta(t-\tau)}\|\Psi^T\Theta\|_2^2 d\tau \\
&\leq c\int_0^t e^{-\delta(t-\tau)}\left(\sum_{k=1}^{m}\phi_k^2\right)d\tau. \qquad \text{(A.11)}
\end{aligned}$$

However, the exponentially weighted norm for the matrix Ψ^T is computed by summing the norm of each column and gives

$$\begin{aligned}
\|\Psi_t^T\|_{2\delta}^2 &= \sum_{i=1}^{m}\|\Psi_{i\ t}^T\|_{2\delta}^2 \\
&= \int_0^t e^{-\delta(t-\tau)}\sum_{i=1}^{m}\|\Psi_i^T\|_2^2 d\tau \\
&= l\int_0^t e^{-\delta(t-\tau)}\sum_{i=1}^{m}\phi_i^2 d\tau. \qquad \text{(A.12)}
\end{aligned}$$

where Ψ_i^T is the i^th column of Ψ^T. Therefore there exists some other finite constant such that

$$\|\Psi^T\Theta_t\|_{2\delta} \leq c\|\Psi_t^T\|_{2\delta} \tag{A.13}$$

Also note that the exponentially weighted norm of Ψ^T can be bounded as

$$\begin{aligned}
\|\Psi_t^T\|_{2\delta}^2 &= l\int_0^t e^{-\delta(t-\tau)}\sum_{i=1}^{m}\phi_i^2 d\tau \\
&= l\int_0^t e^{-\delta(t-\tau)}\left[\sum_{i=1}^{n_c}\left(\|\bar{y}_i\|_2^2 + \|\bar{u}_i\|_2^2\right) + \|r_f\|_2^2\right] d\tau \\
&= l\left[\sum_{i=1}^{n_c}\left(\|\bar{y}_{it}\|_{2\delta}^2 + \|\bar{u}_{it}\|_{2\delta}^2\right) + \|r_{ft}\|_{2\delta}^2\right] \\
&= l\left[\sum_{i=1}^{n_c}\left(\|G_{af,i}(s)y_t\|_{2\delta}^2 + \|G_{af,i}(s)u_t\|_{2\delta}^2\right) + \|G_{af}(s)r_t\|_{2\delta}^2\right] \\
&\leq l\left[\sum_{i=1}^{n_c}\left(c\|y_t\|_{2\delta}^2 + c\|u_t\|_{2\delta}^2\right) + c\|r_t\|_{2\delta}^2\right] \\
&\leq l\left[cn_c\left(\|y_t\|_{2\delta}^2 + \|u_t\|_{2\delta}^2\right) + c\|r_t\|_{2\delta}^2\right] \\
&\leq c\left(\|y_t\|_{2\delta}^2 + \|u_t\|_{2\delta}^2 + 1\right) \\
&= cm_f^2
\end{aligned} \tag{A.14}$$

so long as r is bounded.

Next, note that

$$y - y_m = W_m(s)\left[\Psi^T\tilde{\Theta}\right] \tag{A.15}$$

according to an argument similar to that given in Section 2.5.3 such that

$$y = W_m(s)\left[\Psi^T\tilde{\Theta} + r\right]. \tag{A.16}$$

From Theorem A.0.2 the statement

$$\begin{aligned}\|y\|_2 &\leq c + c\|\Psi^T\tilde{\Theta}_t\|_{2\delta} \\ &\leq c + c\|\Psi_t^T\|_{2\delta}\end{aligned} \tag{A.17}$$

can obtained in a fashion similar to Eq. (A.13) when $\Theta \in \mathcal{L}_\infty$. Use of Eq. (A.14) permits the statement

$$\|y\|_2 \leq cm_f \tag{A.18}$$

and thus $\frac{y}{m_f} \in \mathcal{L}_\infty$.

For (iii), recall that each column of Φ^T is the filtered version of the respective column in Ψ^T. Theorem A.0.2 can be used to state

$$\begin{aligned}\|\Phi_i^T\|_2 &\leq \|G_{cf2}(s)\|_{2\delta}\|\Psi_{it}^T\|_{2\delta} \\ &\leq c\|\Psi_{it}^T\|_{2\delta} \\ &\leq cm_f.\end{aligned} \tag{A.19}$$

The norm for the full matrix can be bounded by the same expression and thus $\frac{\Phi}{m_f} \in \mathcal{L}_\infty$.

Finally, (iv) is demonstrated by expressing the derivative operation in the Laplace domain. From Eq. (A.16), $\dot{y}$ can be expressed as

$$\dot{y} = sW_m(s)\left[\Psi^T\tilde{\Theta} + r\right]. \tag{A.20}$$

The system indicated by $sW_m(s)$ will be proper so long as the previously stated requirement $d_m > d$ is satisfied. Theorem A.0.2 and the required boundedness of r can thus be used to claim that

$$\begin{aligned} \|\dot{y}_t\|_{2\delta} &\leq c\|\Psi_t^T\|_{2\delta} + c \\ &\leq cm_f \end{aligned} \tag{A.21}$$

and thus $\frac{\|\dot{y}\|_{2\delta}}{m_f} \in \mathcal{L}_\infty$. The exponentially weighted norm of the matrix $\dot{\Psi}^T$ can be computed similarly by summing the operation on each column

$$\begin{aligned} \|\dot{\Psi}_t^T\|_{2\delta}^2 &= l \int_0^t e^{-\delta(t-\tau)} \sum_{i=1}^{m} \dot{\phi}_i^2 d\tau \\ &= l \left[\sum_{i=1}^{n_c} \left(\|\dot{\bar{y}}_{it}\|_{2\delta}^2 + \|\dot{\bar{u}}_{it}\|_{2\delta}^2 \right) + \|\dot{r}_{ft}\|_{2\delta}^2 \right] \\ &= l \left[\sum_{i=1}^{n_c} \left(\|sG_{af,i}(s) y_t\|_{2\delta}^2 + \|sG_{af,i}(s) u_t\|_{2\delta}^2 \right) + \|sG_{af}(s) r_t\|_{2\delta}^2 \right] \\ &\leq l \left[\sum_{i=1}^{n_c} \left(c\|y_t\|_{2\delta}^2 + c\|u_t\|_{2\delta}^2 \right) + c\|r_t\|_{2\delta}^2 \right] \\ &\leq l \left[cn_c \left(\|y\|_{2\delta}^2 + \|u\|_{2\delta}^2 \right) + c\|r\|_{2\delta}^2 \right] \\ &\leq c \left(\|y_t\|_{2\delta}^2 + \|u_t\|_{2\delta}^2 + 1 \right) \\ &= cm_f^2 \end{aligned} \tag{A.22}$$

and thus $\frac{\|\dot{\Psi}\|_{2\delta}}{m_f} \in \mathcal{L}_\infty$. □

Next consider the two swapping lemmas that will be used. The first is the more widely known swapping lemma given in Theorem 2.2.7 which will

be used with alteration. The second is presented in the following theorem and has been modified to accommodate nonminimum phase zeros in the filter definition.

Theorem A.0.4 (Swapping lemma 2)**.** *If* $\Psi : \mathbb{R}^+ \to \mathbb{R}^{p\times l}$ *and* $\tilde{\Theta} : \mathbb{R}^+ \to \mathbb{R}^p$ *are differentiable, then*

$$\Psi^T\tilde{\Theta} = F_1(s)\left[\dot{\Psi}^T\tilde{\Theta} + \Psi^T\dot{\Theta}\right] + F(s)\left[\Psi^T\tilde{\Theta}\right] \tag{A.23}$$

where

$$F(s) = \bar{F}\beta_F(s), \tag{A.24}$$

$$\bar{F}(s) = \sum_{i=1}^{l} \frac{\alpha_0^k sign(\beta_{0,i})}{(s+\alpha_0\bar{\beta}_{0,i})^k} e^i, \tag{A.25}$$

and $\beta_F(s)$ *is an* $l \times l$ *diagonal matrix of polynomials where each nonzero entry has no roots at the origin. The parameter* k *must be greater than the degree of* $\beta_F(s)$ *and* $\alpha_0 > 1$ *is necessary. Each* $\beta_{0,i}$ *refers to the constant term of the* i^{th} *diagonal entry of* $\beta_F(s)$ *and* $\bar{\beta}_{0,i} = \sqrt[k]{|\beta_{0,i}|}$*. Additionally,*

$$F_1(s) = \left(I_l - F(s)\right)\frac{1}{s}. \tag{A.26}$$

Further, for $\alpha > \delta$ *where* $\delta \geq 0$*,*

$$\|F_1(s)\|_{\infty\delta} \leq \sum_{i=1}^{k}\left(\frac{c}{\alpha_0} + c\alpha_0^i\right). \tag{A.27}$$

where c *stands for a constant not dependent on* α_0*.*

Proof. The quantity $\Psi^T\tilde{\Theta}$ can be written as

$$\Psi^T\tilde{\Theta} = \frac{s}{s}(I_l - F(s))\left[\Psi^T\tilde{\Theta}\right] + F(s)\left[\Psi^T\tilde{\Theta}\right]. \tag{A.28}$$

Incorporating the definition of $F_1(s)$ and applying s as the differential operator results in

$$\Psi^T\tilde{\Theta} = F_1(s)\left[\dot{\Psi}^T\tilde{\Theta} + \Psi^T\dot{\Theta}\right] + F(s)\left[\Psi^T\tilde{\Theta}\right]. \tag{A.29}$$

For simplicity, now consider the case where $l = 1$ such that each of the transfer function and polynomial matrices become scalar. In this case the general expression for the polynomial $\beta_F(s)$ is given by

$$\beta_F(s) = \beta_m s^m + ... + \beta_1 s + \beta_0. \tag{A.30}$$

The structure required implies that β_m, $\beta_0 \neq 0$ while every other coefficient is unrestricted and that $k > m$. The polynomial can be manipulated to facilitate construction of the transfer function $F(s)$ as

$$\begin{aligned}
\beta_F(s) &= \beta_0\left(\frac{\beta_m}{\beta_0}s^m + ... + \frac{\beta_1}{\beta_0}s + 1\right) \\
&= \beta_0\left(\bar{\beta}_m s^m + ... + \bar{\beta}_1 s + 1\right) \\
&= \text{sign}(\beta_0)|\beta_0|\left(\bar{\beta}_m s^m + ... + \bar{\beta}_1 s + 1\right) \\
&= \text{sign}(\beta_0)\bar{\beta}_0^k\left(\bar{\beta}_m s^m + ... + \bar{\beta}_1 s + 1\right)
\end{aligned} \tag{A.31}$$

where $\bar{\beta}_i \triangleq \frac{\beta_i}{\beta_0}$ for $i = 1...m$ and

$$\bar{\beta}_0^k = |\beta_0|. \tag{A.32}$$

Note that

$$\text{sign}(\beta_0) = \begin{cases} 1 \text{ if } \beta_0 > 0 \\ -1 \text{ if } \beta_0 < 0 \end{cases} \tag{A.33}$$

as β_0 cannot be zero.

An appropriate choice of $\bar{F}(s)$ can be made to produce the desired cancellation of the pole at the origin in $F_1(s)$. Specifically, select

$$\bar{F}(s) = \frac{\text{sign}(\beta_0)\alpha_0^k}{(s+\alpha_0\bar{\beta}_0)^k} \tag{A.34}$$

For this choice of $\bar{F}(s)$ the transfer function $1 - F(s)$ becomes

$$\begin{aligned} 1 - F(s) &= 1 - \bar{F}(s)\beta_F(s) \\ &= \frac{(s+\alpha_0\bar{\beta}_0)^k - \text{sign}(\beta_0)\alpha_0^k\beta_F(s)}{(s+\alpha_0\bar{\beta}_0)^k} \\ &= \frac{\sum_{i=0}^k C_k^i \alpha_0^{k-i}\bar{\beta}_0^{k-i}s^i - \text{sign}(\beta_0)\alpha_0^k\sum_{i=0}^k \beta_i s^i}{(s+\alpha_0\bar{\beta}_0)^k} \\ &= \frac{s\sum_{i=1}^k \left(C_k^i \alpha_0^{k-i}\bar{\beta}_0^{k-i} - \text{sign}(\beta_0)\alpha_0^k\beta_i\right)s^{i-1}}{(s+\alpha_0\bar{\beta}_0)^k} \end{aligned} \tag{A.35}$$

where the two constant terms in the numerator have canceled and a factor of s can be pulled out. Note that

$$C_k^i = \frac{k!}{i!(k-i)!} \tag{A.36}$$

and that $\beta_i = 0$ for $i > m$ since they do not exist. The transfer function $F_1(s)$ then becomes

$$\begin{aligned} F_1(s) &= \big(1 - F(s)\big)\frac{1}{s} \\ &= \frac{\sum_{i=1}^k \left(C_k^i \alpha_0^{k-i}\bar{\beta}_0^{k-i} - \text{sign}(\beta_0)\alpha_0^k\beta_i\right)s^{i-1}}{(s+\alpha_0\bar{\beta}_0)^k}. \end{aligned} \tag{A.37}$$

The norm bound is next established by breaking down the expression

for $F_1(s)$ into components whose bounds are known:

$$\left\| \frac{1}{s+\alpha_0\bar{\beta}_0} \right\|_{\infty\delta} = \frac{2}{2\alpha_0\bar{\beta}_0 - \delta} \leq \frac{2}{\alpha_0\bar{\beta}_0} \tag{A.38}$$

$$\left\| \frac{s^{i-1}}{(s+\alpha_0\bar{\beta}_0)^{i-1}} \right\|_{\infty\delta} = 1, \quad i \geq 1 \tag{A.39}$$

$$\begin{aligned} \left\| \frac{\alpha_0^i \bar{\beta}_0^i}{(s+\alpha_0\bar{\beta}_0)^i} \right\|_{\infty\delta} &= \left(\left\| \frac{\alpha_0\bar{\beta}_0}{(s+\alpha_0\bar{\beta}_0)} \right\|_{\infty\delta} \right)^i \\ &= \left(\frac{2\alpha_0\bar{\beta}_0}{2\alpha_0\bar{\beta}_0 - \delta} \right) \\ &\leq 2^i, \quad i \geq 1 \end{aligned} \tag{A.40}$$

Manipulating the expression for $F_1(s)$ for convenience gives

$$\begin{aligned} F_1(s) &= \frac{\sum_{i=1}^{k} \left(C_k^i \alpha_0^{k-i} \bar{\beta}_0^{k-i} - \text{sign}(\beta_0)\alpha_0^k \beta_i \right) s^{i-1}}{(s+\alpha_0\bar{\beta}_0)^k} \\ &= \frac{1}{(s+\alpha_0\bar{\beta}_0)} \sum_{i=1}^{k} \left(\frac{C_k^i \alpha_0^{k-i} \bar{\beta}_0^{k-i} - \text{sign}(\beta_0)\alpha_0^k \beta_i}{(s+\alpha_0\bar{\beta}_0)^{k-i}} \frac{s^{i-1}}{(s+\alpha_0\bar{\beta}_0)^{i-1}} \right). \end{aligned} \tag{A.41}$$

Note that the norm of first term inside the summation can be bounded as

$$\begin{aligned} \left\| \frac{C_k^i \alpha_0^{k-i} \bar{\beta}_0^{k-i} - \text{sign}(\beta_0)\alpha_0^k \beta_i}{(s+\alpha_0\bar{\beta}_0)^{k-i}} \right\|_{\infty\delta} \leq \\ C_k^i \left\| \frac{\alpha_0^{k-i} \bar{\beta}_0^{k-i}}{(s+\alpha_0\bar{\beta}_0)^{k-i}} \right\|_{\infty\delta} + \alpha_0^k |\beta_i| \left\| \frac{1}{(s+\alpha_0\bar{\beta}_0)^{k-i}} \right\|_{\infty\delta} \end{aligned} \tag{A.42}$$

Substituting the component bounds gives

$$\left\| \frac{C_k^i \alpha_0^{k-i} \bar{\beta}_0^{k-i} - \text{sign}(\beta_0)\alpha_0^k \beta_i}{(s+\alpha_0\bar{\beta}_0)^{k-i}} \right\|_{\infty\delta} \leq C_k^i 2^{k-i} + \alpha_0^k |\beta_i| \left(\frac{2}{\alpha_0\bar{\beta}_0} \right)^{k-i} \tag{A.43}$$

such that the norm of the entire transfer function is bounded by

$$\begin{aligned}\|F_1(s)\|_{\infty\delta} &\leq \frac{2}{\alpha_0\bar{\beta}_0}\sum_{i=1}^{k}\left(C_k^i 2^{k-i} + \alpha_0^k|\beta_i|\left(\frac{2}{\alpha_0\bar{\beta}_0}\right)^{k-i}\right) \\ &\leq \sum_{i=1}^{k}\left(\frac{c}{\alpha_0} + c\alpha_0^i\right). \end{aligned} \tag{A.44}$$

In the MIMO case where $l > 1$, the quantities $\beta_F(s)$ and $F_1(s)$ become matrices. By requiring that $\beta_F(s)$ is diagonal, the same design for $F(s)$ and thus $F_1(s)$ can easily be extended to the matrix case with β_0 replaced by the appropriate $\beta_{0,i}$. Finally, by defining $F_1(s) = \sum_{i=1}^{l} f_{1,i}(s)e^i$ and

$$\|F_1(s)\|_{\infty\delta} = \sum_{i=1}^{l}\|f_{1,i}(s)\|_{\infty\delta}, \tag{A.45}$$

it is clear that the same bound for $\|F_1(s)\|_{\infty,\delta}$ given in Eq. (A.44) still holds. □

To show that the $\Psi^T\tilde{\Theta}$ remains bounded, begin by using the new swapping lemma given Theorem A.0.4 to say

$$\Psi\tilde{\Theta} = F_1(s)\left[\dot{\Psi}^T\tilde{\Theta} + \Psi^T\dot{\Theta}\right] + F(s)\left[\Psi^T\tilde{\Theta}\right] \tag{A.46}$$

with and select $\beta_F(s) = \beta_{du}(s)$. Next use the standard swapping lemma in Theorem 2.2.7 with $W(s) = G_{cf,2}(s)$ to say

$$\Psi^T\tilde{\Theta} = G_{cf,2}^{-1}(s)\left[\Phi^T\tilde{\Theta} - G_{cf,2_C}(s)\left[Q_B\dot{\tilde{\Theta}}\right]\right]. \tag{A.47}$$

Substituting Eq. (A.47) into Eq. (A.46) yields

$$\Psi^T\tilde{\Theta} = F_1(s)\left[\dot{\Psi}^T\tilde{\Theta} + \Psi^T\dot{\Theta}\right] + F(s)G_{cf,2}^{-1}(s)\left[\Phi^T\tilde{\Theta} - G_{cf,2_C}(s)\left[Q_B\dot{\tilde{\Theta}}\right]\right]. \tag{A.48}$$

Note that the presence of $\beta_{du}(s)$ in $F(s)$ and $G_{cf,2}^{-1}(s)$ will cancel such that

$$\begin{aligned}\|FG_{cf,2}^{-1}\|_{\infty\delta} &= \left\| \frac{C_f(s)\alpha_0^k \text{sign}(\beta_0)}{(s+\alpha_0\bar{\beta}_0)^k a_f(s)} \right\|_{\infty\delta} \\ &= \alpha_0^k \left\| \frac{(s+c_1)^{n_c+n_u+d}}{(s+\alpha_0\bar{\beta}_0)^k (s+c_2)^{n_c}} \right\|_{\infty\delta} \end{aligned} \tag{A.49}$$

in the SISO case if $C_f(s)$ has all roots at c_1 and $a_f(s)$ has all roots at c_2. Selecting $c_1 = c_2 = \alpha_0\bar{\beta}_0$ for simplicity and choosing $k = n_c + n_u + d$ gives

$$\|FG_{cf,2}^{-1}\|_{\infty\delta} \leq c\alpha_0^{n_u+d} \tag{A.50}$$

where c is a constant independent of α_0 according to the component bounds. The same bound hold in the MIMO case by an argument similar to that given at the end of Theorem A.0.4.

Taking the norm of Eq. (A.48) and using the established bounds for $F(s)$ and $F_1(s)$ gives

$$\begin{aligned}\|\Psi^T\tilde{\Theta}_t\|_{2\delta} \leq \sum_{i=1}^{k} \left(\frac{c}{\alpha_0} + c\alpha_0^i \right) (\|\dot{\Psi}^T\tilde{\Theta}_t\|_{2\delta} + \|\Psi^T\dot{\Theta}_t\|_{2\delta}) \\ + c\alpha_0^{n_u+d}(\|\Phi^T\tilde{\Theta}_t\|_{2\delta} + \|G_{cf,2_C}(s)\left[Q_B\dot{\tilde{\Theta}}\right]_t\|_{2\delta}).\end{aligned} \tag{A.51}$$

Recall that from Theorem 5.6.1 that $z_s = \Phi^T\tilde{\Theta} = \epsilon + \eta\Phi^T\Phi\epsilon$ such that

$$\begin{aligned}\|\Psi^T\tilde{\Theta}_t\|_{2\delta} \leq \sum_{i=1}^{k} \left(\frac{c}{\alpha_0} + c\alpha_0^i \right) (\|\dot{\Psi}^T\tilde{\Theta}_t\|_{2\delta} + \|\Psi^T\dot{\Theta}_t\|_{2\delta}) \\ + c\alpha_0^{n_u+d}(\|\epsilon_t\|_{2\delta} + \eta\|\Phi^T\Phi\epsilon_t\|_{2\delta} + \|G_{cf,2_C}(s)\left[Q_B\dot{\tilde{\Theta}}\right]_t\|_{2\delta}).\end{aligned} \tag{A.52}$$

Use the normalizing properties from Theorem A.0.3 along with filter definitions, $\tilde{\Theta} \in \mathcal{L}_\infty$, and $m_f \geq 1$ to obtain

$$\|G_{cf,2_C}(s)\left[Q_B\dot{\tilde{\Theta}}\right]_t\|_{2\delta} \leq c\|m_f\dot{\tilde{\Theta}}_t\|_{2\delta} \tag{A.53}$$

$$\|\dot{\Psi}^T\tilde{\Theta}_t\|_{2\delta} \leq c\|\dot{\Psi}_t\|_{2\delta} \leq cm_f \tag{A.54}$$

$$\|\Psi^T\dot{\Theta}_t\|_{2\delta} \leq c\|m_f\dot{\Theta}_t\|_{2\delta} \tag{A.55}$$

$$\|\Phi^T\Phi\epsilon_t\|_{2\delta} \leq c\|m_f\Phi\epsilon_t\|_{2\delta} \tag{A.56}$$

$$\|\epsilon_t\|_{2\delta} \leq \|m_f\epsilon_t\|_{2\delta} \tag{A.57}$$

such that

$$\begin{aligned}\|\Psi^T\tilde{\Theta}_t\|_{2\delta} \leq \sum_{i=1}^{k}\left(\frac{c}{\alpha_0}+c\alpha_0^i\right)(cm_f + c\|m_f\dot{\Theta}_t\|_{2\delta}) \\ + c\alpha_0^{n_u+d}(\|m_f\epsilon_t\|_{2\delta} + c\|m_f\Phi\epsilon_t\|_{2\delta} + c\|m_f\dot{\tilde{\Theta}}_t\|_{2\delta}).\end{aligned} \tag{A.58}$$

Lastly, define $\tilde{g}^2 = \epsilon^T\epsilon + \epsilon^T\Phi^T\Phi\epsilon + \dot{\Theta}^T\dot{\Theta}$ such that

$$\|\Psi^T\tilde{\Theta}_t\|_{2\delta} \leq \sum_{i=1}^{k}\left(\frac{c}{\alpha_0}+c\alpha_0^i\right)(cm_f + c\|m_f\dot{\Theta}_t\|_{2\delta}) + c\alpha_0^{n_u+d}\|m_f\tilde{g}_t\|_{2\delta}. \tag{A.59}$$

Note that $\tilde{g} \in \mathcal{L}_2$ since $\epsilon, \Phi\epsilon, \dot{\Theta} \in \mathcal{L}_2$ according to Theorem 5.6.1. Return to the definition of m_f, include established input and output bounds, and then substitute Eq. (A.59) to obtain

$$\begin{aligned}m_f^2 &= 1 + \|u_t\|_{2\delta}^2 + \|y_t\|_{2\delta}^2 \\ &\leq c + c\|\Psi^T\tilde{\Theta}_t\|_{2\delta}^2 \\ &\leq c + c\left(\sum_{i=1}^{k}\left(\frac{c}{\alpha_0}+c\alpha_0^i\right)(cm_f + c\|m_f\dot{\Theta}_t\|_{2\delta}) + c\alpha_0^{n_u+d}\|m_f\tilde{g}_t\|_{2\delta}\right)^2.\end{aligned} \tag{A.60}$$

From here the procedure is to assume that $\alpha_0 >> 1$ such that the coefficient under in the summation goes to zero. However, the presence of the $c\alpha_0^i$ term does not permit such behavior. This term arises due to the inclusion of $\beta_F(s)$ in $F(s)$ in Theorem A.0.4. If $\beta_F(s)$ were omitted then

$$\bar{F}(s) = \frac{\alpha_0^k}{(s+\alpha_0)} I_l \tag{A.61}$$

would be an acceptable choice and so long as $\alpha_0 > 1$

$$\|F_1(s)\|_{\infty\delta} \leq \frac{c}{\alpha_0} \tag{A.62}$$

would result as the coefficient instead of the summation term.

In the event that the first term of Eq. (A.60) could be dropped, all that remains is to use the Bellman-Gronwall Lemma to conclude that m_f is bounded since $\tilde{g} \in \mathcal{L}_2$. Then the unnormalized version of all the normalized signals shown to be bounded in Theorem A.0.3 are also bounded, notably including Ψ and thus $\Psi\tilde{\Theta}$.

Appendix B

Discrete–time Conversion

This appendix looks at an alternate approach to establish boundedness of the regressor Ψ and related quantity $\Psi^T\tilde{\Theta}$ in the tracking error convergence proof of Chapter 5. The procedure attempts to use a Lyapunov-like function similar to that used in the discrete-time version of the problem that appears in Appendix C of [20]. Here, however, alternate steps must be taken to establish a necessary state-to-input relationship. This is very nearly done by reusing a portion of the signal growth analysis of the Chapter 5 proof, but fails to produce the bound required.

Theorem B.0.1. *For the composite system shown in Fig. 5.3 and the associated x_F dynamics in Eq.* (5.86) *it holds that*

$$\|\Psi(t)\| \leq c_1 + c_2 \sup_{\tau \leq t} \|x_F(\tau)\| \tag{B.1}$$

when $\tilde{\Theta}$ is bounded.

Proof. From the composite system it was established in Eq. (5.90) that

$$\sup_{\tau \leq t} \|\Psi^T(\tau)\tilde{\Theta}(\tau)\| = \mathcal{O}\left[\sup_{\tau \leq t} \|\bar{x}(\tau)\|\right]. \tag{B.2}$$

Additionally it was shown in Eq. (5.96) that

$$\sup_{\tau \leq t} \|x_G(\tau)\| = \mathcal{O}\left[\sup_{\tau \leq t} \|x_F(\tau)\|\right] \tag{B.3}$$

such that

$$\sup_{\tau \leq t} \|\bar{x}(\tau)\| \sim \sup_{\tau \leq t} \|x_F(\tau)\| \tag{B.4}$$

through use of Theorem 2.3.2. However, use of this theorem as stated relies on the assumption that the vector $\bar{x}$ grows unbounded. Fortunately one direction of Theorem 2.3.2 holds without unbounded growth of the vector. Specifically, for a vector $x = [x_1^T \; x_2^T]^T$ it holds that

$$\sup_{\tau \leq t} \|x_1(\tau)\| = \mathcal{O}\left[\sup_{\tau \leq t} \|x_2(\tau)\|\right] \Rightarrow \sup_{\tau \leq t} \|x_2(\tau)\| \sim \sup_{\tau \leq t} \|x(\tau)\|. \tag{B.5}$$

Thus, it is permissible here to still use Eq. (B.3) to claim that Eq. (B.4) holds.

Combining Eqs. (B.2) and (B.4) gives

$$\sup_{\tau \leq t} \|\Psi^T(\tau)\tilde{\Theta}(\tau)\| = \mathcal{O}\left[\sup_{\tau \leq t} \|x_F(\tau)\|\right] \tag{B.6}$$

or equivalently

$$\sup_{\tau \leq t} \|\Psi(\tau)\| = \mathcal{O}\left[\sup_{\tau \leq t} \|x_F(\tau)\|\right] \tag{B.7}$$

since $\tilde{\Theta}$ can still be shown to be bounded by Theorem 5.6.1. Use of Theorem 2.3.1 allows the supremum on the left to be dropped

$$\|\Psi(t)\| = \mathcal{O}\left[\sup_{\tau \leq t} \|x_F(\tau)\|\right]. \tag{B.8}$$

Substituting the definition of $\mathcal{O}$ notation leads to the stated result

$$\|\Psi(t)\| \leq c_1 + c_2 \sup_{\tau \leq t} \|x_F(\tau)\|. \tag{B.9}$$

□

The Ψ bound obtained in Theorem B.0.1 is not quite what is necessary to proceed. Instead, the preferred bound would be a similar relationship that lacks the supremum on the right side. The following theorem assumes that this preferred bound holds to demonstrate the remainder of the proof procedure.

Theorem B.0.2. *For the problem description in Section 5.1 and adaptive system in Section 5.2, it can be established that* Ψ *and* $\Psi^T\tilde{\Theta}$ *are bounded so long as*

$$\|\Psi(t)\| \leq c_1 + c_2\|x_F(t)\| \tag{B.10}$$

holds.

Proof. Recall the x_F dynamics from the composite system presented in Eq. (5.86) of Theorem 5.6.3

$$\dot{x}_F = A_F x_F + B_F z_f. \tag{B.11}$$

Construct the related quadratic function

$$J(x_F(t)) = x_F^T P_F x_F \tag{B.12}$$

where $P_F = P_F^T > 0$ and $Q_F = Q_F^T > 0$ are define by the Lyapunov equation for the stable matrix A_F

$$A_F^T P_F + P_F A_F = -Q_F. \tag{B.13}$$

Taking the derivative yields

$$\dot{J}(x_F(t)) = -x_F^T Q_F x_F + 2z_f^T B_F^T P_F x_F \tag{B.14}$$

which can be bounded as

$$\dot{J}(x_F(t)) \leq -k_1\|x_F\|^2 + k_2\|z_f\|^2 \tag{B.15}$$

where k_1 and k_2 are positive constants.

A Lyapunov-like function can be constructed using $J(x_F(t))$ as

$$V(x_F(t)) = \ln\left(1 + J(x_F(t))\right). \tag{B.16}$$

Taking the derivative and using the bound in Eq. (B.15) along with a quadratic form eigenvalue bound results in

$$\begin{aligned}
\dot{V}(x_F(t)) &= \frac{\dot{J}}{1+J} \\
&\leq \frac{-k_1\|x_F\|^2 + k_2\|z_f\|^2}{1 + x_F^T P_F x_F} \\
&\leq \frac{-k_1\|x_F\|^2 + k_2\|z_f\|^2}{1 + \lambda_{\min}(P_F)\|x_F\|^2} \\
&= \frac{-k_1\|x_F\|^2}{1 + \lambda_{\min}(P_F)\|x_F\|^2} + \frac{k_2\|z_f\|^2}{1 + \lambda_{\min}(P_F)\|x_F\|^2} \\
&= -W(x_F(t)) + k_2\ell^2(t)
\end{aligned} \tag{B.17}$$

where

$$W(x_F(t)) = \frac{k_1\|x_F\|^2}{1 + \lambda_{\min}(P_F)\|x_F\|^2} \tag{B.18}$$

$$|\ell(t)| = \frac{\|z_f\|}{\sqrt{1 + \lambda_{\min}(P_F)\|x_F\|^2}}. \tag{B.19}$$

Next proceed by establishing that $\ell \in \mathcal{L}_2$. Recall from the surrogate tracking error definition in Eq. (5.21) that the filtered tracking error can be

written as

$$\begin{aligned} z_f &= z_s - \Phi^T\Theta + u_f \\ &= z_s - G_{cf,2}(s)\left[\Psi^T\right]\Theta + G_{cf,2}(s)\left[\Psi^T\Theta\right]. \end{aligned} \tag{B.20}$$

Use of the swapping lemma presented in Theorem 2.2.7 on the last two terms results in

$$z_s = z_s + G_{cf,2_C}(s)\left[G_{cf,2_B}(s)\left[\Psi^T\right]\dot{\Theta}\right]. \tag{B.21}$$

Define $Q_B^T = G_{cf,2_B}(s)\left[\Psi^T\right]$ to reach the simpler expression

$$z_f = z_s + G_{cf,2_C}(s)\left[Q_B^T\dot{\Theta}\right]. \tag{B.22}$$

The norm of z_f can be bounded as

$$\begin{aligned} \|z_f\| &\leq \|z_s\| + c\|Q_B^T\dot{\Theta}\| \\ &\leq \|z_s\| + c\|Q_B^T\|\|\dot{\Theta}\| \\ &\leq \|z_s\| + c\|\Psi^T\|\|\dot{\Theta}\| \end{aligned} \tag{B.23}$$

where c is used to represent a finite constant since $G_{cf,2_B}(s)$ and $G_{cf,2_C}(s)$ are stable systems. Including this bound in the expression for ℓ gives

$$|\ell(t)| \leq \frac{\|z_s\|}{\sqrt{1+\lambda_{\min}(P_F)\|x_F\|^2}} + \frac{c\|\Psi^T\|\|\dot{\Theta}\|}{\sqrt{1+\lambda_{\min}(P_F)\|x_F\|^2}}. \tag{B.24}$$

Using the result $\|\Psi^T\| \leq c_1 + c_2\|x_F\|$ from Eq. (B.10) allows $\ell(t)$ to be expressed as

$$|\ell(t)| \leq \frac{\|z_s\|}{\sqrt{1+\lambda_{\min}(P_F)\|x_F\|^2}} + \frac{(c+c\|x_F\|)\|\dot{\Theta}\|}{\sqrt{1+\lambda_{\min}(P_F)\|x_F\|^2}}. \tag{B.25}$$

Note that the structure of the denominator permits the statements

$$\frac{1}{\sqrt{1+\lambda_{\min}(P_F)\|x_F\|^2}} \leq 1 \tag{B.26}$$

and

$$\frac{\|x_F\|}{\sqrt{1+\lambda_{\min}(P_F)\|x_F\|^2}} \leq \max\left(1, \frac{1}{\sqrt{\lambda_{\min}(P_F)}}\right) \tag{B.27}$$

such that the second term $\ell(t)$ is reduced to provide the bound

$$|\ell(t)| \leq \frac{\|z_s\|}{\sqrt{1+\lambda_{\min}(P_F)\|x_F\|^2}} + c\|\dot{\Theta}\|. \tag{B.28}$$

Next, recall the normalized surrogate tracking error definition $z_s = \Omega^2\epsilon$ and the results of Theorem 5.6.1. Using the normalized expression a bound for z_s can be found that explicitly contains terms that were established to be $\mathcal{L}_2$ as

$$\begin{aligned} \|z_s\| &= \|\epsilon + \eta\Phi^T\Phi\epsilon\| \\ &\leq \|\epsilon\| + \eta\|\Phi\|\|\Phi\epsilon\|. \end{aligned} \tag{B.29}$$

Again using Eq. (B.10) gives

$$\|z_s\| \leq \|\epsilon\| + (c + c\|x_F\|)\|\Phi\epsilon\|. \tag{B.30}$$

Substituting this result into the expression for $\ell(t)$ and again using the the component bounds in Eqs. (B.26) and (B.27) leads to

$$|\ell(t)| \leq c\|\epsilon\| + c\|\Phi\epsilon\| + c\|\dot{\Theta}\|. \tag{B.31}$$

Finally, it is evident that $\ell \in \mathcal{L}_2$ since $\epsilon, \Phi\epsilon, \dot{\Theta} \in \mathcal{L}_2$ according the Theorem 5.6.1.

Next it must be shown that $W(x_F(t))$ is bounded. Since $W(x_F(t))$ is positive Eq. (B.17) can be rearranged to obtain

$$0 \leq W(x_F(t)) \leq -\dot{V}(x_F(t)) + k_2 \ell^2(t). \tag{B.32}$$

Integrating both sides of the inequality and noting that $V(x_F(t))$ is positive leads to

$$\begin{aligned} 0 &\leq \lim_{t\to\infty} \int_0^t W(x_F(\tau))d\tau \\ &= \lim_{t\to\infty} \int_0^t -\dot{V}(x_F(\tau))d\tau + \lim_{t\to\infty} k_2 \int_0^t \ell^2(\tau)d\tau \\ &= V(x_F(0)) - \lim_{t\to\infty} V(x_F(t)) + \lim_{t\to\infty} k_2 \int_0^t \ell^2(\tau)d\tau \\ &\leq V(x_F(0)) + k_2 \int_0^t \ell^2(\tau)d\tau. \end{aligned} \tag{B.33}$$

Since $\ell \in \mathcal{L}_2$ and $V(x_F(0))$ in finite both the upper and lower limits exist. Therefore

$$\lim_{t\to\infty} \int_0^t W(x_F(\tau))d\tau \tag{B.34}$$

exists and $W(x_F(\tau))$ is bounded.

Ultimately x_F is bounded since $W(x_F(t))$ is a positive definite function of x_F. From there Eq. (B.10) permits the claim that Ψ is bounded. Finally, $\Psi^T\tilde{\Theta}$ is also bounded due to previously established boundedness of $\tilde{\Theta}$. $\square$

Bibliography

[1] B.D.O. Anderson and A. Dehghani. Challenges of adaptive control: Past, permanent and future. *Annual Reviews in Control*, 32(2):123–135, 2008.

[2] S.A. Jacklin. Closing the certification gaps in adaptive flight control software. In *AIAA Guidance, Navigation and Control Conference*, August 2008.

[3] S.A. Jacklin, M.R. Lowry, J.M. Schumann, P.P. Gupta, J.T. Bosworth, E. Zavala, J.W. Kelly, K.J. Hayhurst, C.M. Belcastro, and C.M. Belcastro. Verification, validation, and certification challenges for adaptive flight-critical control system software. In *AIAA Guidance, Navigation, and Control Conference*, August 2004.

[4] R.L. Butchart and B. Shackcloth. Synthesis of model reference adaptive control systems by liapunov's second method. In *IFAC Symposium on Adaptive Control*, 1966.

[5] P.C. Parks. Liapunov redesign of model reference adaptive control systems. *IEEE Transactions on Automatic Control*, 11:326–367, 1966.

[6] K.S. Narendra and L.S. Valavani. Stable adaptive controller design–direct control. *IEEE Transactions on Automatic Control*, 23(4):570–583, 1978.

[7] S. Sastry and M. Bodson. *Adaptive control: Stability, convergence, robustness*. Dover, 2011.

[8] P.A. Ioannou and J. Sun. *Robust adaptive control*. Dover, 2012.

[9] K.S. Narendra and A.M. Annaswamy. *Stable adaptive systems*. Prentice Hall, Englewood Cliffs, NJ, 1989.

[10] K.S. Narendra and R.P. Singh. A globally stable adaptive controler for multivariable systems. In *IEEE Conference on Decision and Control*, pages 973–974, December 1981.

[11] L. Hsu and R.R. Costa. Mimo direct adaptive control with reduced prior knowlede of the high frequency gain. In *IEEE Conference on Decision and Control*, pages 3303–3308, December 1999.

[12] R.R. Costa, L. Hsu, A.K. Imai, and P. Kokotovic. Lyapunov-based adaptive control of mimo system. *Automatica*, 39(7):1251–1257, 2003.

[13] D. Bayard. Extended horizon liftings for stable inversion of nonminimum-phase systems. *IEEE Transactions on Automatic Control*, 39(10):1333–1338, 1994.

[14] D.E. Miller. Model reference adaptive control for nonminimum phase systems. *Systems and Control Letters*, 26(3):167–176, 1995.

[15] R. Lozano and X. Zhao. Adaptive pole placement without excitation probing signals. *IEEE Transactions on Automatic Control*, 39(1):47–58, 1994.

[16] E. Lavretsky. Adaptive output feedback design using asymptotic properties of lqg/ltr controllers. *IEEE Transactions on Automatic Control*, 57(6):1587–1591, June 2012.

[17] E. Lavretsky and K.A. Wise. *Robust and Adaptive Control with Aerospace Applications*. Springer, 2013.

[18] P. Misra. Numerical algorithms for squaring–up non–square systems part ii: General case. In *American Control Conference*, 1993.

[19] I. Barkana. Parallel feedforward and simplified adaptive control. *International Journal of Adaptive Control and Signal Processing*, 1(2):95–109, 1987.

[20] J.B. Hoagg and D.S. Bernstein. Retrospective cost model reference adaptive control for nonminimum-phase systems. *Journal of Guidance, Control, and Dynamics*, 35(6):1767–1786, 2012 2012.

[21] J.B. Hoagg. Model reference adaptive control for nonminimum-phase systems using a surrogate tracking error. In *IEEE Conference on Decision and Control*, 2011.

[22] J.B. Hoagg. Multi-input multi-output direct model reference adaptive control for systems with known nonminimum-phase zeros. In *American Control Conference*, June 2012.

[23] A.M. D'Amato, E.D. Sumer, K.S. Mitchell, A.V. Morozov, J.B. Hoagg, and D.S. Bernstein. Adaptive output feedback control of the NASA GTM

model with unknown nonminimum-phase zeros. In *AIAA Guidance, Navigation, and Control Conference*, 2001.

[24] I. Barkana. Classical and simple adaptive control for nonminimum phase autopilot design. *Journal of guidance, control, and dynamics*, 28:631–638, 2005.

[25] N. Nguyen, K. Krishnakumar, and J. Kaneshige. Flight dynamics and hybrid adaptive control of damaged aircraft. *Journal of Guidance, Control, and Dynamics*, 31(3):751–764, 2008.

[26] K.A. Ackerman, E. Xargay, R. Choe, N. Hovakimyan, M.C. Cotting, R.B. Jeffrey, M.R. Blackstun, T.P. Fulkerson T.R. Lau, and S.S. Stephens. L1 stability augmentation system for calspan's variable-stability learjet. In *AIAA SciTech*, 2016.

[27] K.A. Wise and E. Lavretsky. Asymptotic properties of LQG/LTR controllers in flight control problems. In *AIAA Guidance, Navigation, and Control Conference*, August 2012.

[28] T.E. Gibson, A.M. Annaswamy, and E. Lavretsky. On adaptive control with closed-loop reference models: Transients, oscillations, and peaking. *IEEE Access*, 1:703–717, 2013.

[29] T.E. Gibson. *Closed-Loop Reference Model Adapitve Control: with Application to Very Flexible Aircraft*. PhD thesis, Massachusetts Institute of Technology, 2014.

[30] Z. Qu and A.M. Annaswamy. Adaptive output-feedback control with closed-loop reference models for very flexible aircraft. *Journal of Guidance, Control, and Dynamics*, 39(4):873–888, 2016.

[31] W. MacKunis, P.M. Patre, M.K. Kaiser, and W.E. Dixon. Asymptotic tracking for aircraft via robust and adaptive dynamic inversion methods. *IEEE Transactions on Control Systems Technology*, 18(6):1448–1456, 2010.

[32] K.A. Wise, E. Lavretsky, and N. Hovakimyan. Adaptive control of flight: Theory, applications, and open problems. In *Proceedings of the 2006 American Control Conference*, pages 5966–5971, 2006.

[33] M.L. Fravolini, T. Yucelen, D. Wagner, B. Gruenwald, and N. Nguyen. A design, analysis, and verification framework for adaptive flight control. In *AIAA SciTech*, 2015.

[34] K.L Roger and G.E. Hodges. Active flutter suppression-a flight test demonstration. *Journal of Aircraft*, 12(6):551–556, June 1975.

[35] V. Mukhopadhyay. Transonic flutter suppression control law design and wind-tunnel test results. *Journal of Guidance, Control, and Dynamics*, 23(5):930–937, 2000.

[36] J.M. Barker and G.J. Balas. Comparing linear parameter-varying gain-scheduled control techniques for active flutter suppression. *Journal of Guidance, Control, and Dynamics*, 23(5):948–955, 2000.

[37] M.R. Waszak. Robust multivariable flutter suppression for benchmark active control technology wind-tunnel model. *Journal of Guidance, Control, and Dynamics*, 24(1):147–153, 2001.

[38] G. Platanitis and T.W. Straganac. Control of a nonlinear wing section using leading- and trailing-edge surfaces. *Journal of Guidance, Control, and Dynamics*, 27(1):52–58, January–February 2004.

[39] T. Theodorsen. General theory of aerodynamic instability and the mechanism of flutter. Technical Report NACA Rept. 496, National Advisory Committee for Aeronautics, Hampton, VA, 1940.

[40] E.H. Dowel. *A Modern Course in Aeroelasticity.* Kluwer Academic Publishers, 1995.

[41] K.W. Lee and S.N. Singh. Multi-input noncertainty–equivalent adaptive control of an aeroelastic system. *Journal of Guidance, Control, and Dynamics*, 33(3):1451–1460, 2010.

[42] K.W. Lee and S.N. Singh. Control of a wing section using leading– and trailing–edge flaps by $\mathcal{L}_1$ adaptive feedback despite disturbances. In *AIAA Aerospace Sciences Meeting*, January 2013.

[43] N. Nguyen, I. Tuzcu, T. Yucelen, and A. Calise. Longitudinal dynamics and adaptive control application for an aeroelastic generic transport model. In *AIAA Atmospheric Flight Mechanics Conference*, 2011.

[44] M. Cassaro, M. Battipede, P. Marzocca, and A. Behal. Comparison of adaptive control architectures for flutter suppression. *Journal of Guidance, Control, and Dynamics*, 38(2), February 2015. 346–354.

[45] A. Hjartarson, P.J. Seiler, and G.J. Balas. LPV aeroservoelastic control using the LPVTools toolbox. In *AIAA Atmospheric Flight Mechanics Conference*, 2013.

[46] C.M. Shearer ans C.E.S. Cesnik. Trajectory control for very flexible aircraft. *Journal of Guidance, Control, and Dynamics*, 31(2), 2008.

[47] P. Suh, A. Chin, and D. Mavris. Robust modal filtering for control of flexible aircraft. In *AIAA Atmospheric Flight Mechanics Conference*, 2013.

[48] Z. Qu and A.M. Annaswamy. Adaptive output-feedback control with closed-loop reference models for very flexible aircraft. *Journal of Guidance, Control, and Dynamics*, 39(4):873–888, 2016.

[49] X. Xie. Stability and robustness analysis of mimo mrac using kp=l2d2s2 factorization. *International Journal of Systems Science*, 39(3):265–278, 2008.

[50] K.S. Narendra, A.M. Annaswamy, and R.P. Singh. A general approach to the stability analysis of adaptive systems. *International Journal of Control*, 41(1):193–216, 1985.

[51] H.K. Khalil. *Nonlinear Systems*. Prentice Hall, 2002.

[52] B.L. Stevens and F.L. Lewis. *Aircraft Control and Simulation*. Wiley, 2003.

[53] J.B Hoagg and D.S. Bernstein. Nonminimum-phase zeros - much to do about nothing - classical control - revisited part ii. *IEEE Control Systems*, 27(3):45–57, 2007.

[54] R.F. Stengel. *Flight Dynamics*. Princeton University Press, 2004.

[55] Ilan Kroo. Design and development of the SWIFT: A foot-launched sailplane. In *18th Applied Aerodynamics Conference*, 2000.

[56] A. Preumont. *Vibration Control of Active Structures*. Springer, 2011.

[57] D.K. Miu. *Mechatronics–Electromechanics and Contromechanics*. Springer, 1993.

[58] V.A. Spector and H. Flashner. Sensitivity of structural models for non-collocated control systems. *ASME Journal of Dynamic Systems Measurement and Control*, 111(4):646–655, 1989.

[59] ZONA Technology, Inc. *ZAERO Theoretical Manual, Version 8.5*, 2011.

[60] W.J. Rugh. *Linear Systems Theory*. Prentice Hall, 2nd edition, 1995.

[61] A.S. Morse. A gain matrix decomposition and some of its applications. *Systems & Control Letters*, 21(1):1–10, July 1993.

[62] Z. Iwai, I. Mizumoto, and Y. Nakashima. Multivariable stable pid controller design with parallel feedforward compensator. In *SICE-ICASE International Joint Conference*, October 2006.

[63] I. Bar-Kana and H. Kaufman. Global stability and performance of a simplified adaptive algorithm. *International Journal of Control*, 42(6):1491–1505, 1985.

[64] I. Mizumoto, T. Egashira, and Z. Iwai. Simple adaptive control for mimo plants with unmodeled dynamics. In *Asian Control Conference*, 1997.

[65] B. Moore. Principal component analysis in linear systems: Controllability, observability, and model reduction. *IEEE Transactions on Automatic Control*, 26(1):17–31, 1981.

[66] K.E. Hashemi, M.R. Akella, and C. Pak. Tracking error convergence for multi-input multi-output model reference adaptive control with known nonminimum phase zeros. In *IEEE Conference on Decision and Control*, December 2015.

[67] E.J. Davison and S.H. Wang. New results on the controllability and observability of general composite systems. *IEEE Transactions on Automatic Control*, 20(1):123–128, February 1975.

[68] E.G. Gilbert. Controllability and observability in multivariable control systems. *Journal of SIAM Control*, 2(1):128–151, 1963.

[69] J.R. Wright and J.E. Cooper. *Introduction to Aircraft Aeroelasticity and Loads*. Wiley, 2008.

[70] J.K. Mahesh, C.R. Stone, W.L. Garrard, and H.J. Hunt. Control law synthesis for flutter suppresssion using linear quadratic gaussian theory. *Journal of Guidance, Control, and Dynamics*, 4(4):415–422, 1981.

[71] J.R. Newsom. Control law synthesis for active flutter suppression using optiaml control theory. *Journal of Guidance, Control, and Dynamics*, 2(5):388–394, 1979.

[72] L. Nicolai, K. Hunten, S. Zink, and P. Flick. System benefits of active flutter suppression for a sensorcraft-type vehicle. In *13th AIAA/ISSMO Multidisciplinary Analysis Optimization Conference*, 2010.

[73] B.S. Liebst, W.L. Garrard, and J.A. Farm. Design of a multivariable flutter suppression/gust load alleviation system. *Journal of Guidance, Control, and Dynamics*, 11(3):220–229, 1988.

[74] R.V. Doggett Jr., H.G. Morgan, and A.G. Rainey. An experimental investigation of aerodynamic effects of airfoil thickness on transonic flutter characteristics. Technical Report NASA-TM-X-79, NASA Langley Research Center, November 1959.

[75] K.L. Roger. Airplane math modeling methods for active control design. In *AGARD-CP-228*, 1977.